



DE83011185

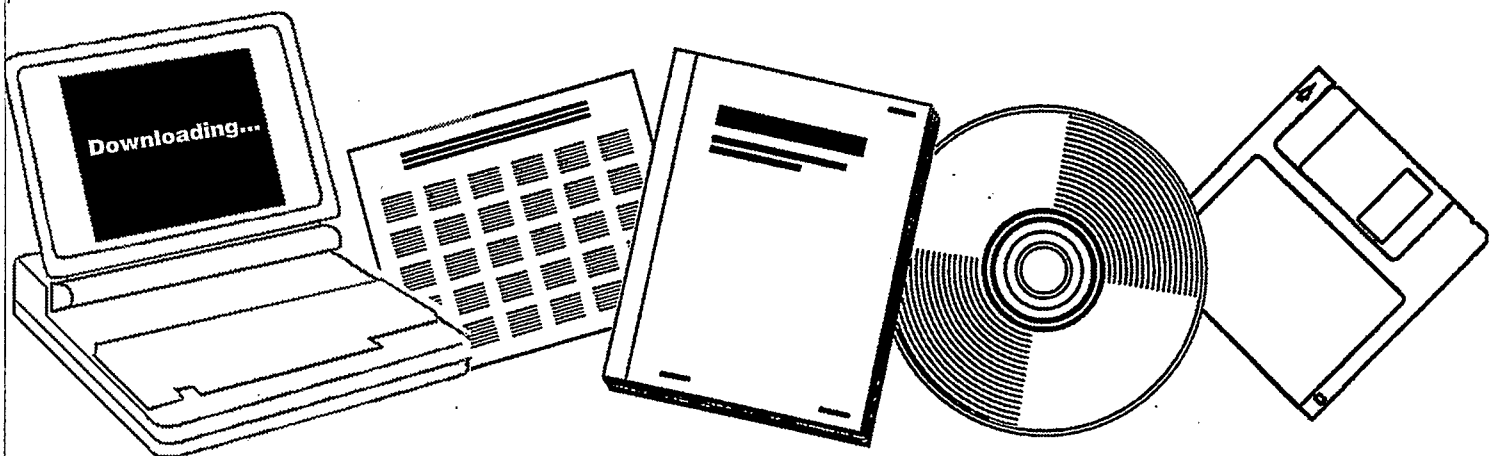
NTIS

One Source. One Search. One Solution.

**FISCHER-TROPSCH SYNTHESIS FROM A LOW H SUB
2 :CO GAS IN A DRY FLUIDIZED-BED SYSTEM.
TECHNICAL PROGRESS REPORT, SEPTEMBER 1,
1982-MARCH 31, 1983**

VIRGINIA POLYTECHNIC INST. AND STATE
UNIV., BLACKSBURG. DEPT. OF CHEMICAL
ENGINEERING

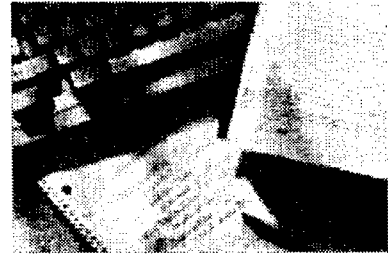
1983



U.S. Department of Commerce
National Technical Information Service

One Source. One Search. One Solution.

NTIS



Providing Permanent, Easy Access to U.S. Government Information

National Technical Information Service is the nation's largest repository and disseminator of government-initiated scientific, technical, engineering, and related business information. The NTIS collection includes almost 3,000,000 information products in a variety of formats: electronic download, online access, CD-ROM, magnetic tape, diskette, multimedia, microfiche and paper.



Search the NTIS Database from 1990 forward

NTIS has upgraded its bibliographic database system and has made all entries since 1990 searchable on www.ntis.gov. You now have access to information on more than 600,000 government research information products from this web site.

Link to Full Text Documents at Government Web Sites

Because many Government agencies have their most recent reports available on their own web site, we have added links directly to these reports. When available, you will see a link on the right side of the bibliographic screen.

Download Publications (1997 - Present)

NTIS can now provide the full text of reports as downloadable PDF files. This means that when an agency stops maintaining a report on the web, NTIS will offer a downloadable version. There is a nominal fee for each download for most publications.

For more information visit our website:

www.ntis.gov



U.S. DEPARTMENT OF COMMERCE
Technology Administration
National Technical Information Service
Springfield, VA 22161

DOE/PC/50791-T1

(DE83011185)

Distribution Category UC-90d

DE83011185



A Technical Progress Report
for the Period of
September 1, 1982 to March 31, 1983.

FISCHER-TROPSCH SYNTHESIS FROM A LOW H₂:CO GAS
IN A DRY FLUIDIZED-BED SYSTEM

Y. A. Liu, Arthur M. Squires and Kenneth Konrad
Department of Chemical Engineering
Virginia Polytechnic Institute and State University
Blacksburg, Virginia 24061

Prepared for

U. S. Department of Energy
Pittsburgh Energy Technology Center
Grant No. DE-FG-82P50791
Project Manager: Dr. Sayeed Akhtar

ABSTRACT

The objective of this project is to experimentally develop and demonstrate a novel dry fluidized-bed reactor system (called "heat tray") for Fischer-Tropsch synthesis from a low $H_2:CO$ gas. The new reactor involves conducting catalytic synthesis reactions primarily in a horizontal conveying zone, in which fine particles of iron catalyst are carried in a relatively dilute suspension by a large flow of reacting gas. A secondary reaction zone, in the form of a shallow fluidized bed of catalyst particles, is situated beneath the primary reaction zone. This shallow bed also has immersed horizontal heat-transfer tubes for removing reaction heat. A major thrust of the new reactor development is to prevent carbon deposits from forming on the iron catalyst, which cause deactivation and physical degradation. This is to be achieved by conducting the Fischer-Tropsch synthesis in an unsteady-state mode, particularly by alternately exposing the iron catalyst to a large flow of low $H_2:CO$ gas for a short period of time and to a small flow of H_2 -rich gas for a long period of time.

During the past several months, the design, construction and steady-state testing of a fully-automated vibrofluidized microreactor system have been successfully completed, and a computer-controlled gas chromatographic (GC) system for gas product analysis has also been tied to the reactor system. Work on unsteady-state Fischer-Tropsch synthesis experiments is to be initiated shortly. In addition, supporting hydrodynamic and heat transfer studies in several shallow fluidized-bed systems have produced some encouraging data. The results indicate very high heat transfer coefficients of $300-400 \text{ W/m}^2\text{-}^\circ\text{K}$ between a shallow bed and its immersed horizontal heat-transfer tube, and of about $7,000 \text{ W/m}^2\text{-}^\circ\text{K}$ between a supernatant gas stream and a shallow bed which closely simulates the microreactor system in use.

ACKNOWLEDGEMENT

This project is supported by the U.S. Department of Energy, Pittsburgh Energy Technology Center (PETC), grant number DE-FG-82P50791, under the program on new and improved concepts in coal liquefaction. Dr. Sayeed Akhtar of PETC serves as the project manager. Partial project cost-sharing is provided by grants from the Exxon Educational Foundation and the Mobil Foundation. The continued interest and support in this project given by Drs. Barry L. Tarmy, Gerry C. Lahn, and Robert M. Koros, and Mr. W. Robert Epperly of the Exxon Research and Engineering Company, and by Drs. D. Duayne Whitehurst and Paul B. Weisz of the Mobil Research and Development Corporation, are gratefully acknowledged. Special appreciation is also extended to Messrs. John H. Boyd, Hao-Hsin Huang, Gary K. Whiting and Jyh-Shing Yang, chemical engineering graduate students at Virginia Tech, for their significant contributions to this project; and to Mrs. Jan Chance for her patient and competent typing of this report.

TABLE OF CONTENTS

	<u>Page</u>
ABSTRACT	i
ACKNOWLEDGEMENT	ii
1. PROJECT SCOPE AND STATUS	1
1.1 Technical Background: Basic Concepts of the Fischer-Tropsch Synthesis from a Low H ₂ :CO Gas in a Dry Fluidized-Bed System	1
1.2 Project Tasks and Current Status	3
2. TRANSIENT FISCHER-TROPSCH SYNTHESIS FROM A LOW H ₂ :CO GAS IN A VIBROFLUIDIZED MICROREACTOR SYSTEM	5
2.1 Relevant Literature	5
2.1.1 Modern Views of Fischer-Tropsch Synthesis Reaction Kinetics and Mechanisms	5
2.1.2 Transient Methods for Fischer-Tropsch Kinetics Studies	8
2.1.3 Catalyst Selection for Fischer-Tropsch Synthesis	10
2.1.4 Product Analysis in Fischer-Tropsch Synthesis	11
2.2 Experimental Systems	12
2.2.1 Vibrofluidized Microreactor System	12
2.2.2 Feeding and Pulsing Sequences of Reactant Gases	23
2.2.3 Analytical Method and System	32
2.3 Scope of Experimental Tests	34
2.4 Experimental Results and Discussion	37

	<u>Page</u>
3. SUPPORTING FLUIDIZATION STUDIES	44
3.1 Hydrodynamics in a Shallow Fluidized Bed	44
3.1.1 Introduction	44
3.1.2 Experimental System	48
3.1.3 Experimental Results and Discussion	48
3.2 Heat Transfer in a Shallow Fluidized Bed	53
3.2.1 Relevant Literature	53
3.2.2 Experimental System	62
3.2.3 Experimental Results and Discussion	62
3.3 Heat Transfer in a Heat Tray	78
3.3.1 Experimental System	78
3.3.2 Experimental Results and Discussion	83
4. LITERATURE CITED	87
5. APPENDICES	91
5.1 Safety Provisions of the Fischer-Tropsch Synthesis Microreactor System	91
5.1.1 Location of the Microreactor System	91
5.1.2 Ventilation of the Microreactor System	91
5.1.3 High Temperature and Pressure Precautions	95
5.1.4 Electrical System	95
5.1.5 Emergency Equipment	95
5.1.6 Emergency Shutdown Procedures	98
5.2 Related Literature on the Fischer-Tropsch Synthesis	100

	<u>Page</u>
5.3 Development of Working Equations for Measurements of Heat Transfer Coefficient Between Flowing Supernatant Gas and a Shallow Fluidized Bed in a Heat Tray	116
5.3.1 Heat Tray System Diagram and Simplifying Modeling Assumptions	116
5.3.2 Notations Used in Heat Transfer Model Development	116
5.3.3 The Upper Half or Freeboard Zone of the Heat Tray	121
5.3.4 The Lower Half or Fluidized-Bed Zone of the Heat Tray	123
5.3.5 The Working Equation for Measurements of Heat Transfer Coefficient Between a Flowing Supernatant Gas and a Shallow Fluidized Bed in a Heat Tray	125

LIST OF FIGURES

	<u>Page</u>
1.1 A Simplified Schematic Diagram of a New Dry Fluidized-Bed System ("Heat Tray") for Fischer-Tropsch Synthesis for a Low $H_2:CO$ Gas	2
2.1 A Schematic Diagram of Fischer-Tropsch Synthesis Kinetics: S=Active Site on Catalyst Surface	6
2.2 Equipment Symbols Used in Figures of Experimental Systems	13
2.3 The Vibrofluidized Microreactor System for Unsteady-State Fischer-Tropsch Studies	14
2.4 A Stainless-Steel Vibrofluidized Microreactor for Fischer-Tropsch Kinetics Studies (A Side View)	15
2.5 Key Components of the Vibrofluidized Microreactor for Fischer-Tropsch Kinetics Studies	16
2.6 The Plenum Zone of the Vibrofluidized Microreactor	18
2.7 The Reaction Zone of the Vibrofluidized Microreactor	19
2.8 The Freeboard Zone of the Vibrofluidized Microreactor	20
2.9 Product Gas Exit Zone of the Vibrofluidized Microreactor	21
2.10 A Schematic Diagram of the Leaf-Spring Suspension System for the Vibrofluidized Microreactor	22
2.11 A Cold Model of the Reaction Zone in the Vibrofluidized Reactor	24
2.12 High Flow Rate (e.g., $2,500 \text{ mm}^3/\text{sec}$) of S-Gas Feed through Valve E for a Short Duration (e.g., 2 sec)	25
2.13 Plenum Purge of S-Gas by High Flow Rate (e.g., $11,950 \text{ mm}^3/\text{cc}$) of F-Gas through Valves A, B, and C for a Very Short Duration (e.g., 0.1 sec)	26

	<u>Page</u>
2.14 Reaction Zone Purge by Relatively High Flow Rate (e.g., 250 mm ³ /sec) of F-Gas through Valves B and C for a Short Duration (e.g., 1 sec)	27
2.15 Low Flow Rate (e.g., 14.7 mm ³ /sec) of F-Gas Feed into the Reaction Zone through Valve C for a Long Duration (e.g., 17 sec)	28
2.16 Plenum Purge of F-Gas by High Flow Rate (e.g., 11,500 mm ³ /sec) of S-Gas through Valves D and E for a Very Short Duration (e.g., 0.1 sec)	29
2.17 Flow Rates and Feeding/Purging Times of Both F-Gas and S-Gas in an Initial Unsteady-State Fischer-Tropsch Kinetics Experiment	30
2.18 A Schematic Diagram of the On-Line GC Analytical System for Gas Products in the Sample Mode	33
2.19 A Schematic Diagram of the On-Line GC Analytical System for Gas Products in the Backflush Mode	35
2.20 The Vibrofluidized Microreactor System for Unsteady-State Fischer-Tropsch Synthesis	38
2.21 A Computer-Controlled On-Line Gas Chromatographic System for Product Analysis	39
2.22 Isothermal Chromatogram of Reactor Feed	41
2.23 Isothermal Chromatogram of Light Gas Products of Fischer-Tropsch Synthesis at 315°C and 28 atm	42
3.1 Three Flow Regimes in a Shallow Fluidized Bed	46
3.2 The Experimental System for Pressure Drop Measurements in a Shallow Fluidized Bed	49
3.3 A Photograph of the Experimental System for Shallow Fluidized-Bed Hydrodynamic and Heat-Transfer Studies	50
3.4 (a) The Bed Pressure Drop in a Shallow Fluidized Bed of Spherical Alumina Particles (-12+20 Mesh)	54
(b) The Bed Pressure Drop in a Shallow Fluidized Bed of Spherical Alumina Particles (-12+20 Mesh)	55
(c) The Bed Pressure Drop in a Shallow Fluidized Bed of Spherical Alumina Particles (-12+20 Mesh)	56

	<u>Page</u>
3.5 (a) The Bed Pressure Drop in a Shallow Fluidized Bed of Spherical Alumina Particles (-20+40 Mesh)	57
(b) The Bed Pressure Drop in a Shallow Fluidized Bed of Spherical Alumina Particles (-20+40 Mesh)	58
(c) The Bed Pressure Drop in a Shallow Fluidized Bed of Spherical Alumina Particles (-20+40 Mesh)	59
3.6 A Schematic Diagram of the Experimental System for Shallow-Bed Heat Transfer Studies	63
3.7 (a) Minimum Fluidization Velocity of -40+60 Mesh Alumina Particles (Mean Particle Diameter = 310 μm)	65
(b) Minimum Fluidization Velocities of -10+20 Mesh Alumina Particles (Mean Particle Diameter = 610 μm)	66
(c) Minimum Fluidization Velocity of -12+20 Mesh Alumina Particles (Mean Particle Diameter = 1,100 μm)	67
3.8 (a) Effect of Superficial Gas Velocity on the Bed-to-Surface Heat Transfer Coefficient in a Shallow Fluidized Bed of -40+60 Mesh Alumina Particles with a Laminated Distributor Plate	68
(b) Effect of Superficial Gas Velocity on the Bed-to-Surface Heat Transfer Coefficient in a Shallow Fluidized Bed of -40+60 Mesh Alumina Particles with a Perforated Distributor Plate	69
3.9 (a) Effect of Static Bed Height on the Bed-to-Surface Heat Transfer Coefficient in a Shallow Fluidized Bed of -40+60 Mesh Alumina Particles with a Perforated Distributor Plate	71
(b) Effect of Static Bed Height on the Bed-to-Surface Heat Transfer Coefficient in a Shallow Fluidized Bed of -40+60 Mesh Alumina Particles with a Laminated Distributor Plate	72
3.10 (a) Effect of Heat-Transfer Tube Elevation on the Bed-to-Surface Heat Transfer Coefficient in a Shallow Fluidized Bed of -40+60 Mesh Alumina Particles with a Laminated Distributor Plate and at a Static Bed Height of 20 mm	73

(b) Effect of Heat-Transfer Tube Elevation on the Bed-to-Surface Heat Transfer Coefficient in a Shallow Fluidized Bed of -40+60 Mesh Alumina Particles with a Laminated Plate and at Superficial Gas Velocity of 0.67 m/s	74
(c) Effect of Heat-Transfer Tube Elevation on the Bed-to-Surface Heat Transfer Coefficient in a Shallow Fluidized Bed of -40+60 Mesh Alumina Particles with a Perforated Distributor Plate and at a Superficial Gas Velocity of 0.67 m/s	75
3.11 Effects of Particle Size and Distributor Type on the Bed-to Surface Heat Transfer Coefficient in Shallow Fluidized Beds of Alumina Particles at Different Superficial Gas Velocities	77
3.12 A Schematic Diagram of the Heat Tray System	79
3.13 A Photograph of the Heat Tray System	80
3.14 (a) A Front View of the Heat Tray	81
(b) A Side View of the Heat Tray	82
3.15 Effect of Ratio of F-Gas to S-Gas Mass Flow Rates on the Heat Transfer Coefficient Between a Flowing S-Gas Stream and a Shallow Fluidized Bed of -40+60 Mesh Norton Masterbeads at Different S-Gas Exit Nozzle Openings	85
3.16 Effect of S-Gas Inlet Velocity on the Heat Transfer Coefficient Between a Flowing S-Gas Stream and a Shallow Fluidized Bed of -40+60 Mesh Norton Masterbeads	86
5.1 A Schematic of the Location of the Fischer-Tropsch Synthesis Microreactor System ("Reactor Lab")	92
5.2 A Schematic Diagram of the Control Volume for Mass and Energy Balances for the Heat Tray	117
5.3 A Schematic Diagram of the Control Volume for Mass and Energy Balances for the Upper Half (Freeboard) of the Heat Tray	118
5.4 A Schematic Diagram of the Control Volume for Mass and Energy Balances for the Lower Half (Fluidized Bed) of the Heat Tray	119

LIST OF TABLES

	<u>Page</u>
2.1 Design Features of Key Zones of the Vibrofluidized Microreactor	17
2.2 Volumetric Flow Rates and Feeding/Pulsing Times for Needle Valves A to E in the Initial Operational Sequences Illustrated in Figures 2.12 to 2.16	31
2.3 Conditions for Initial Steady-State Synthesis Experiments with H ₂ :CO and H ₂	40
3.1 A Comparison of Key Features of Deep and Shallow Fluidized Beds	45
3.2 Relationships Between the Pressure Drop Across the Orifice Meter (ΔP_0) and Volumetric Flow Rate (V) and Superficial Velocity (u) of the Air Stream in the Shallow Fluidized Bed	51
3.3 Range of Experimental Variables and Conditions in Initial Pressure Drop Measurements Across a Shallow Fluidized Bed	52
3.4 A Summary of Representative Investigations on Heat Transfer from Shallow Fluidized Beds to Immersed Heat-Transfer Surface	60
3.5 Range of Experimental Variables and Conditions in Initial Bed-to-Surface Heat Transfer Measurements in a Shallow Fluidized Bed	64
3.6 Range of Experimental Variables and Conditions in Initial Measurements of Heat Transfer Coefficient Between a Flowing Supernatant Gas (S-Gas) Stream and a Shallow Fluidized Bed	84
5.1 Estimates of Microreactor System Volumes and Room Air Renewal Rates	94
5.2 Upper Limits of Operating Temperatures and Pressure for Different Components of the Vibrofluidized Microreactor System	96

1. PROJECT SCOPE AND STATUS

1.1 Technical Background: Basic Concepts of the Fischer-Tropsch Synthesis from a Low H₂:CO Gas in a Dry Fluidized-Bed System

Figure 1.1 shows a simplified schematic diagram of a new dry fluidized-bed reactor system (called "heat tray") for Fischer-Tropsch synthesis from a low H₂:CO gas. There are two gas feeds to the system. The first feed is a H₂-rich fluidizing gas (F-gas) furnished at a low flow rate (e.g., 0.05-0.1 m/s) to a shallow fluidized bed (about 5 to 10 cm in depth) of fine particles of iron catalyst. The second feed is a low H₂:CO supernatant gas (S-gas) provided at a far higher flow rate (e.g., 1.5-3.0 m/s) to the supernatant space (freeboard zone) above the shallow bed. In the new reactor system, the supernatant space serves as the primary reaction zone, in which fine particles of iron catalyst are carried in a relatively dilute suspension by a large flow of reacting gas of low H₂:CO ratio, and most catalytic reaction occurs. The shallow fluidized bed of fine particles of iron catalyst serves as a secondary reaction zone, in which further catalytic reactions take place. This shallow bed also has immersed horizontal heat-transfer tubes in order to take advantage of the excellent bed-to-surface heat transfer rates observed in shallow beds (see, for example, Ali and Broughton, 1977) for removing reaction heat.

A major thrust of the new reactor development is to prevent carbon deposits from forming on the iron catalyst which cause deactivation and physical degradation. This is to be achieved by conducting the Fischer-Tropsch synthesis in an unsteady-state mode, particularly by alternately exposing the iron catalyst to a large flow of low H₂:CO gas (S-gas) for a short period of time and to a smaller flow of H₂-rich gas (F-gas) for a long period of time. This approach is based, in part, on an important experimental observation known by industrial practitioners for Fischer-Tropsch synthesis for many years that the carbon deposition rate on an iron catalyst can be minimized by increasing the hydrogen partial pressure (Day, 1980; Squires, 1982). It is hoped that the relatively long residence-time of an iron catalyst particle within the shallow bed fluidized by a H₂-rich gas will prevent production of carbon deposits on the particle.

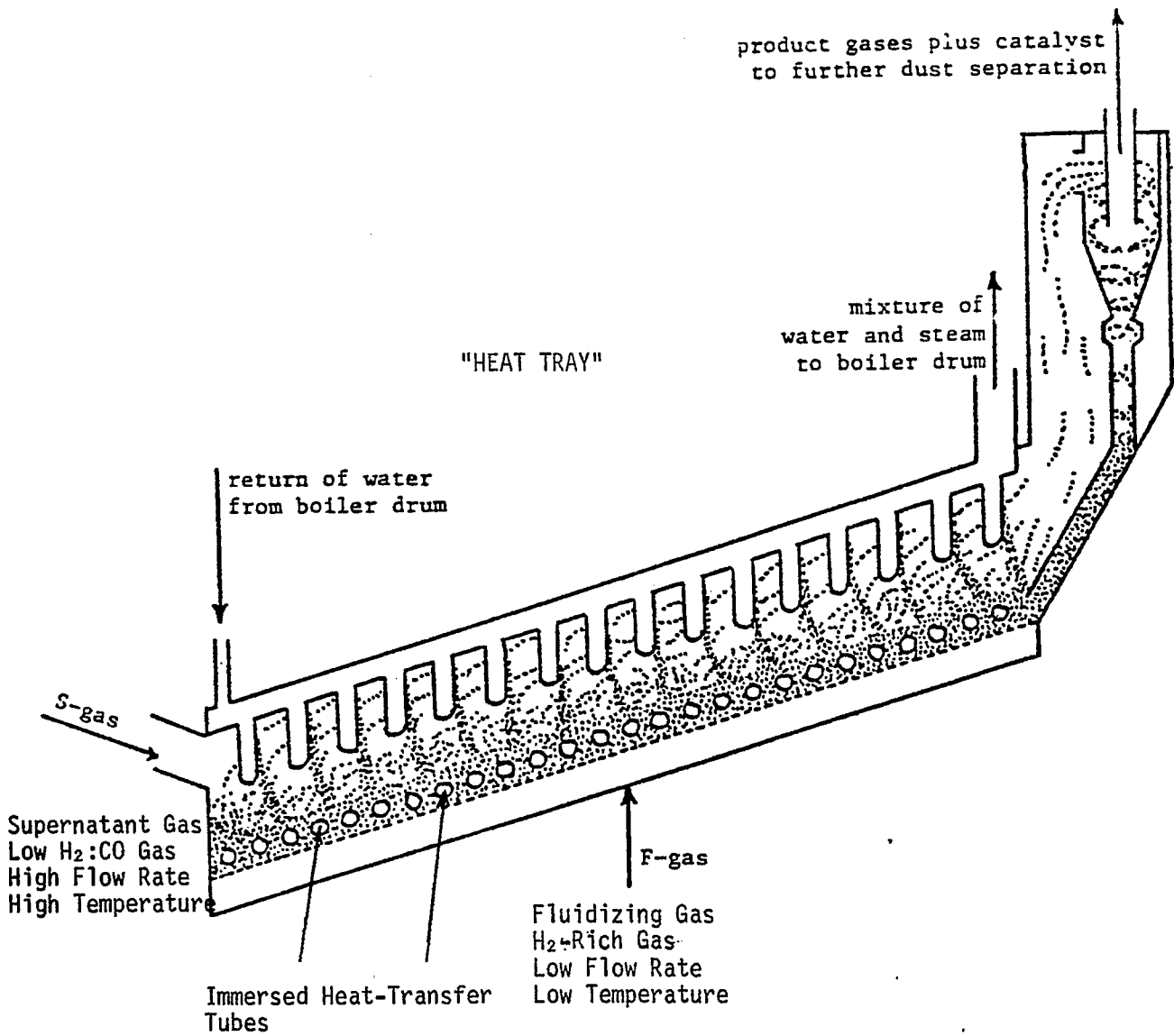


Figure 1.1 A Simplified Schematic Diagram of a New Dry Fluidized-Bed System ("Heat Tray") for Fischer-Tropsch Synthesis from a Low H₂:CO Gas.

1.2 Project Tasks and Current Status

The specific tasks of this research include the following:

A. Studies of unsteady-state Fischer-Tropsch synthesis kinetics in a vibrofluidized microreactor simulating the life history of an iron catalyst particle in the proposed reactor (Figure 1.1), i.e., alternating back and forth between a brief exposure to a large flow of low H₂:CO S-gas and a longer exposure to a small flow of H₂-rich F-gas.

B. Supporting fluidization studies, including:

(1) studies of hydrodynamics in a shallow fluidized bed and of the rate of exchange of particles between a shallow fluidized bed and a horizontal flow of supernatant gas above the bed;

(2) studies of heat transfer from a shallow fluidized bed to immersed heat-transfer tubes within the bed;

(3) studies of heat transfer from a flowing supernatant gas to a shallow fluidized bed.

The key accomplishments of the project thus far may be summarized as follows.

(1) A fully-automated vibrofluidized microreactor system has been successfully designed, constructed and tested. Safety provisions for the operation of the reactor system have been thoroughly investigated and established. A computer-controlled on-line gas chromatographic (GC) system for product analysis has also been tied to the reactor system. Both the reactor and GC systems have performed very well in initial steady-state Fischer-Tropsch synthesis experiments with H₂:CO and H₂ gases over an iron catalyst. Unsteady-state Fischer-Tropsch synthesis experiments are to be initiated shortly with detailed catalyst composition analysis and temperature-programmed GC analysis of all gas products (see Sections 2 and 5.1).

(2) An experimental system has been designed and constructed for studies of hydrodynamics and heat transfer characteristics in a shallow fluidized bed. Experiments have been conducted for measurements of the pressure drop across the shallow bed and of the heat transfer from the bed to its immersed heat-transfer tube. The results show a relatively high bed-to-surface heat transfer coefficient of 300 to 400 W/m²-°K, and demonstrate a significant effect of distributor type on both bed pressure drop and heat transfer coefficient in a shallow bed (see Sections 3.1 and 3.2).

(3) A heat tray system has been designed and constructed for measurements of heat transfer coefficient between a flowing supernatant gas and a shallow fluidized bed. Available experimental results have indicated very high heat transfer coefficients of about $1,240 \text{ Btu/hr-ft}^2\text{-}^\circ\text{F}$ ($7,040 \text{ W/m}^2\text{-}^\circ\text{K}$). This high rate of heat transfer has provided encouraging support of the new fluidized-reactor concept for Fischer-Tropsch synthesis, particularly in the use of immersed heat-transfer surface for recovering reaction heat in a shallow bed (see Sections 3.3 and 5.3).

2. TRANSIENT FISCHER-TROPSCH SYNTHESIS FROM A LOW $H_2:CO$ GAS IN A VIBROFLUIDIZED MICROREACTOR SYSTEM

2.1 Relevant Literature

2.1.1 Modern Views of Fischer-Tropsch Reaction Kinetics and Mechanisms

Research conducted during the past few years has provided many new insights to the kinetics and mechanisms of Fischer-Tropsch synthesis since the early reviews by Storch, et al. (1951) and Pichler (1952). In particular, a number of papers and reviews have been published which describe proposed mechanisms along with their supporting evidence for Fischer-Tropsch synthesis over Group VIII catalysts. Notable are those by Bell (1981), Biloen (1979), Biloen, et al. (1979), Brady (1981), Deluzarche, et al. (1981), Eidus (1967), Henrici-Olive and Olive (1976), Muetterties and Stein (1979), Ponce (1978), Rofer-DePoorter (1981), Schulz and Zeweldeen (1977), and Vannice (1976). The modern views of the Fischer-Tropsch synthesis kinetics and mechanisms described in these publications have set the stage for the current project, and it is worthwhile to briefly summarize them below. A short version of this summary appears in Squires (1982).

Figure 2.1 shows a schematic diagram of Fischer-Tropsch reaction kinetics over iron catalysts. Reaction equations 1 through 12 are after Bell (1981), and equation 13 has been added to the list to indicate the unwanted reactions converting the surface carbon to unreactive forms, here represented by C_n . Essentially, Fischer-Tropsch reaction kinetics over iron catalysts involve the following steps.

(1) Adsorptions of CO and H_2 on active sites on an iron catalyst and the subsequent dissociations into adsorbed atoms of C and O , and into adsorbed atoms of H , respectively (reaction equations 1 through 3).

(2) Removal of adsorbed atoms of O by reaction with H_2 or CO to form H_2O or CO_2 , respectively (reaction equations 4a and 4b).

(3) Competition among reactions of

(i) adding an adsorbed atom of H to an adsorbed atom of C to form adsorbed CH (reaction equation 5);

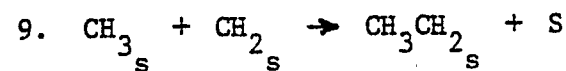
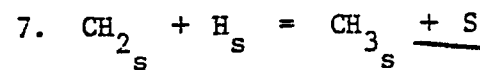
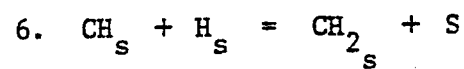
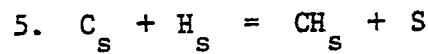
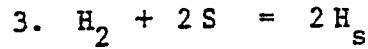
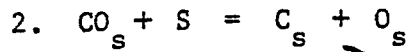
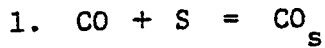
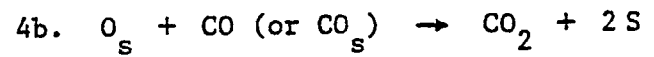
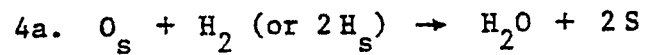
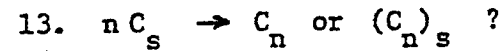
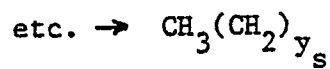
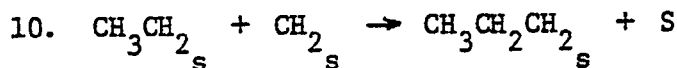
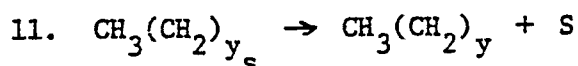
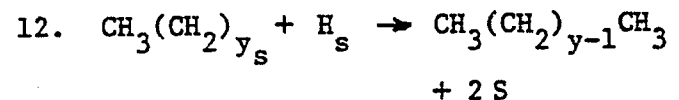
I. Initiation of hydrocarbon chainV. Removal of adsorbed oxygenVI. "Sintering" of surface carbonVII. Production of methaneII. Propagation of chainIII. Chain termination with formation of an olefinIV. Chain termination with formation of saturate

Figure 2.1. A Schematic Diagram of Fischer-Tropsch Synthesis Kinetics (Bell, 1981): S=Active Site on Catalyst Surface; Subscript "s" Denotes an Adsorbed Species.

(ii) "sintering" of an adsorbed atom of C to an unreactive form of carbon (unwanted reaction equation 13);

(iii) formation of iron carbides through diffusion of adsorbed atoms of C into the interiors of iron catalyst particles (unavoidable; not represented in Figure 2.1).

(4) Further reactions of adsorbed CH groups with adsorbed atoms of H to yield adsorbed groups of CH₂ and CH₃ (reaction equations 6 and 7).

(5) Competition between reactions of

(i) adding an adsorbed atom of H to an adsorbed CH₃ group to yield CH₄ gas (unwanted; reaction equation 8);

(ii) Insertion of an adsorbed CH₂ group to an adsorbed CH₃ group to yield an adsorbed CH₃CH₂ group, and thereby initiating a hydrocarbon chain (reaction equations 9 and 10).

(6) Competition between chain termination reactions with

(i) formation of an olefin, CH₃(CH₂)_y (reaction equation 11);

(ii) formation of a saturated hydrocarbon, CH₃(CH₂)_{y-1}CH₃ (reaction equation 12).

Results from recent research have provided some evidence which supports the above reaction steps. This research was done in a number of laboratories, many in mutual communication; and it is difficult to construct a precise order of discovery of seminal facts and ideas. Wentrcek, et al. (1976) have experimentally demonstrated the dissociation of CO on the surface of a nickel methanation catalyst, with subsequent addition of hydrogen to an adsorbed carbon atom. McCarty and Wise (1979) and McCarty, et al. (1981) have shown not only the great initial reactivity of adsorbed atoms of carbon toward hydrogen and steam, but also their tendency to react to form a number of progressively less active forms of carbon. Niemantsverdriet and van der Kraan (1981) have brought into this picture the further competition for carbon by reactions which carry it within the interior of an iron catalyst particle to form iron carbide. Dautzenberg et al. (1977), seemingly unaware of Wentrcek, et al.'s demonstration of the role of surface carbon atoms (1976), have data for kinetics of hydrocarbon chain growth which were not marred by their apparent lack of understanding of the mechanism for hydrocarbon chain initiation.

Dry (1980) has presented an experimental correlation between the carbon deposition rate on an iron catalyst and the ratio $p_{CO}/p_{H_2}^2$, where p_{CO} and p_{H_2} are partial pressure of H_2 and CO , respectively. This correlation confirms what was known by industrial practitioners for Fischer-Tropsch synthesis some 35 years ago about the role of hydrogen in limiting the lifetime of adsorbed atoms and in preventing their "consolidation" or "sintering" into less reactive atomic configuration, as described by Squires (1982). This correlation also suggests that the rate of carbon deposition depends strongly on the hydrogen partial pressure, p_{H_2} , while it does not depend on the carbon monoxide partial pressure, p_{CO} , nearly as much. Based on this observation, it is hopeful that the new fluidized bed reactor concept being explored in the current project, shown in Figure 1.1, in which the iron catalysts in the fluidized bed spend most of their residence times in a hydrogen-rich atmosphere, will minimize the production of carbon deposits on catalyst particles. It is also expected that the relatively long residence times of iron catalysts in the hydrogen-rich atmosphere in the new fluidized bed reactor will limit the concentration of the adsorbed carbon atom, C_s , and thus suppress the unwanted "sintering" of adsorbed carbon atoms (reaction step 13 in Figure 2.1). This long residence time in hydrogen should tend to favor the hydrocarbon chain termination reactions (reaction steps 11 and 12 in Figure 2.1), over reaction step 13; and it would decrease the oxidation of iron catalysts. Further, it is believed that there should be a sufficient residence time (although relatively short) in the atmosphere of low $H_2:CO$ ratio in the freeboard region (i.e., the supernatant zone) of the new fluidized-bed reactor to foster the initiation of hydrocarbon chains (reaction steps 1 to 3, and 5 to 9, in Figure 2.1).

2.1.2 Transient Methods for Fischer-Tropsch Kinetics Studies

Transient methods for kinetics studies typically involve sending an input signal, such as a pulsed amount of reactant gases, into a reactor and then observing the time-dependent changes of certain reaction variables, such as reaction temperatures and species concentration. In order for the transient response to truly reflect the kinetics of the reaction being investigated, the reactor must be operated under conditions that it is free of heat- and mass-transfer limitations. A recent monograph edited by Bell and Hegedus (1982) includes many articles on catalysis under transient conditions; and two review papers by Bennett (1976 and 1982) describe in some detail the basic theory and application of transient methods in heterogeneous catalysis.

Transient methods have been used to identify the reaction intermediates and rate-limiting steps in Fischer-Tropsch synthesis. For example, Matsumoto and Bennett (1978) and Reymond, et al. (1980) applied the transient method to study the kinetics of the reduction of carbon monoxide with hydrogen to methane using a fused, promoted catalyst in a tubular reactor at 250°C and atmospheric pressure. When a stream of the reaction mixture (H₂:CO=9:1) flowing over the catalyst in a steady state was suddenly changed to pure hydrogen; the surface of the catalyst was found to be covered mostly by a carbon intermediate and the bulk of the catalyst was identified to be Hägg carbide, Fe₂C. The rate-determining step was found to be the hydrogenation of the surface carbon. Dautzenberg, et al. (1977) investigated the transient kinetics of Fischer-Tropsch synthesis of paraffins from an equimolar mixture of H₂ and CO. A plug-flow reactor was used along with Ru/γ-A₂O₃ catalysts to study the rate constants of the propagation reaction of hydrocarbon chains. Under transient operating conditions, it was found that the overall activity of these catalysts was very low. The latter observation was thought to be caused by the very low intrinsic activity of the exposed Ru atoms and not by the low number of active surface atoms. In a later transient kinetics study, Kieffer, et al. (1982) suggested that the rate of propagation of hydrocarbon chains could not be the rate-determining step of the Fischer-Tropsch synthesis. This study was done in a microreactor packed with precipitated iron-zinc catalysts at 277°C and 2.5 atm.

Transient methods have also been used to increase the yield of a particular product by influencing the selectivity to that product. For example, in the paper on the Fischer-Tropsch synthesis of paraffins from H₂ and CO by Dautzenberg, et al. (1977) cited previously, it was shown that transient operating conditions could be manipulated to limit production of species of high molecular weight. Also, a number of examples of improved product yields resulted from transient kinetics studies that have been cited by Bennett (1982). Recently, Feimer, et al. (1982) studied the effect of forced cycling of feed H₂ and CO concentrations over a precipitated, copper-potassium promoted iron catalyst in a fixed-bed reactor at 246°C and 3.8 atm. Differential conversions were measured using pulsed amounts of hydrogen-rich and hydrogen-poor mixtures of H₂ and CO for different time periods varying from 1 to 30 minutes and various cycle split-ratios. Steady-state measurements were also undertaken to supplement the cycling studies. The results showed that under rapid cycling with one cycle containing pure hydrogen, methane was produced at a rate 80% higher than the corresponding reactions at steady-state conditions. This was taken as evidence that methane was produced in at least two parallel reactions, while the higher hydrocarbons (C₂ to C₉) were produced sequentially. The results also indicated

that a decrease in the time period between hydrogen-rich and hydrogen-poor pulses increased the time-averaged production rates of the higher hydrocarbons. Although the production rates were smaller than those observed at steady-state conditions. These investigators thus suggested that under their experimental conditions, no significant improvement in rate or selectivity to liquid hydrocarbons could be achieved with transient operations compared to steady-state conditions. A major objective of the current project is to demonstrate how transient operations in a dry fluidized-bed system can optimize the product yield and selectivity and minimize the production of carbon deposits on catalysts.

An objective of the present study is to investigate if cycling of the feed gases between high and low $H_2:CO$ ratios would decrease both catalyst oxidation and carbon deposition. For this purpose, a non-nitrided fused iron catalyst promoted with potassium is chosen for initial studies. This catalyst is prepared by the United Catalyst, Inc., catalog number C73-1-01, with the following compositions: 30-37% FeO, 65-68% Fe_2O_3 , 2-3% Al_2O_3 , 0.5-0.8% K_2O and 0.7-1.2% CaO. Other iron catalysts may be tested as the experiments progress.

2.1.3 Catalyst Selection for Fischer-Tropsch Synthesis

Since the inception of the Fischer-Tropsch synthesis, extensive research has been conducted on the catalysis for the reaction between H_2 and CO over Group VIII metals. In an important paper, Vannice (1975) reported the specific activities and product distribution of all the Group VIII metals except osmium (Os). Based on his results, the effectiveness of different metal catalysts for the methanation reaction ranked in a decreasing order of specific activity was identified as: ruthenium (Ru), iron (Fe), nickel (Ni), cobalt (Co), rhodium (Rh), palladium (Pd) and iridium (Ir). This ranking was different from similar comparisons in older studies which had not taken into account the variations in metal surface area.

Because iron catalysts are much less expensive than ruthenium catalysts, and also less expensive than nickel and cobalt catalysts, nearly all commercial processes have used iron catalysts. For those processes utilizing fluidized-bed reactors, catalysts with greater mechanical strength, such as fused iron catalysts, are often used (Storch, 1951). Iron catalysts generally have high specific activities. However, these catalysts tend to promote the formation of iron oxides and carbides, leading to changes in product selectivity (Storch, 1951).

Both the lifetime and activities of iron catalysts have been found to increase with increasing pressure up to 30 atmospheres in the Fischer-Tropsch synthesis experiments by Shah and Perrotta (1976). The use of alkaline promoters has been shown to cause a decrease in the rate of methane formation, an increase in the rate of carbon deposition, and a shift in selectivity towards the formation of longer-chain molecules (Bonzel and Krebs, 1981). By contrast, the use of nitrided iron catalysts has been found to increase the rate of methane formation, decrease the rate of carbon deposition and shift the selectivity towards the formation of lower-molecular-weight compounds (particularly alcohols) (Bonzel and Krebs, 1981).

2.1.4 Product Analysis in Fischer-Tropsch Synthesis

Many different techniques have been developed for analyzing the products of the Fischer-Tropsch synthesis. Most of the earlier techniques involved condensation of high-boiling components and subsequent chromatographic separations. Stockinger (1977) has developed an on-line gas chromatographic (GC) system for the quantitative analysis of gaseous products obtained from the Mobil process for catalytic conversion of methanol to gasoline.

The system involves two sample injection valves. One valve is followed by a packed column and a thermal conductivity detector for analyzing light gases, including CO, CO₂ and CH₄. The other valve is connected to a capillary column and a flame ionization detector for analyzing C₁ to C₆ hydrocarbons. Both columns are placed inside a temperature-programmed oven, in which the temperature is varied from sub-ambient (-70°C) to 100°C in order to obtain good peak resolutions.

An improved version of Stockinger's on-line GC technique for analyzing the products from a Fischer-Tropsch reactor has been developed recently by Nijs and Jacobs (1981). The two-detector and two-column setup used by Stockinger is retained, but the entire product stream is analyzed instead of just analyzing the gaseous products. This is done by keeping the Fischer-Tropsch synthesis products in the gaseous phase by holding them at the reaction temperature (about 200°C) until they are automatically injected into the GC column. Argon is used as an internal standard in order that an accurate carbon mass balance in the reactor system can be made. This technique has been used to successfully identify nearly 120 compounds. Ar, CO, CO₂ and CH₄ are separated on the packed column in less than 10 minutes, while the separation of hydrocarbons takes about two hours.

A very recent report by Diffenbach, et al. (1982) has also described the use of the two-detector and two-column technique for identifying the Fischer-Tropsch synthesis products. The product stream is kept at the reaction temperature in a manner similar to that adopted by Nijs and Jacobs (1981), but no internal standard is used to aid in making the carbon balance.

In this investigation, the on-line GC technique of Nijs and Jacobs (1981) will be adopted for product analysis.

2.2 Experimental Systems

2.2.1 Vibrofluidized Microreactor System

Figure 2.2 summarizes the equipment symbols used in figures of experimental systems described in this Section.

Figure 2.3 shows a schematic diagram of a vibrofluidized microreactor system for unsteady-state Fischer-Tropsch kinetics studies. The system includes four gas reservoirs labelled P_1 (two), P_2 and P_3 , and eight solenoid valves numbered 1 to 8 for use in cycling different feed gas streams (H_2 and H_2 -CO-Ar or N_2 and N_2 -He). Six needle valves labelled A to F are provided to set the desired flow rates with the aid of two Brooks thermal mass flow meters, as indicated by FT. System pressures near gas reservoirs P_2 and P_3 are monitored using Schaevitz Engineering pressure transducers of strain-gage type, as depicted by PIT, in conjunction with an Analog Devices digital panel meter. A back-pressure relief valve is also used to regulate the system pressure with the aid of a nitrogen gas stream.

The design features of the vibrofluidized microreactor are illustrated in Figures 2.4 and 2.5. Figure 2.4 gives a side view of the microreactor, and Figure 2.5 shows different components of the microreactor. As shown, the microreactor consists of four primary zones: (1) "plenum" zone, (2) reaction zone, (3) freeboard zone, and (4) product gas exit zone. The specific design features of these zones are summarized in Table 2.1 and illustrated in Figures 2.6 to 2.9.

The microreactor is suspended in a Techne fluidized constant-temperature bath using a leaf-spring suspension system as shown in Figure 2.10. A Ling Dynamic Systems vibration generator is suspended above the bed in order to impart the desired vibratory motion to the microreactor through the suspension system. The catalyst bed contained in the microreactor is fluidized by vibrations rather than by the energy imparted by

LEGEND




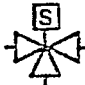


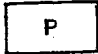





	Two - way Valve	O ₁	Valve Oven
	Needle Valve	O ₂	G.C. Oven
	Solenoid Valve	P	F-T Products
	Three-way Solenoid	V ₁	6-Port Sample Valve
	Check Valve	V ₂	10 - Port Sample Valve
	Pressure Relief Valve	S ₁	0.03 ml Sample Loop
	Gas Reservoir	S ₂	0.2 ml Sample Loop
	Flow Transducer	C ₁	Capillary Column
	Pressure Element	C ₂	Packed Column
	Analysis Point (G.C.)	INT	Reporting Integrator
	Microreactor	FID	Flame Ionization Detector
	Flexible S.S. Hose	TCD	Thermal Conductivity Detector

Figure 2.2. Equipment Symbols Used in Figures of Experimental Systems.

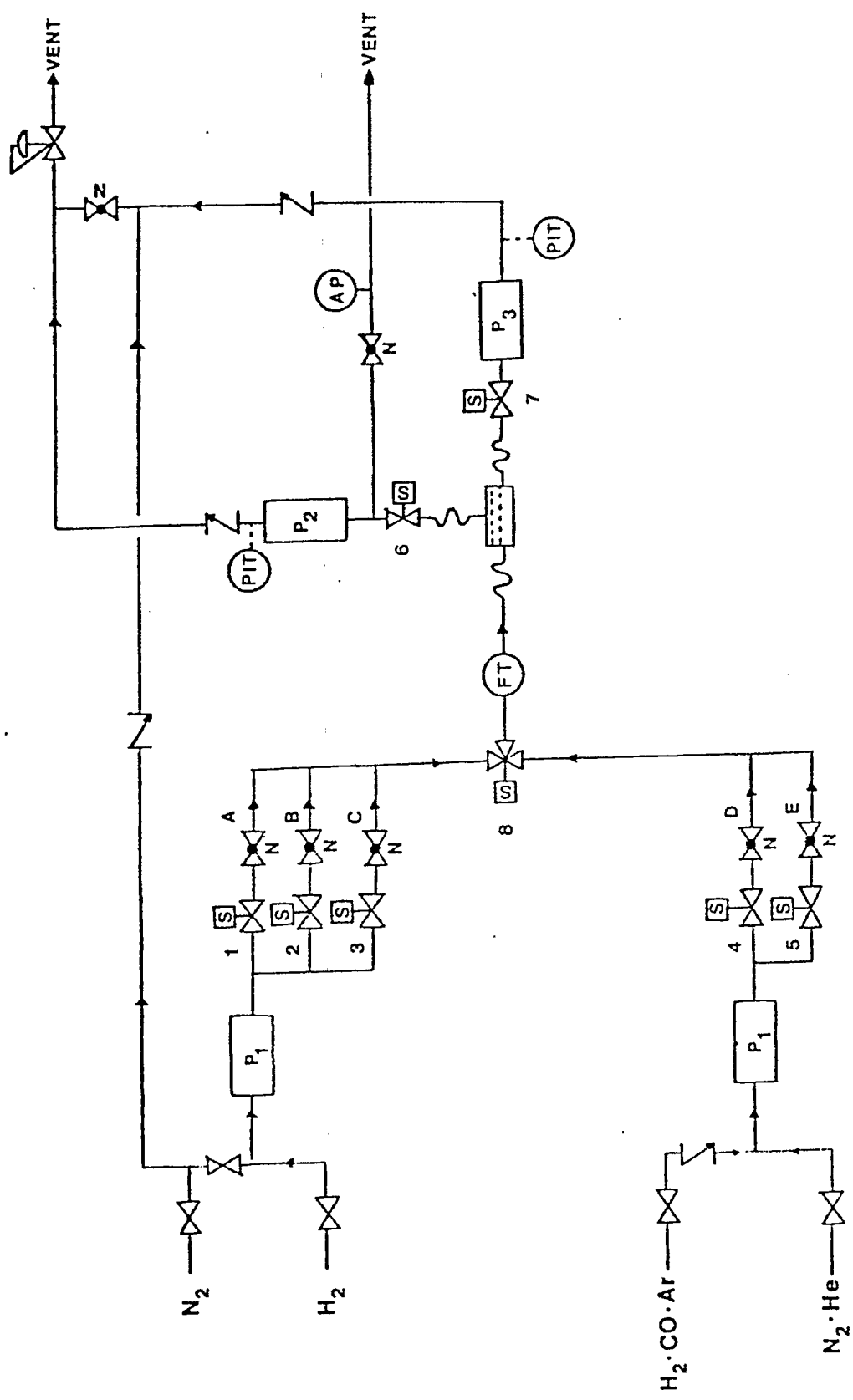


Figure 2.3. The Vibrofluidized Microreactor System for Unsteady-State Fischer-Tropsch Studies.

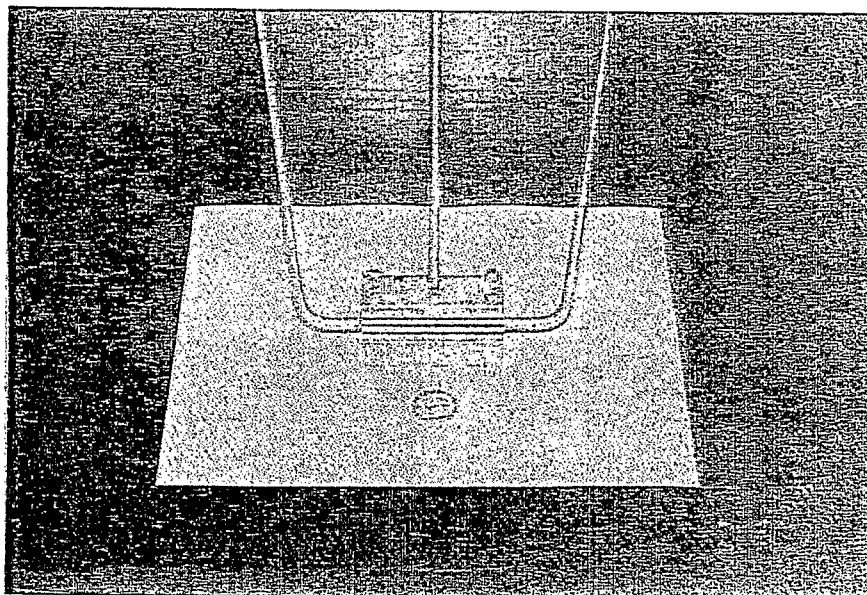


Figure 2.4. A Stainless-Steel Vibrofluidized Microreactor for Fischer-Tropsch Kinetics Studies (A side view).

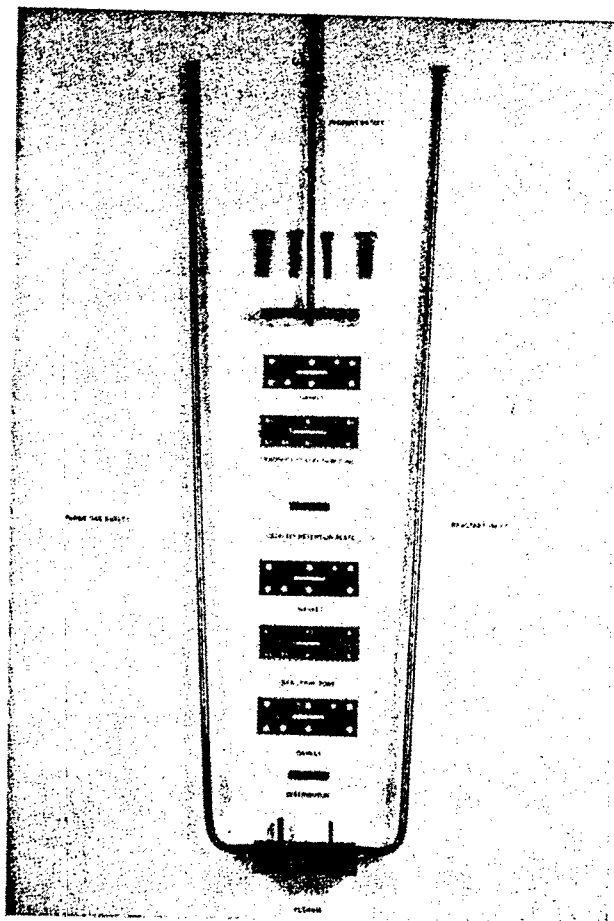


Figure 2.5. Key Components of the Vibrofluidized Microreactor for Fischer-Tropsch Kinetics Studies.

Table 2.1

Design Features of Key Zones of the Vibrofluidized Microreactor

Reactor Zone	Design Features	Figure Number
1. Plenum Zone	A 5.46-mm I.D. tube into which a 2.54x2.54 mm slot has been milled along with a recessed support for sintered stainless-steel distributor plate.	Figure 2.6
2. Reaction Zone	A 2.54 mm x 2.54 mm x 4.70 mm slot with rounded ends. An 0.08 mm O.D. thermocouple extends into this zone.	Figure 2.7
3. Freeboard Zone	A 2.54 mm x 2.54 mm x 4.70 mm slot with a recessed portion to accommodate a sintered stainless-steel catalyst retention plate.	Figure 2.8
4. Product Gas Exit Zone	A 5.46 mm I.D. exit hole and tube.	Figure 2.9

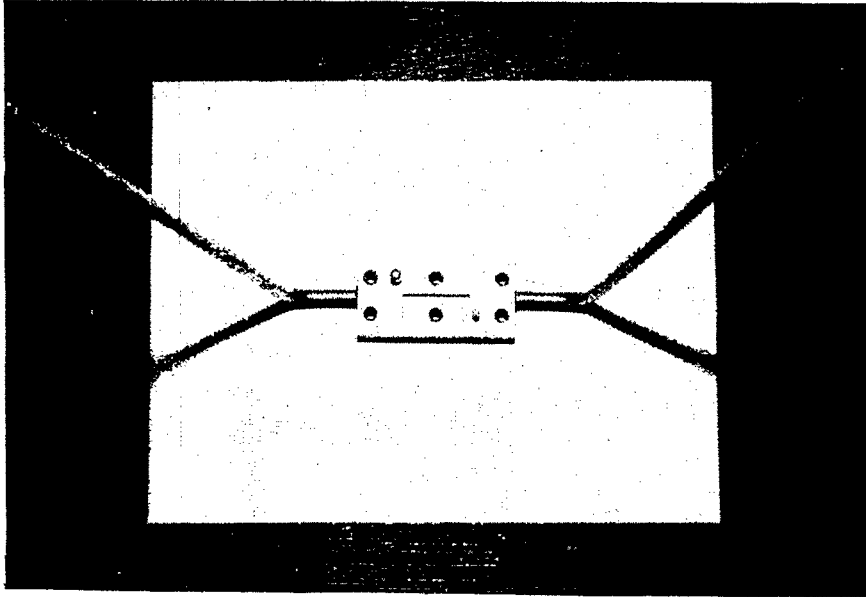


Figure 2.6. The Plenum Zone of the Vibrofluidized Microreactor.

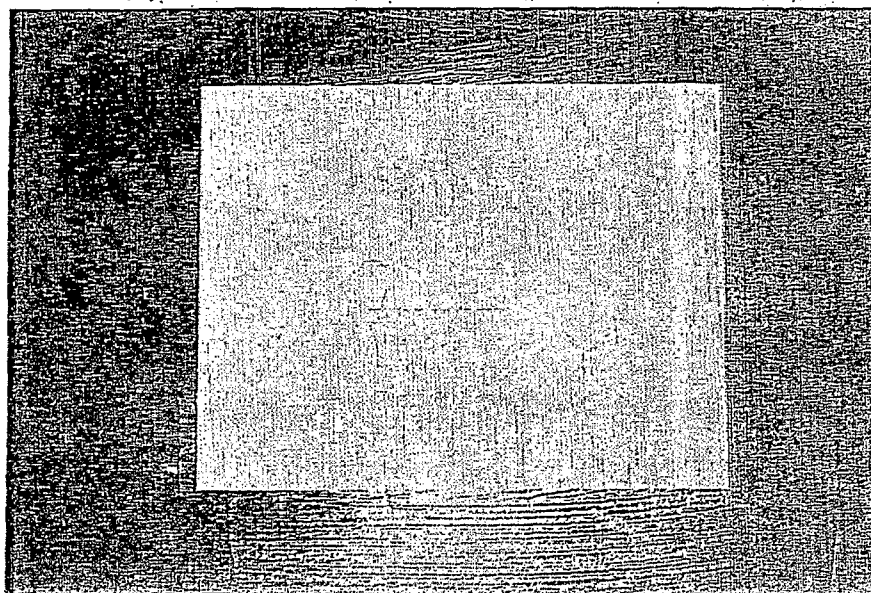


Figure 2.7. The Reaction Zone of the Vibrofluidized Microreactor.

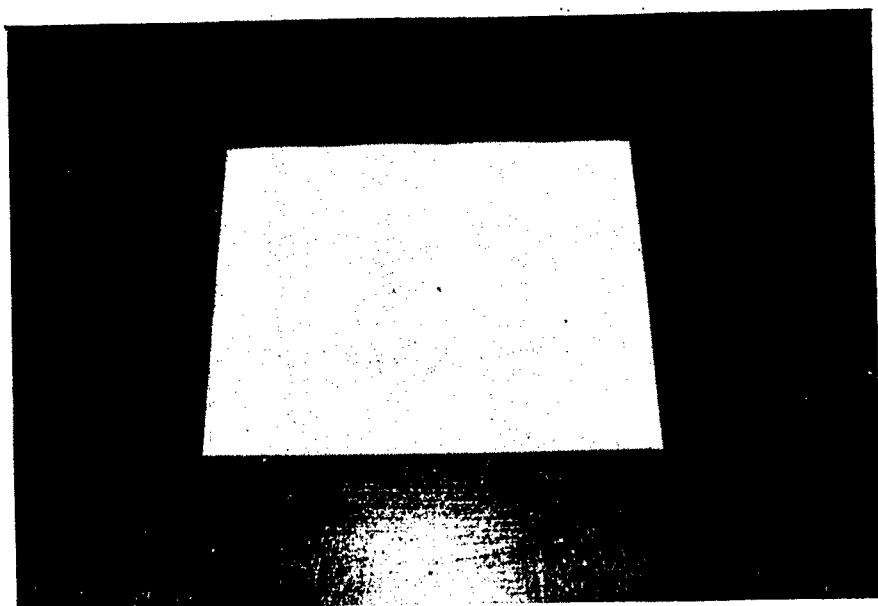


Figure 2.8. The Freeboard Zone of the Vibrofluidized Microreactor.

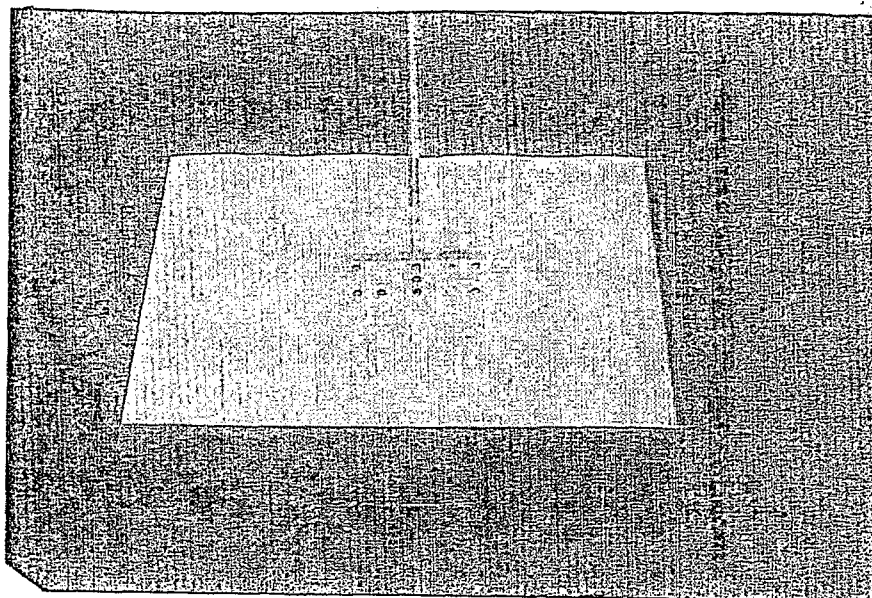


Figure 2.9. Product Gas Exit Zone of the Vibrofluidized Microreactor.

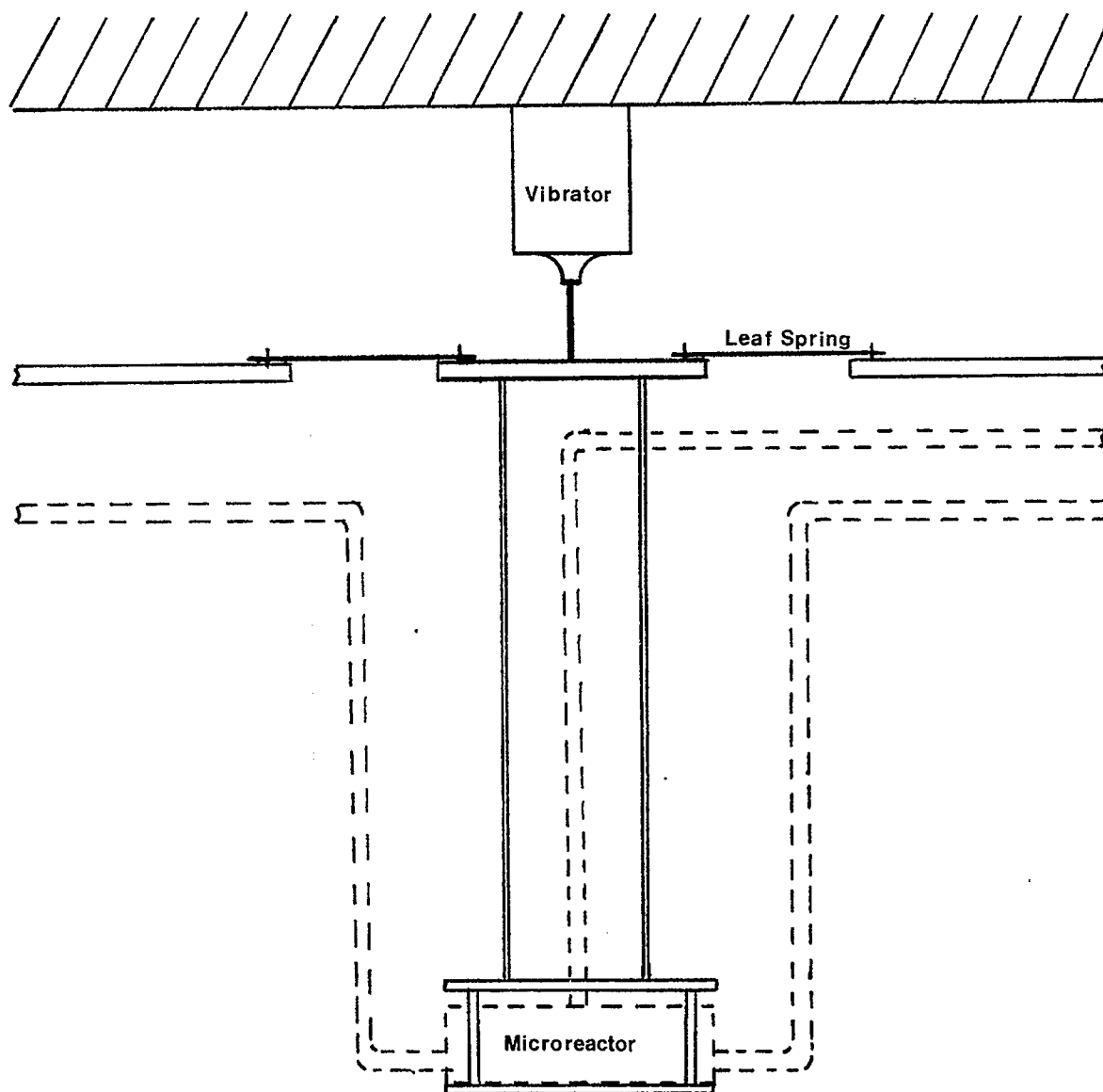


Figure 2.10. A Schematic Diagram of the Leaf-Spring Suspension System for the Vibrofluidized Microreactor.

the gases entering the reaction zone. This vibration-induced fluidization ensures uniform mixing and heat transfer characteristics of the catalyst bed, which would not be possible otherwise because of the varying gas flow rates throughout the pulsed feed and purging cycles of the unsteady-state kinetics studies.

Figure 2.11 illustrates an atmospheric mock-up of the reaction zone of the microreactor. This cold-flow model is used for investigating the catalyst particle size, gas flow rate, frequency and amplitude of vibration and distributor plate porosity in the reaction zone which will ensure good catalyst circulation and minimize fine catalyst entrainment inside the vibrofluidized microreactor.

2.2.2 Feeding and Pulsing Sequences of Reactant Gases

As mentioned in Section 1, two of the key concepts of the new fluidized bed reactor for Fischer-Tropsch synthesis from a low $H_2:CO$ gas are: (1) to provide good contact between catalyst and a low $H_2:CO$ gas in the supernatant gas, where most chemical reactions occur; and (2) to force the catalyst to spend a relatively long time in a H_2 -rich gas (fluidizing gas), but to spend only a very short time in a low $H_2:CO$ gas (supernatant gas) so as to minimize carbon formation and catalyst oxidation. In order to experimentally demonstrate the technical feasibility of these concepts, several sequences for feeding and pulsing reactant gases are to be investigated.

An initial sequence being tested subjects the catalysts to 17 seconds of a H_2 -rich fluidizing gas (F-gas) at a low flow rate and also to 2 seconds of a low $H_2:CO$ supernatant gas (S-gas) at a high flow rate. Figures 2.12 to 2.16 show the schematic diagrams of five key steps in this initial sequence of feeding and pulsing of reactant gases, and Figure 2.17 presents a graphical summary of the five steps expressed in terms of flow rates and feeding/pulsing times of both the F-gas and S-gas.

In the initial experiments, the volumetric flow rates and feeding/pulsing times of F-gas and S-gas for needle valves A to E in the operational sequences illustrated in Figures 2.12 to 2.16 are listed in Table 2.2. The specific feeding and pulsing operations in the initial experiments are as follows:

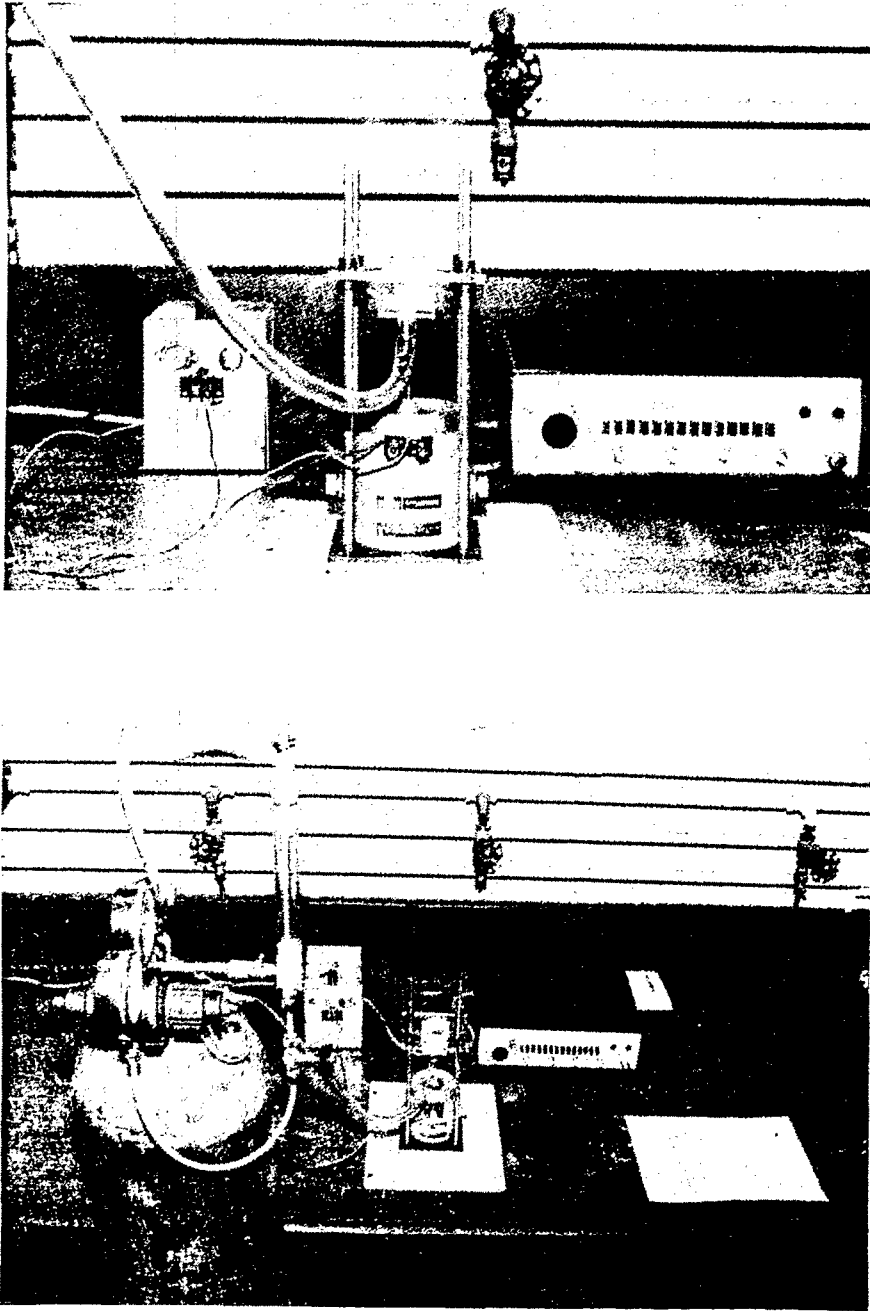


Figure 2.11. A Cold Model of the Reaction Zone in the Vibrofluidized Reactor.

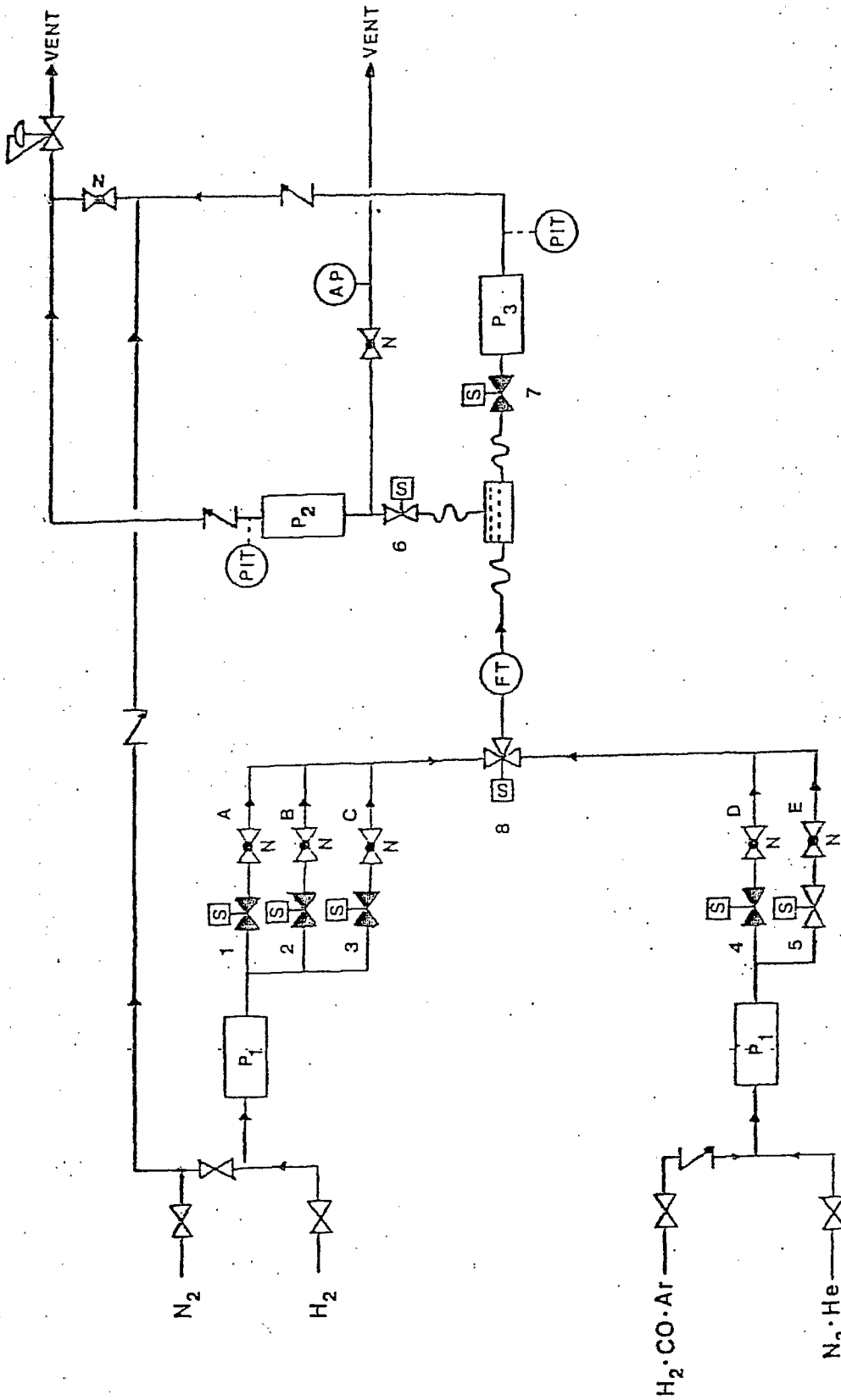


Figure 2.12. High Flow Rate (e.g., 2,500 mm³/sec) of S-Gas Feed through Valve E for a Short Duration (e.g., 2 sec).

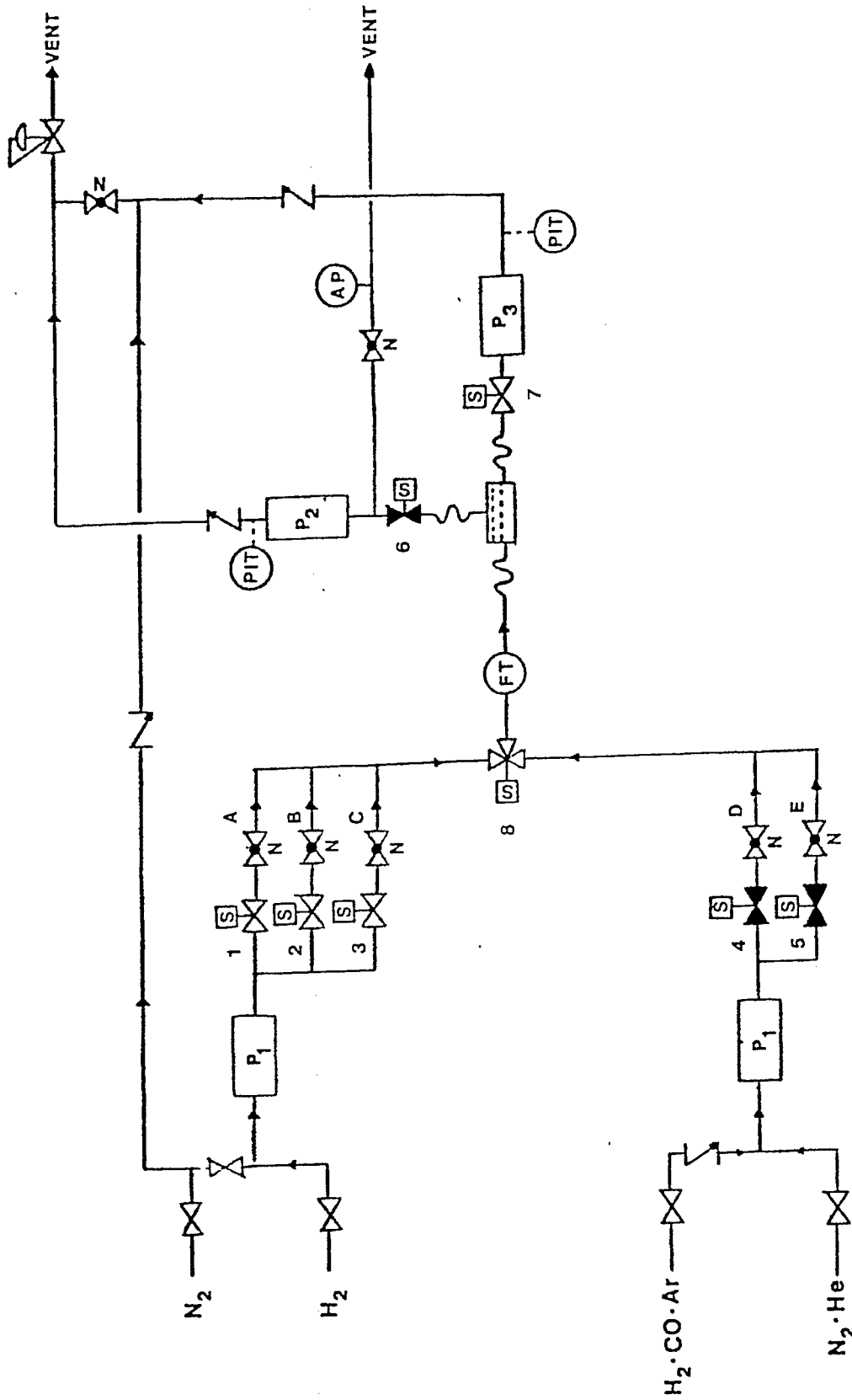


Figure 2.13. Plenum Purge of S-Gas by High Flow Rate (e.g., 11,950 mm³/cc) of F-Gas through Valves A, B, and C for a Very Short Duration (e.g., 0.1 sec).

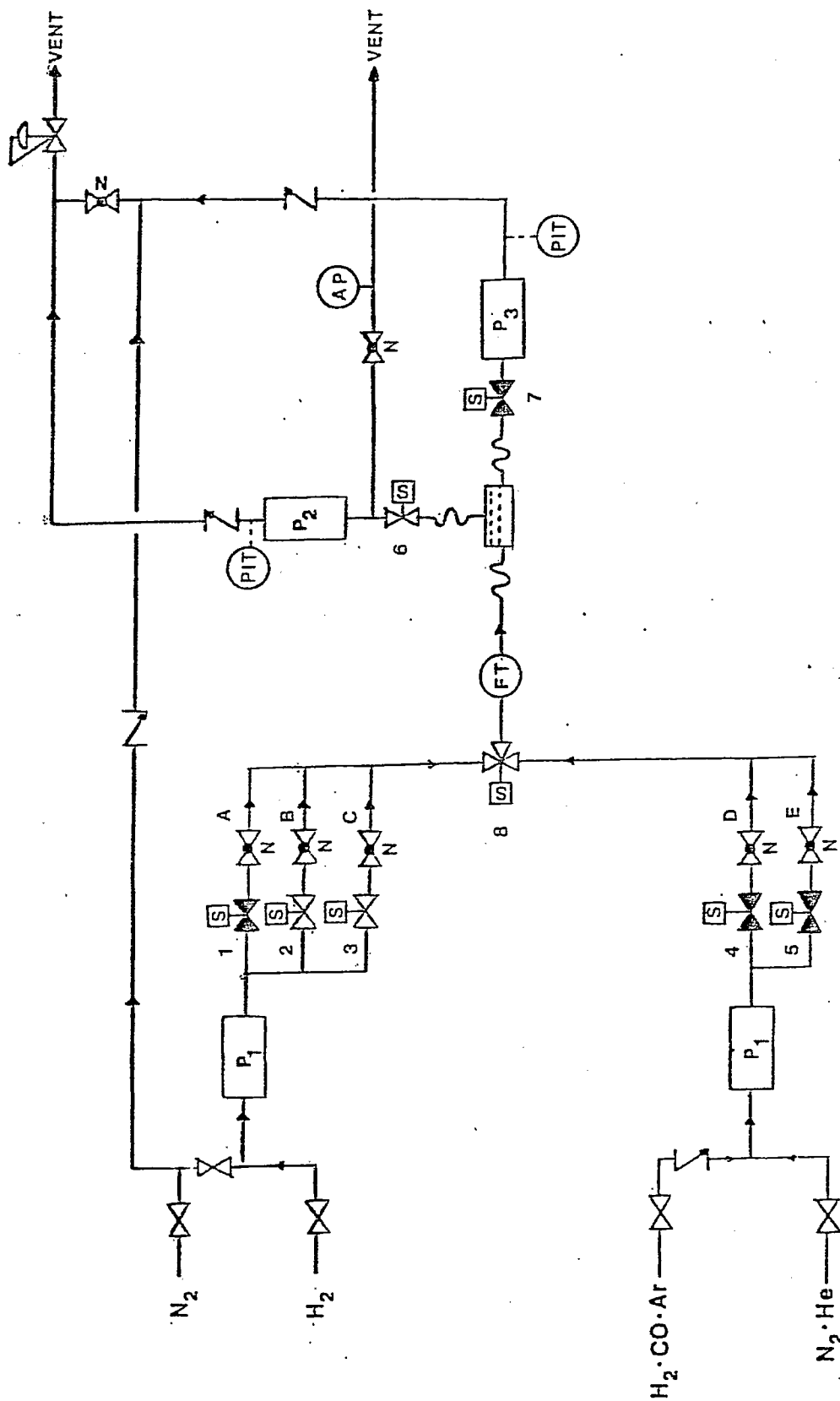


Figure 2.14. Reaction Zone Purge by Relatively High Flow Rate (e.g., 250 mm³/sec) of F-Gas through Valves B and C for a Short Duration (e.g., 1 sec).

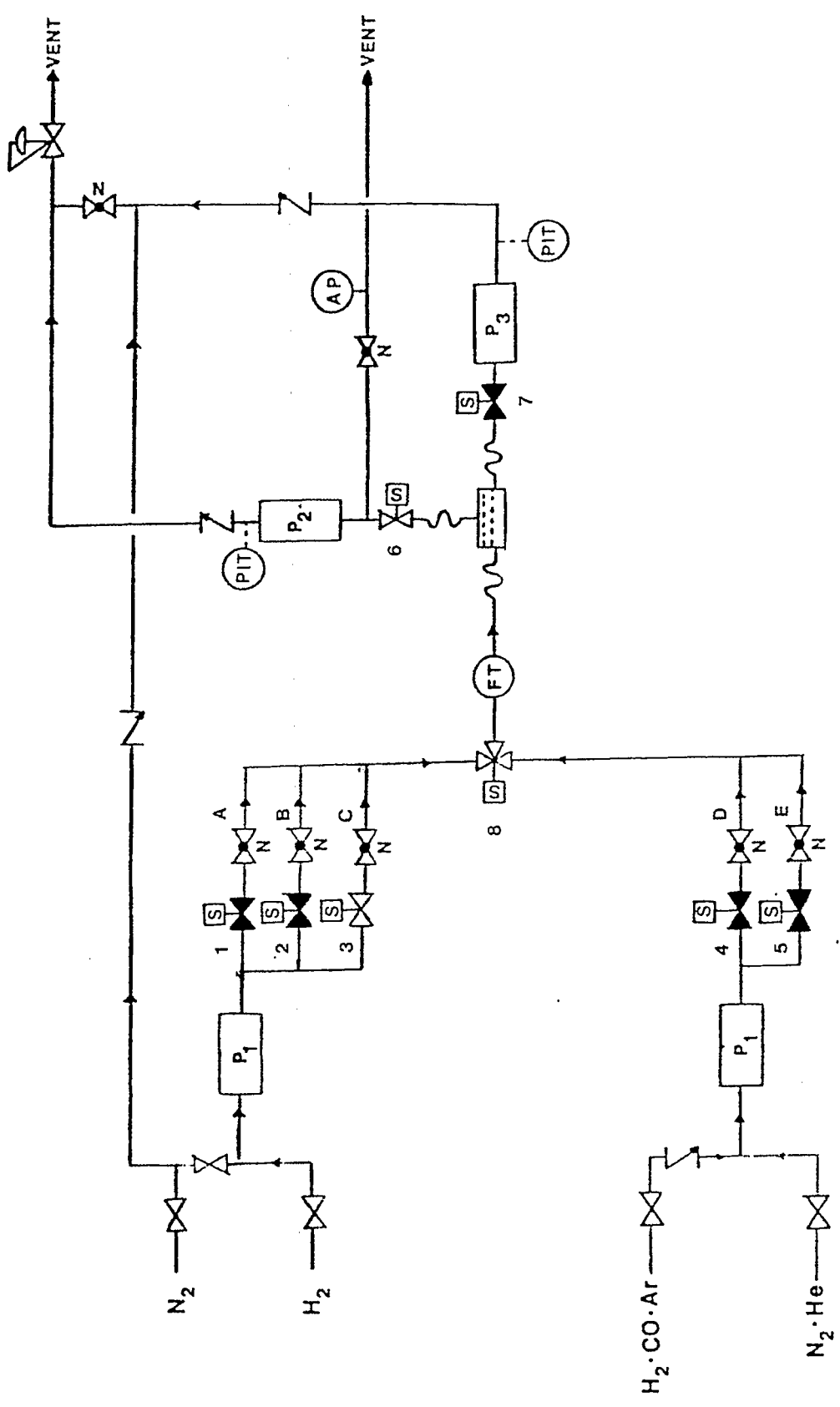


Figure 2.15. Low Flow Rate (e.g., $14.7 \text{ mm}^3/\text{sec}$) of F-Gas Feed into the Reaction Zone through Valve C for a Long Duration (e.g., 17 sec).

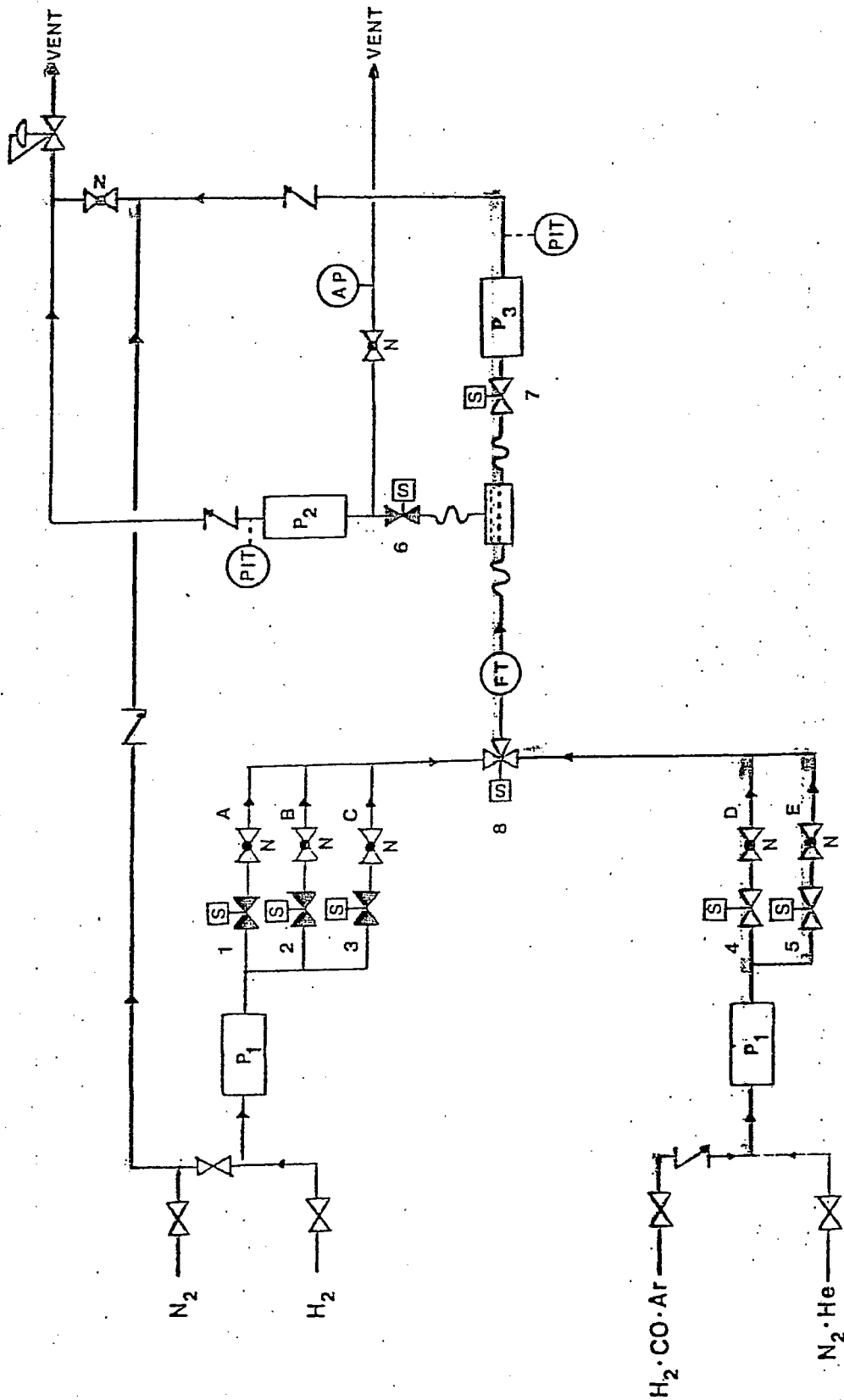


Figure 2.16. Plenum Purge of F-Gas by High Flow Rate (e.g., 11,500 mm³/sec) of S-Gas through Valves D and E for a Very Short Duration (e.g., 0.1 sec).

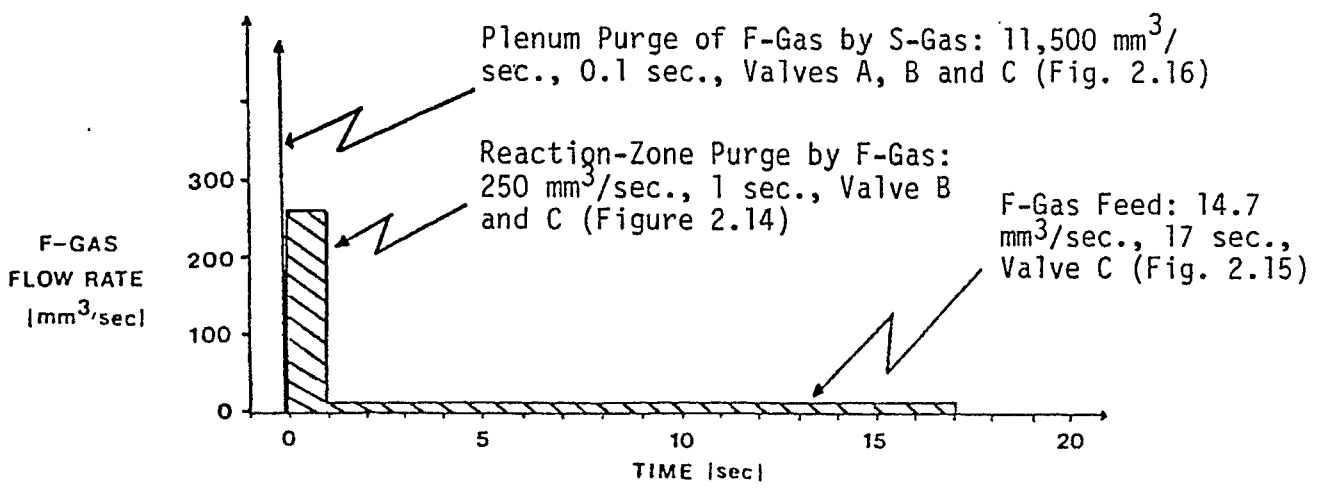
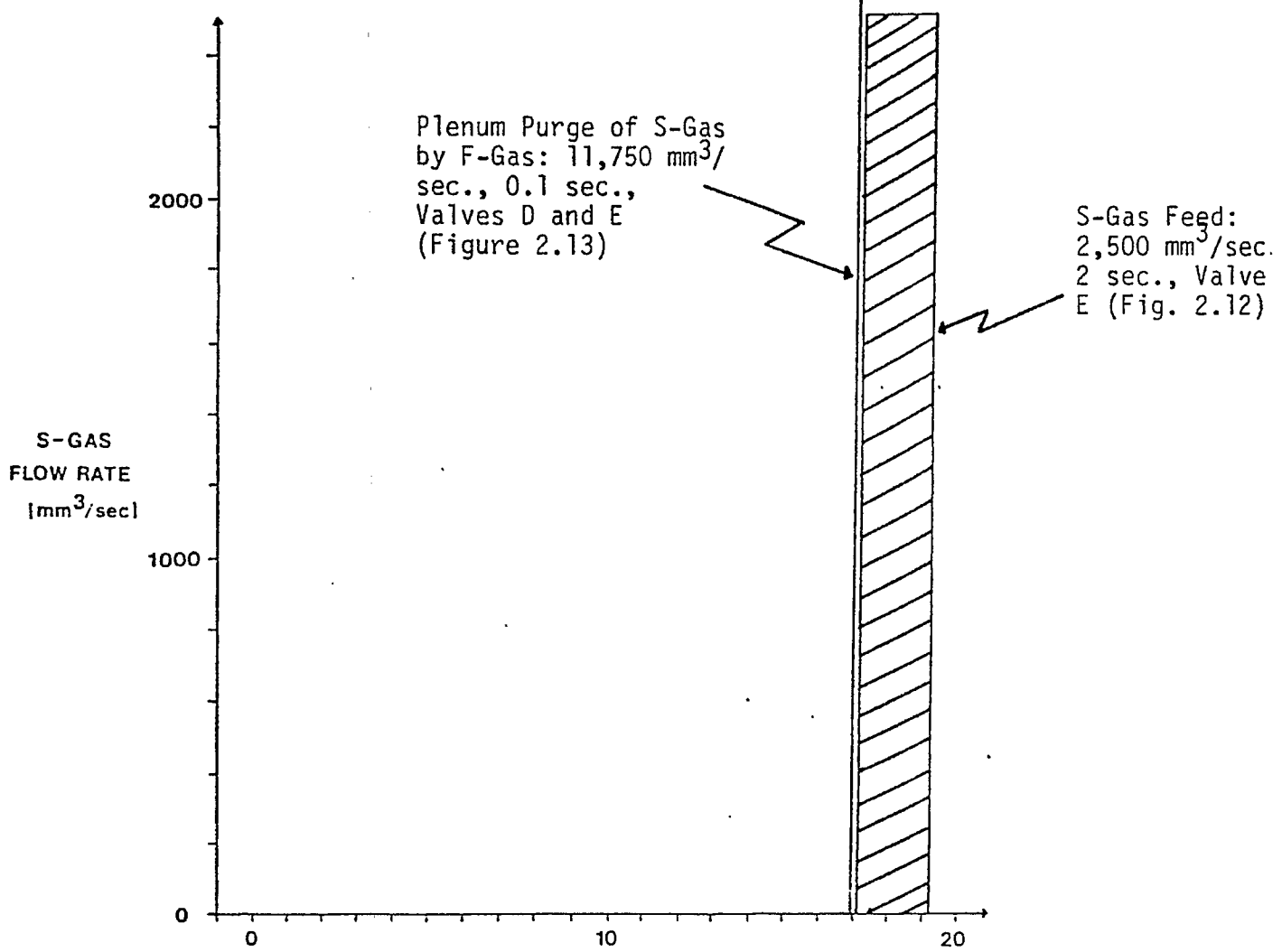


Figure 2.17. Flow Rates and Feeding/Purging Times of Both F-Gas and S-Gas in an Initial Unsteady-State Fischer-Tropsch Kinetics Experiment.

Table 2.2

Volumetric Flow Rates and Feeding/Pulsing Times for Needle Valves A to E in the Initial Operational Sequences Illustrated in Figures 2.12 to 2.16

Needle Valve Number	Gas Flow	Volumetric Flow Rate, mm ³ /sec, at 3150C and 27 atm	Feeding/Pulsing Duration, sec.	Total Gas Volume, mm ³	Space Velocity 1/sec.
A	F-gas (purge)	11,250	0.1 (purge)	1,125 (purge)	--
B	F-gas	235.3	1.0	235.3	--
C	F-gas	14.7	17	250	--
D	S-gas (purge)	9,250	0.1 (purge)	925 (purge)	--
E	S-gas	2,500	2	5,000	10

(i) S-gas feed at the beginning of a cycle (Figure 2.12). Valves 1, 2, 3, 4 and 7 are closed. Three-way valve 8 is shifted to permit a high flow rate (e.g., 2,500 mm³/sec) of S-gas (H₂:CO•Ar) into the microreactor through valve E for a short duration (e.g., 2 seconds). This flow should be able to sweep out the gas inventory in the reaction zone of the microreactor approximately 20 times.

(ii) Plenum purge of S-gas by F-gas (Figure 2.13). Valves 4, 5 and 6 are closed and three-way valve 8 is shifted to permit the F-gas to flow. At this time, valves 1, 2, 3 and 7 are opened simultaneously for a relatively high flow rate (e.g., 11,500 mm³/sec) of F-gas through needle valves A, B and C into the base plenum zone of the microreactor for a very short duration (e.g., 0.1 second). This flow should be able to purge the gas contained in the plenum zone completely.

(iii) Reaction-zone purge by F-gas (Figure 2.14). Valves 1 and 7 are closed and valve 6 is opened. This permits a relatively high flow rate (e.g., 250 mm³/sec) of F-gas through needle valves B and C for a short duration (e.g., 1 second) in order to purge the reaction zone approximately once.

(iv) F-gas feed into the reaction zone (Figure 2.15). Valve 2 is closed and valves 3 and 6 remain opened. A low flow rate (e.g., 14.7 mm³/sec) of F-gas passes through valves 3 and C into the reaction zone for a long duration (e.g., 17 seconds).

(v) Plenum purge of F-gas by S-gas (Figure 2.16). Valves 3 and 6 are closed, and valves 4, 5 and 7 remain opened. Three-way valve 8 is shifted to its original position which allows for the S-gas to flow into the plenum zone through valves D and E at a high flow rate (e.g., 11,500 mm³/sec) for a very short duration (e.g., 0.1 second). This flow should be able to sweep out the gas contained in the plenum space in the microreactor.

2.2.3 Analytical Method and System

As discussed in Section 2.1.4, the on-line GC technique of Nijs and Jacobs (1981) has been adopted in this investigation for identifying and analyzing the Fischer-Tropsch synthesis products. Figure 2.18 shows a schematic diagram of the on-line analytical system in the sample mode. This system consists of two sample injection valves which are connected to

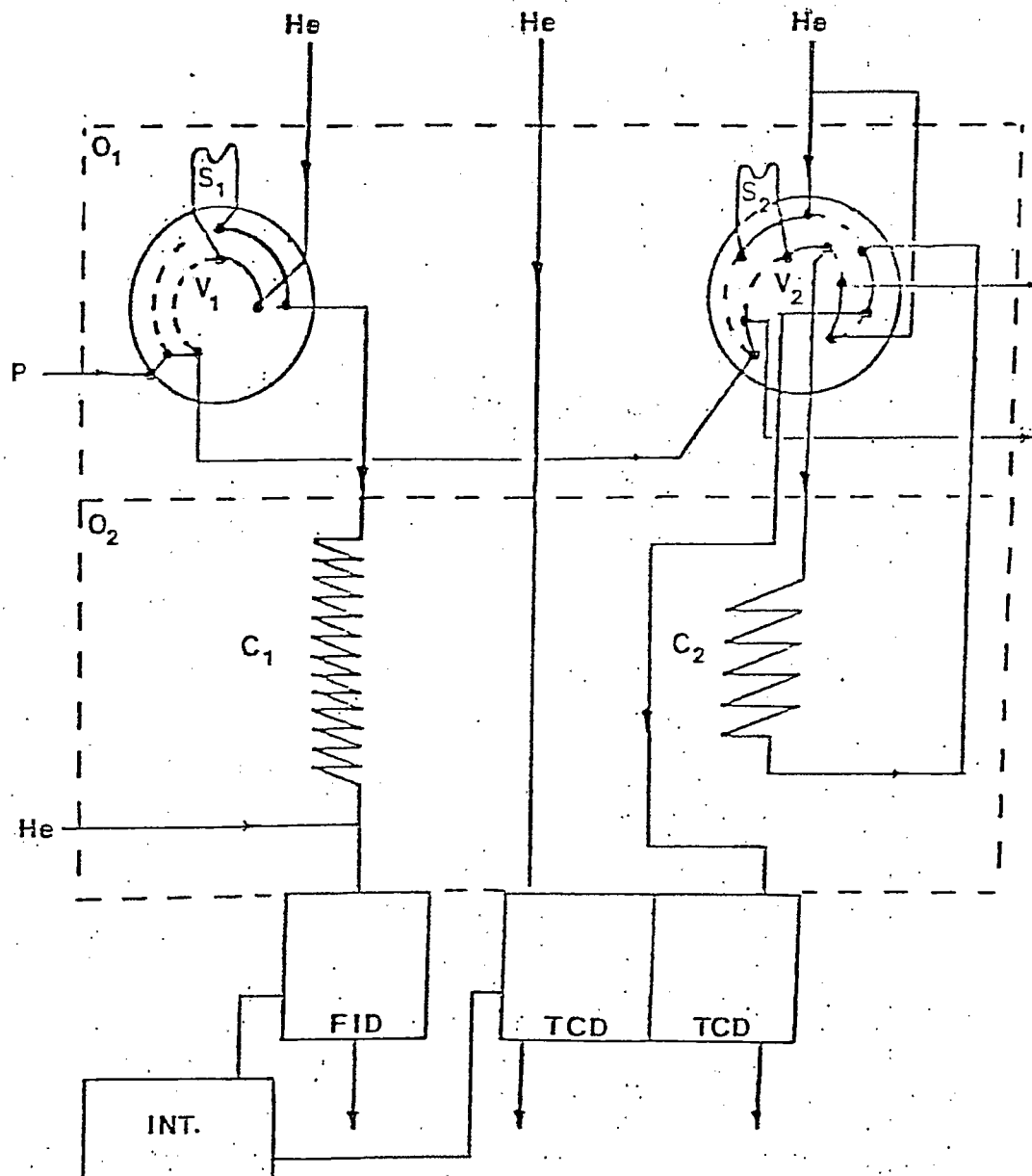


Figure 2.18. A Schematic Diagram of the On-Line GC Analytical System for Gas Products in the Sample Mode.

GC columns. The first sampling valve (V1) is a 6-port valve for injecting 0.03-ml samples into a (C1) 60-ft Durabond DB1 fused silica capillary column, which is connected to a flame ionization detector for identifying and analyzing C₁ to C₁₂ hydrocarbons. The other sampling valve (V2) is a 10-port valve for injecting 0.2 ml samples into a 6-ft., Spherocarb 60/80-mesh packed column (C2), which is connected to a thermal conductivity detector (TCD) for identifying and analyzing light gases, including CO, CO₂, light hydrocarbons and argon (an internal standard). Both sample valves are held in a heating mantle at approximately 200°C.

Actual product analyses are initiated and controlled by a Zenith Z-89 microcomputer. Product gas samples are simultaneously injected into the capillary and packed columns, both of which are placed inside a temperature-programmed oven. The temperature program of the Hewlett-Packard 5730A controller begins at -50°C and increases at a rate of 10°C per minute. The output from the TCD is monitored by a GC peak-area integrator (INT.) until carbon monoxide is eluted from the packed column (C2). At this time, the temperature program is shifted to a heating rate of 1°C per minute and the packed column (C2) is then backflushed to remove heavy hydrocarbons, as illustrated in the schematic diagram of Figure 2.19. After approximately two hours, a detailed product identification and analysis, including C₁ to C₄ alcohols, C₁ to C₁₂ paraffins and olefins and alkyl aromatics, can be obtained.

In the current analytical system for initial experiments, Fischer-Tropsch synthesis products continuously flow from the microreactor to a small sample collection cylinder, in which they will mix with gas products collected from several preceding feeding/pulsing cycles to yield an integrated product for GC analyses. In future experiments, attempts will be made to withdraw samples for GC analyses during different parts of the feeding/pulsing sequence. This will provide some insight into the kinetics and mechanism of the transient Fischer-Tropsch synthesis.

2.3 Scope of Experimental Tests

The specific experimental tests to be carried out in this investigation can be categorized as follows:

- (i) cold-flow vibrofluidization experiments;
- (ii) steady-state synthesis experiments with H₂:CO and H₂;

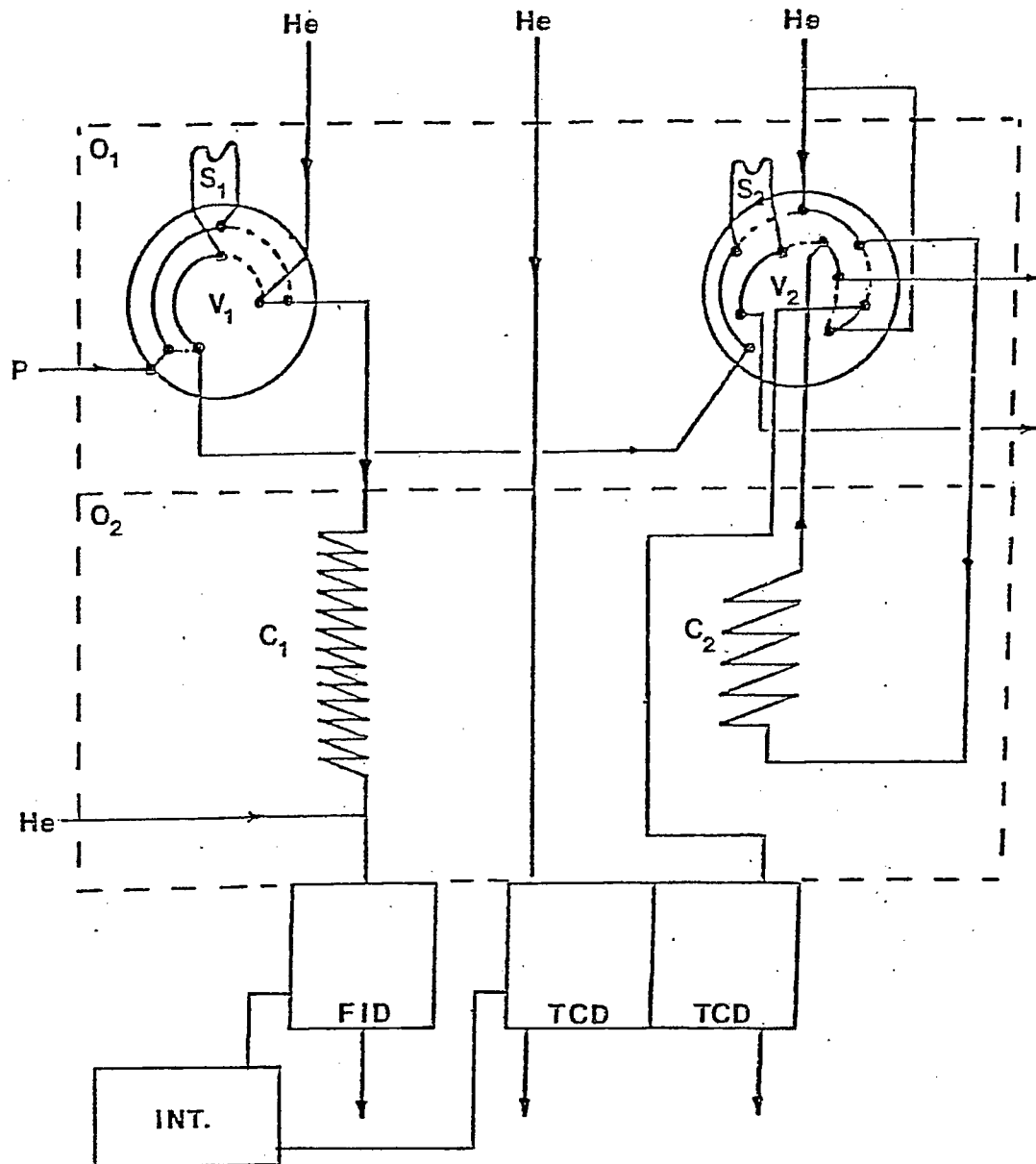


Figure 2.19. A Schematic Diagram of the On-Line GC Analytical System for Gas Products in the Backflush Mode.

- (iii) pulsing system experiments with $N_2:He$ and N_2 ;
- (iv) transient synthesis experiments with $H_2:CO$ and H_2 .

The objectives of cold-flow vibrofluidization experiments, using the system shown in Figure 2.11, are to determine the approximate entrainment velocities of different size ranges of fused iron catalysts, while varying the catalyst bed depth, distributor plate porosity, and amplitude and frequency of vibration. These experiments will provide proper vibrofluidization conditions to ensure that the catalyst is not being transported and held against the retaining plate during the actual kinetics experiments in the vibrofluidized microreactor.

The purposes of steady-state kinetics experiments with $H_2:CO$ and H_2 are two-fold. First, any technical problems which may develop in operating the vibrofluidized microreactor system (Figure 2.3) can be corrected without the added complexity introduced in transient experiments. Secondly, the steady-state experiments will provide reference data on carbon deposition, carbide formation, catalyst oxidation, trends in catalyst activity, as well as product yield and selectivity for future comparison with results from transient kinetics experiments.

Pulsing system experiments are to be undertaken by using N_2 as a surrogate fluidizing-gas (F-gas) and an $N_2:H_2$ mixture as a surrogate supernatant gas (S-gas) in the vibrofluidized microreactor system shown in Figure 2.3. A fast-response thermal conductivity cell will be placed into the system at strategic locations in order to determine the extent of gas peak dispersion. These locations include the downstream of the three-way valve (valve 8 in Figure 2.3), the downstream of the reaction zone, and the downstream of the base plenum zone. The specific pulsing system experiments will provide operational guidelines which ensure distinct transitions between F-gas and S-gas in the reaction zone of the vibrofluidized microreactor system.

The objectives of transient synthesis experiments with $H_2:CO$ and H_2 , using the feeding/pulsing sequence illustrated in Figures 2.12 to 2.17, are to investigate the effects of compositions and residence times of both F-gas and S-gas on product yield and selectivity, and catalyst history (characterized by iron oxidation, carbide formation and carbon deposition). A series of factorially-designed experiments will be carried out to minimize the number of necessary tests and to ensure a meaningful interpretation of experimental results. Future transient synthesis experiments may be conducted with supported or precipitated iron catalysts, nitrided iron catalysts and bifunctional catalysts. Also, other group VIII metal catalysts may be tried.

2.4 Experimental Results and Discussion

Initial steady-state Fischer-Tropsch synthesis experiments were initiated in late February, 1983, using the vibrofluidized microreactor system shown in Figure 2.3 and the on-line GC analytical system illustrated in Figures 2.18-2.19. Figures 2.20 to 2.21 show the pictures of the complete microreactor and analytical systems. The primary objectives of the initial experiments was to test the reliability of the microreactor system for high-pressure operations, and to identify any mechanical problems associated with the current equipment design.

Table 2.3 summarizes the operating conditions and catalyst parameters of an initial experiment. This experiment began with reducing a fused-iron catalyst with hydrogen in the microreactor at 400°C and 5 atm for 6 hours. After the catalyst was reduced, the reactor temperature was decreased to 315°C, and the reactor pressure was raised to 28 atm. A 1,500-SCCM mixture of H₂ and CO at a molar ratio of 2:1 was then fed to the reactor. Based on available results from supporting fluidization experiments using the cold-flow model shown in Figure 2.11, it was known that at this flow rate, the iron catalysts used could be fluidized by the reactant gas flow; and the vibration system was thus not used. The reactor was run for six hours with samples of light product gases being collected once every 20 minutes.

The microreactor system performed very well in the initial experiments. Pressure fluctuations were within 1% and flow rate fluctuations were within 3%. Essentially no technical difficulty was encountered in reactor operations and product sampling. Figures 2.22 and 2.23 show examples of a reactant chromatogram and a light gas product chromatogram.

As a result of the initial experiments, two necessary modifications of system design and product analysis must be made. First, the steady-state synthesis experiments have suggested the needs for pressure taps upstream of the needle valves and for alternative gasket sealing method for the microreactor. The present gasket sealer presently uses a graphite in a water-based solution. This sealer is applied to asbestos-impregnated rubber gasket between two sections of the microreactor. There is a possibility that this sealer may interfere with catalyst characterization when the iron catalyst is analyzed for graphite after an experiment. Therefore, other gasket sealers are being tested for use in the microreactor. Another modification to be made is in the

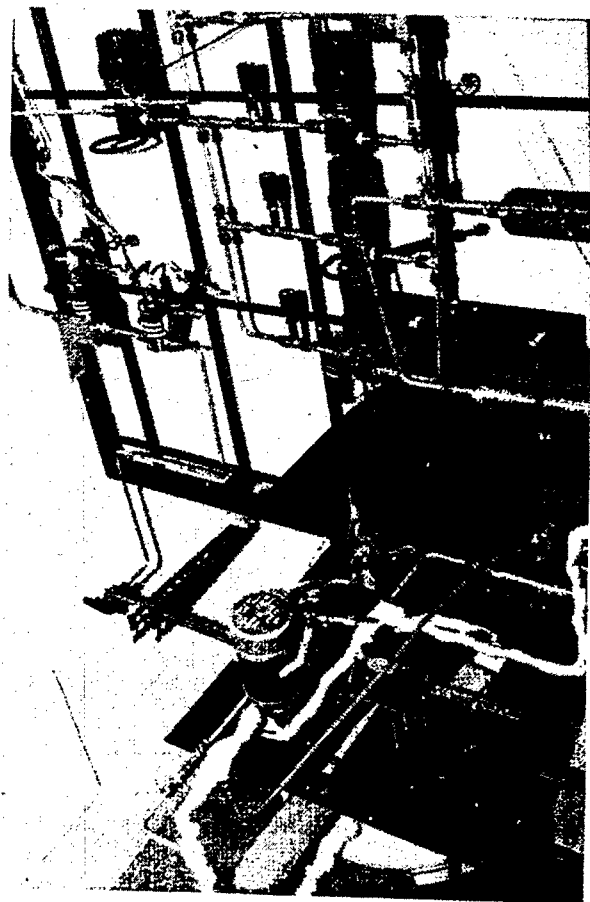


Figure 2.20 The Vibrofluidized Microreactor System for Unsteady-State Fischer-Tropsch Synthesis.

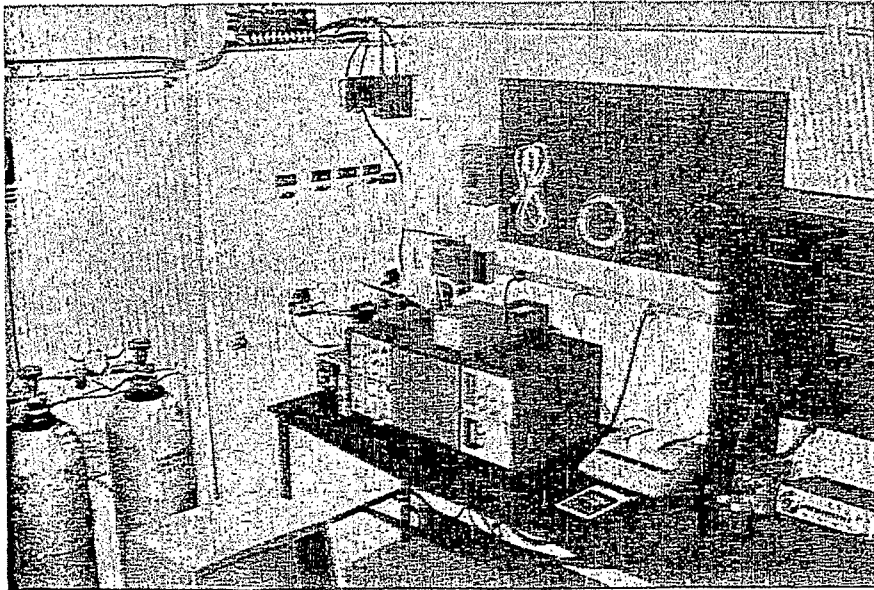
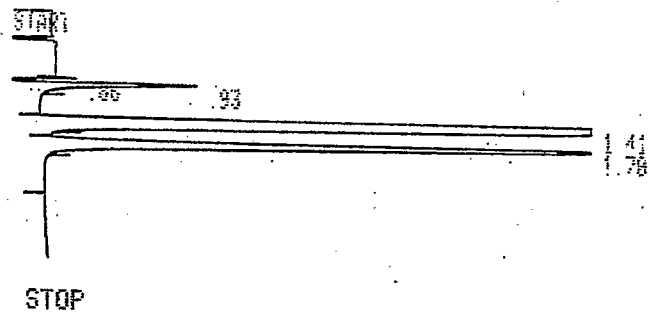


Figure 2.21 A Computer-Controlled On-Line Gas Chromatographic System for Product Analysis. Room Behind the Gas Cylinders in the Figure is the Reactor Box. The Reactor Control Panel is the Black Box on the Right of the Figure.

Table 2.3
 Conditions for Initial Steady-State Synthesis Experiments
 with H₂:CO and H₂

Item	Condition
A. Operating Conditions	
1. Reactor temperature, °C	315
2. Reactor pressure, atm	28
3. H ₂ :CO ratio	2:1
4. Feed flow rate, SCCM	1,500
5. Reaction time, hrs.	6
B. Catalyst parameters	
1. Charge, gm	0.8148
2. Composition, wt%	98.2% Fe, 1.4% Cu, 0.4% K ₂ CO ₃
3. Size distribution, μm	150-300
C. Catalyst reduction conditions	
1. Temperature, °C	400
2. Pressure, atm	5
3. Reducing hydrogen flow, SCCM	37.5
4. Reduction time, hrs.	6

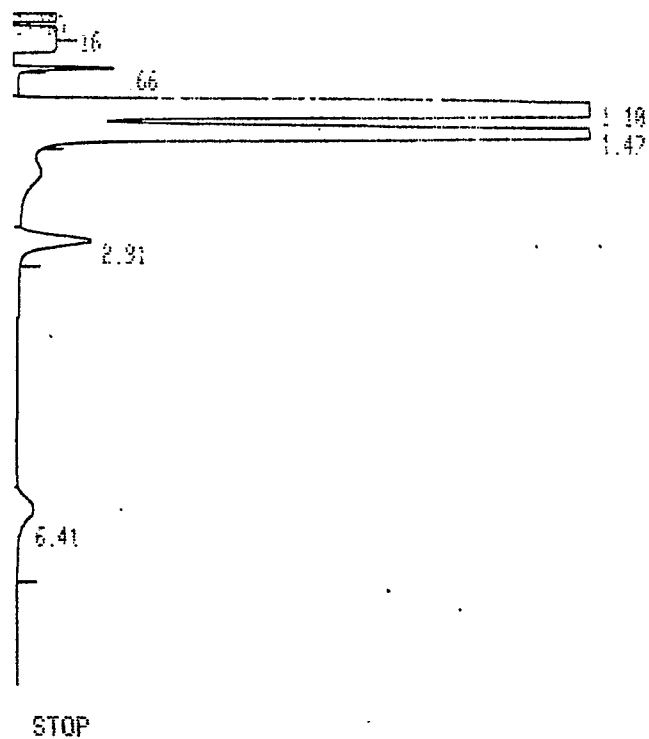


RUN # 20 FEB/25/83 01:01:34

RT	AREA	TYPE	AR/HT	AREA%
0.86	3596	D BP	0.031	1.586
0.93	18155	PB	0.077	8.006
1.41	164590	PB	0.067	72.585
1.78	40415	BB	0.078	17.823

TOTAL AREA= 226760
 MUL FACTOR= 1.0000E+00

Figure 2.22. Isothermal Chromatogram of Reactor Feed.
 62.5% H₂:31.25% CO:6.25% Ar



RUN # 7 MAR/01/83 19:51:35

RT	AREA	TYPE	HR/HT	AREA%
0.16	18808	BB	0.100	0.990
0.66	257330	PB	0.154	13.540
1.10	1335500	PV	0.114	70.269
1.47	271960	VB	0.123	14.310
2.91	11009	BB	0.171	0.579
6.41	5955	BB	0.376	0.313

TOTAL AREA= 1900500
MUL FACTOR= 1.0000E+00

Figure 2.23. Isothermal Chromatogram of Light Gas Products of Fischer-Tropsch Synthesis at 315°C and 28 atm.

area of product analyses. Presently, a fused-silica capillary column is on order and a sub-ambient temperature-programmed oven is being installed in the GC system. In addition, a suitable temperature-programming scheme is needed to obtain good resolution of light gases and hydrocarbons; and the quantitative identification of product peaks must be undertaken using calibration gases.

Once the above system modifications have been completed, unsteady-state Fischer-Tropsch synthesis experiments will be initiated together with detailed catalysis composition analysis and temperature-programmed GC analysis of all gas products.

3. SUPPORTING FLUIDIZATION STUDIES

3.1 Hydrodynamics in a Shallow Fluidized Bed

3.1.1 Introduction

Shallow fluidized beds refer to those beds with static bed heights on the order of only about 0.1 m or less. The study of shallow beds is a relatively new subject in the field of fluidization, and one that is worth exploring because of the following notable advantages of shallow beds over conventional deep beds (Ali and Broughton, 1977):

- (1) Pressure drop across a shallow bed is low.
- (2) Heat transfer coefficient between a shallow bed and its immersed heating surface is high.
- (3) Slugging seldom occurs in a shallow bed.
- (4) Scale-up of a shallow bed and multistage shallow-bed design are relatively easy.

Table 3.1 compares a number of key features of both shallow and deep fluidized beds.

Very little is known about the hydrodynamic behavior of shallow fluidized beds. Squires (1982) has suggested that three "regimes" can be generally seen when a fine powder is fluidized from a static bed height on the order of only about 10 cm or less. Figure 3.1 illustrates schematically the three regimes. At the bottom is a shallow dense bubbling zone having a sharp upper surface. Above this is something not usually seen in deep-bed fluidization, namely, a "cloud zone" that resembles the "turbulent fluidization" first described by Kehoe and Davison (1970) and later studied by Squires (1976) and his colleagues: Yerushalmi, et al. (1978), Yerushalmi and Cankurt (1979) and Avidan (1982). In the literature, the term "cloud phase" was mentioned briefly in writings by former colleagues of Elliott's -- Al-Ali and Broughton (1977). The available information seems to suggest that the transition to turbulence occurs at much lower velocities in shallow beds than in deep beds, but only for an upper part of the bed. If the bed is sufficiently shallow, or the gas velocity sufficiently high, the dense zone of Figure 3.1 disappears, and the cloud zone rests on the grid. Above the cloud zone is a spray zone of highly dilute particles, some of which travel upward at remarkably high velocities.

Table 3.1

A Comparison of Key Features of Deep and Shallow Fluidized Beds

Key Features	Deep Beds	Shallow Beds
1. Bed pressure drop	Large	Small
2. Bed expansion (%)	20 to 40	50 to 250
3. Transport disengaging height	More than 1 m	1 m usually adequate
4. Heat transfer coefficient between the bed and immersed heating surfaces	150 to 500	150 to 800 W/m ² -K (usually higher)
5. Bed slugging	common	seldom occurs
6. Bubble sizes	about 1 m	about 0.1 m
7. Entry effects	usually small	often important
8. Bed temperature	usually uniform	gradients often occur
9. Multistage design	seldom practical	fairly easy
10. Bed scale-up	often difficult due to slugs, particularly in small beds	relatively easy

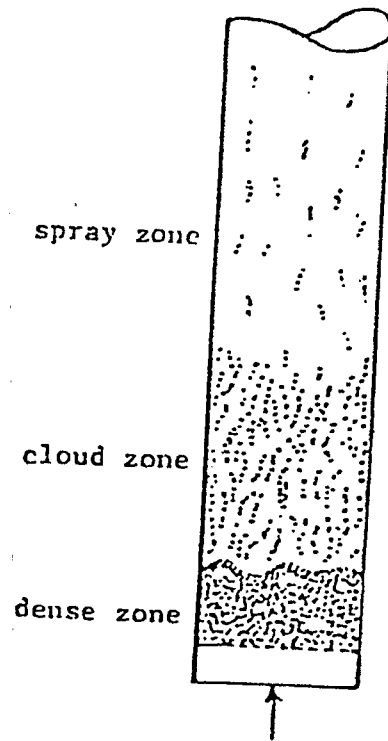


Figure 3.1 Three Flow Regimes in a Shallow Fluidized Bed.

If the shallow bed is fluidized in a tall cylinder, the spray zone may extend a meter or more above the cloud zone. The surface between cloud and spray zones is somewhat diffuse, yet unmistakable.

Pugh (1974) experimentally investigated the dependence of shear stress on shear rate for gas-particle suspensions in an inclined, shallow fluidized bed. His experimental data were correlated by a power-law expression:

$$\tau = m(\gamma)^n$$

where

τ = shear stress, Pa

γ = shear rate, 1/s

m, n = parameters

The parameters m and n were found to be dependent upon the static bed height, superficial fluidization velocity and solid particle properties. In particular, the parameter m in the above equation is closely related to the concept of apparent viscosity of gas-particle suspensions in fluidized beds. The available literature has shown that the apparent viscosity is quantitatively affected by a number of factors (Zenz and Othmer, 1960; pp. 116-127 and 237-240):

(1) The apparent viscosity increases with increasing static bed height and solid particle density.

(2) The apparent viscosity decreases with increasing superficial fluidization velocity, reaching a minimum near the point of minimum fluidization velocity.

(3) The apparent viscosity is not significantly dependent upon the solid particle size, particle shape and particle surface roughness.

(4) The apparent viscosity is dependent upon the design of the distributor (Botterill and van der Kolk, 1971).

Essentially no data have been reported on the bed expansion and pressure drop measurements in shallow fluidized beds. These measurements are important to quantitatively characterizing the three proposed regimes in a shallow fluidized bed (see Figure 3.1). In what follows, initial pressure drop data in a shallow fluidized bed are presented.

3.1.2 Experimental System

Figure 3.2 shows the experimental system for pressure drop measurements in a shallow fluidized bed. The bed is a pyrex glass column with an inside diameter of 10.16 cm. A ruler with a reading range of 40 cm is attached on the outside wall of the glass column to indicate the bed height during the fluidization experiment. Figure 3.3 shows a photograph of the fluidized bed.

Room-temperature building air is used as the fluidizing medium. A pressure regulator and a control valve are used to adjust the air flow for fluidization experiments. The specific air fluidization velocity is measured by an orifice meter, which is calibrated by a standard rotameter. Table 3.2 illustrates the relationships between the pressure drop across the orifice meter (ΔP_o in Figure 3.2) and the volumetric flow rate and the superficial velocity of the air stream in the bed.

The bed pressure drop is measured by a specially-designed pressure probe connected to a manometer filled with Meriam oil of a specific gravity of 0.827. This probe is made of a 5-mm polyethylene tube. Pressure measurements are made through a hole drilled at the sealed end of the polyethylene tube, which is placed inside the fluidized bed. A 200-mesh screen is used to cover that hole to prevent the fluidized particles from penetrating into the manometer.

A 2-layer Dynapore 401430 laminate is used as a gas distributor in initial bed pressure drop measurements. The characteristic equation for the distributor, as provided by the manufacturer, is as follows:

$$P_1^2 - P_2^2 = 10.8G + 0.054 G^2$$

where

P_1 = pressure measured upstreams, in. of H_2O .

P_2 = pressure measured downstreams, in. of H_2O .

G = flow rate at upstream, SCFM/ft².

Initial bed pressure drop measurements are made using the range of experimental variables and conditions summarized in Table 3.3, and the results are described below.

3.1.3 Experimental Results and Discussion

Typical bed pressure drop measurements using the experimental system of Figure 3.2 and under the experimental

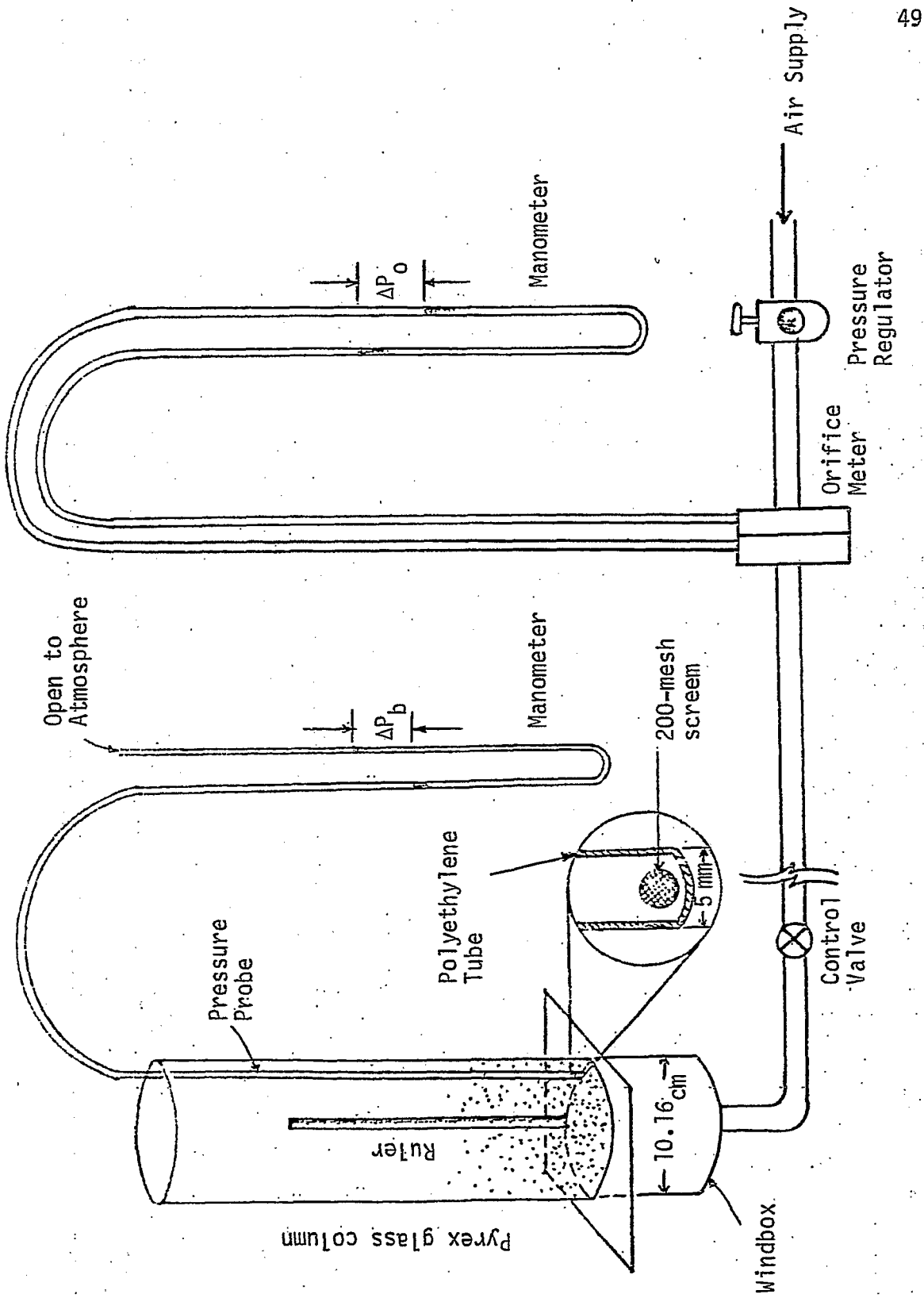


Figure 3.2 The Experimental System for Pressure Drop Measurements in a Shallow Fluidized Bed

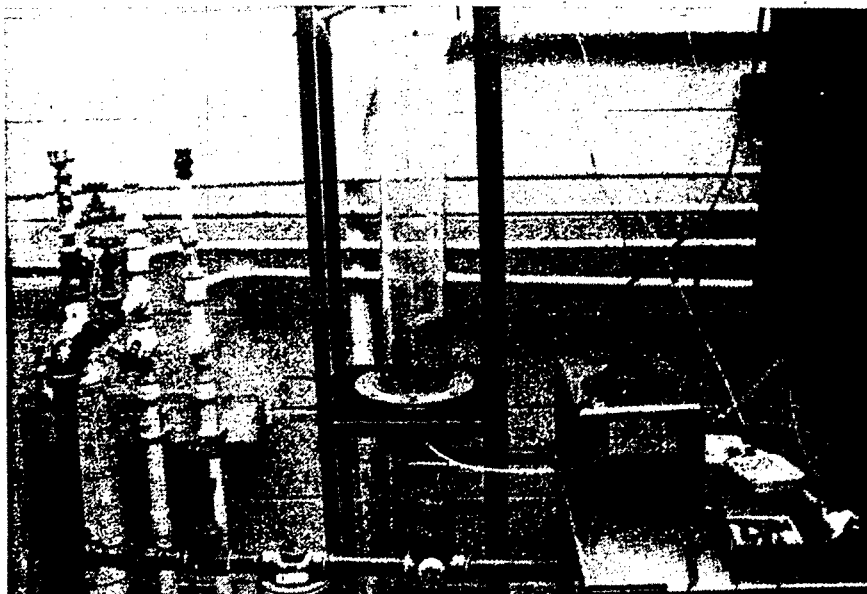


Figure 3.3 A Photograph of the Experimental System for Shallow Fluidized-Bed Hydrodynamic and Heat-Transfer Studies.

Table 3.2

Relationships Between the Pressure Drop Across the Orifice Meter (ΔP_o) and Volumetric Flow Rate (V) and Superficial Velocity (u) of the Air Stream in the Shallow Fluidized-Bed

ΔP_o (In. H ₂ O)	V (SCFM, °C)	u (m/s, 21°C)
0.0	0.000	0.000
1.0	8.160	0.532
3.0	14.265	0.929
5.0	18.302	1.192
10.0	25.370	1.653
20.0	34.589	2.253
30.0	41.046	2.674
40.0	46.072	3.001

Table 3.3

Range of Experimental Variables and Conditions in Initial
Pressure Drop Measurements Across a Shallow
Fluidized Bed

1. Distributor plate:	A 2-layer Dynapore laminate
2. Fluidized particles:	Spherical aluminum particles
3. Particle sizes:	-12+20, -20+40, -40+60 mesh
4. Fluidizing medium:	Room-temperature air
5. Superficial fluidization velocity:	0.53 to 3.00 m/s
6. Static bed height:	0.5 to 11 cm

conditions of Table 3.3 are illustrated in Figures 3.4(a)-(c) and 3.5(a)-(c). In these figures, the bed pressure ratio is defined by:

$$\text{pressure ratio} = \frac{\text{bed pressure drop}}{\text{static bed pressure}}$$

Note that the bed pressure drop is indicated by ΔP_b in Figure 3.2, and the static bed pressure represents the total weight of the fluidized particles per unit cross-sectional area of the bed.

An important observation from Figures 3.4 and 3.5 is that significant bed pressure drop, expressed in terms of pressure ratio, does not exist across a shallow fluidized bed, even with a static bed height of less than 4 cm. This fact represents a key difference between shallow and deep fluidized beds.

Both Figures 3.4 and 3.5 show that at low superficial fluidization velocities and with small static bed heights, the fluctuations in bed pressure drop are relatively significant [see, for example, 3.4(a)]. With large static bed heights, the bed pressure drop tends to approach a constant fraction of the static bed pressure, resulting in a constant value of the bed pressure ratio. A comparison of Figures 3.4 and 3.5 also shows that as expected, the bed pressure drop increases with increasing superficial fluidization velocity and with decreasing solid particle size. Further experiments are being conducted to study the bed expansion and pressure drop across shallow fluidized beds of other solid particles, such as FCC and Fischer-Tropsch iron catalysts, which are of interest to the present investigation.

3.2 Heat Transfer in a Shallow Fluidized Bed

3.2.1 Relevant Literature

Very few experimental studies on heat transfer measurements between a shallow fluidized bed and its immersed heat-transfer surface have been reported in the literature. Table 3.4 summarizes the representative investigations reported thus far. The reported data on the bed-to-surface heat transfer coefficients in shallow beds represent considerable variations in the effects of bed configurations, fluidization conditions and particle properties.

Pillai (1976) and A. Baker (1981) both observed that bed-to-surface heat transfer coefficients decreased with decreasing tube elevation when the heat-transfer tube was placed close to the distributor plate. Atkinson (1974) and Andeen and Glicksman (1976), however, found that bed-to-surface heat transfer coefficients

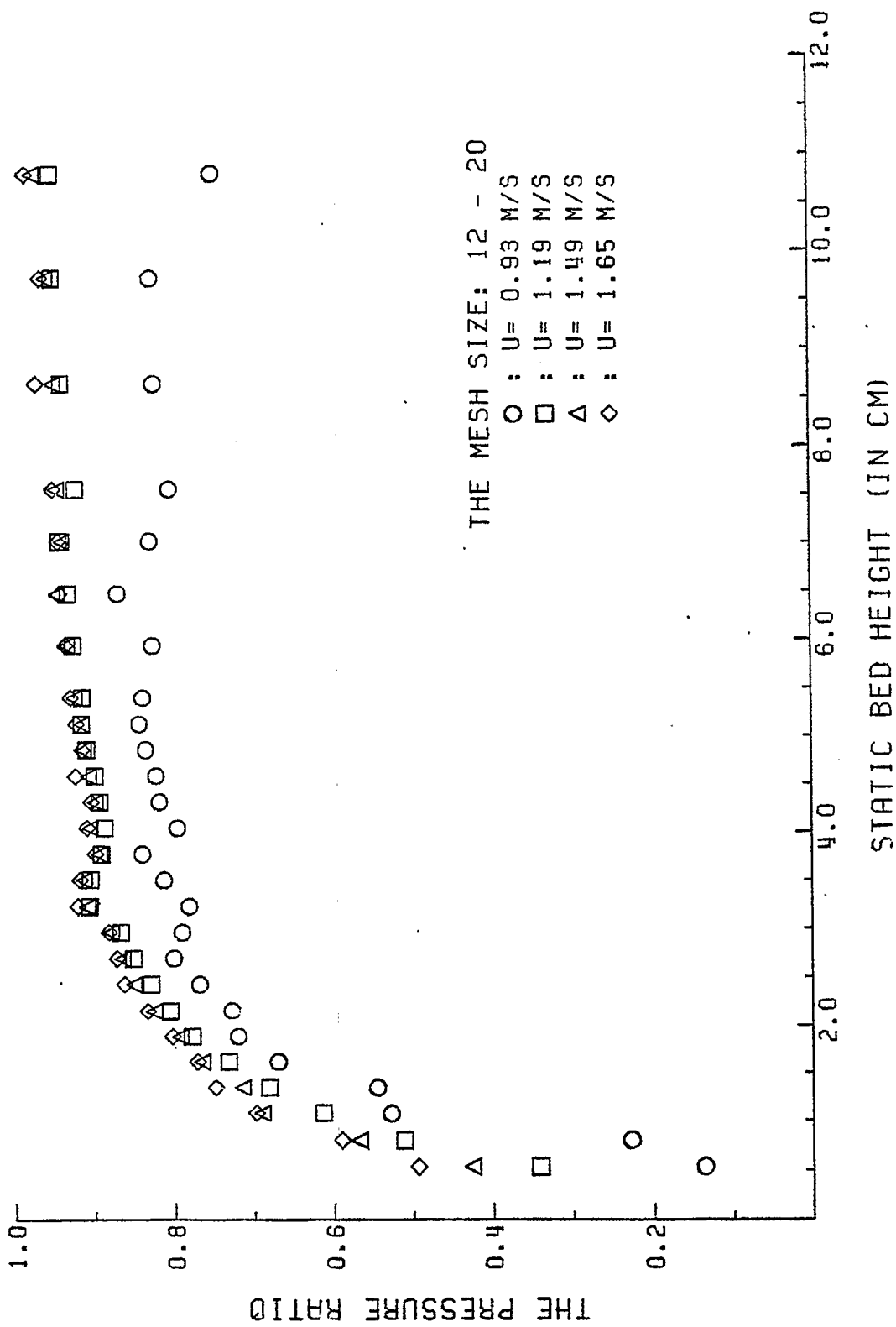


Figure 3.4(a) The Bed Pressure Drop in a Shallow Fluidized Bed of Spherical Alumina Particles (-12+20 Mesh).

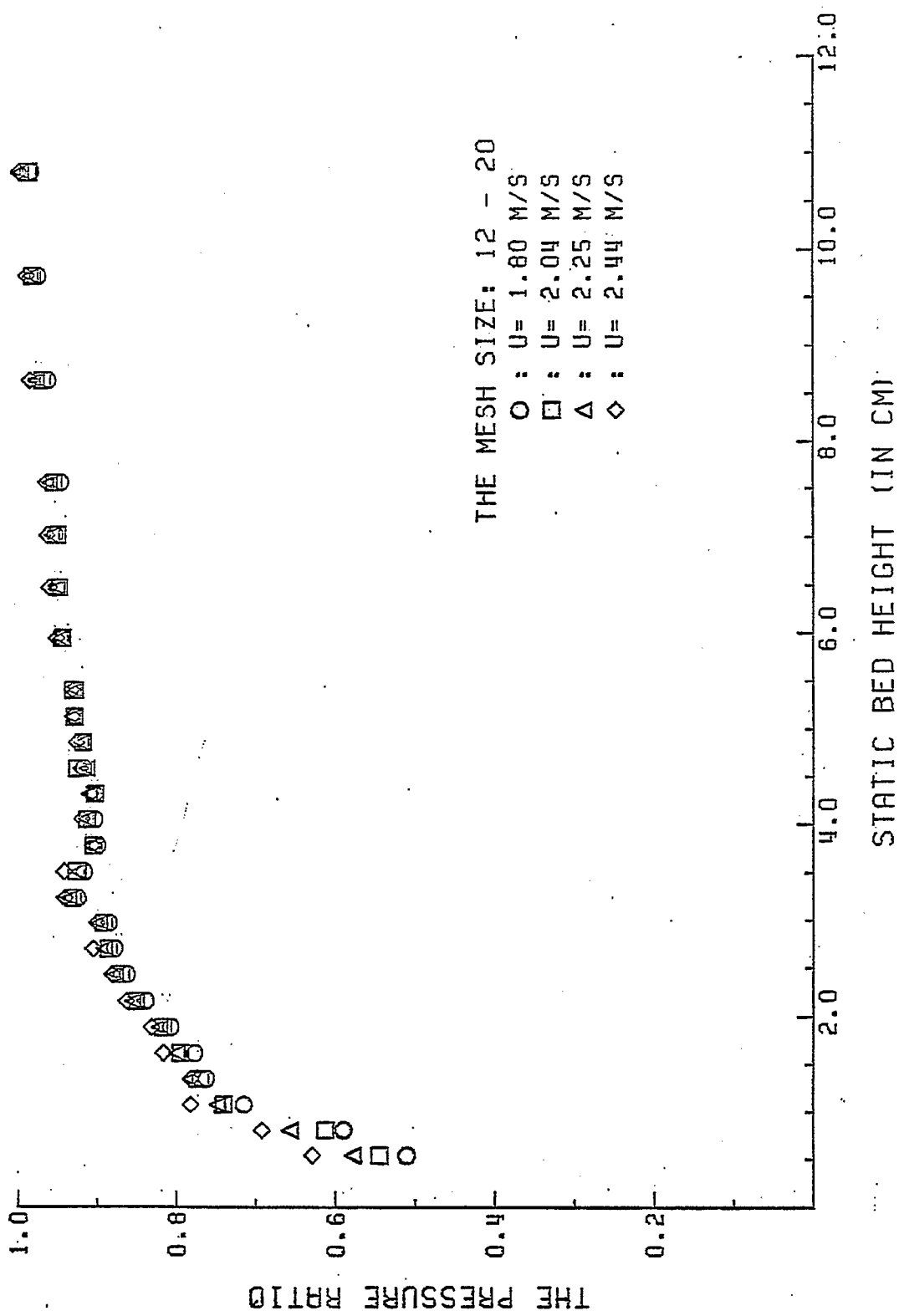


Figure 3.4(b) The Bed Pressure Drop in a Shallow Fluidized Bed of Spherical Alumina Particles (-12+20 Mesh).

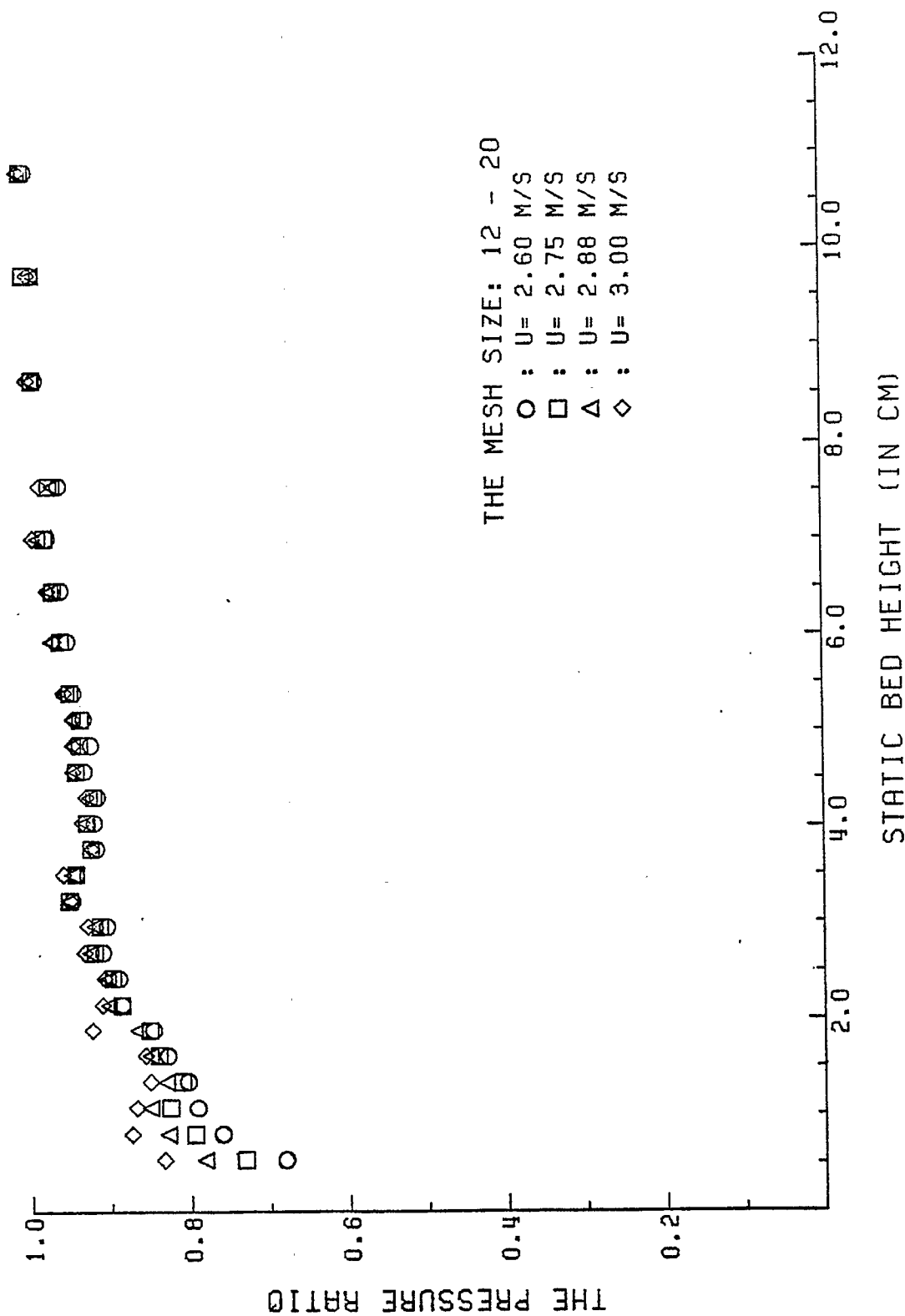


Figure 3.4(c) The Bed Pressure Drop in a Shallow Fluidized Bed of Spherical Alumina Particles (-12+20 Mesh).

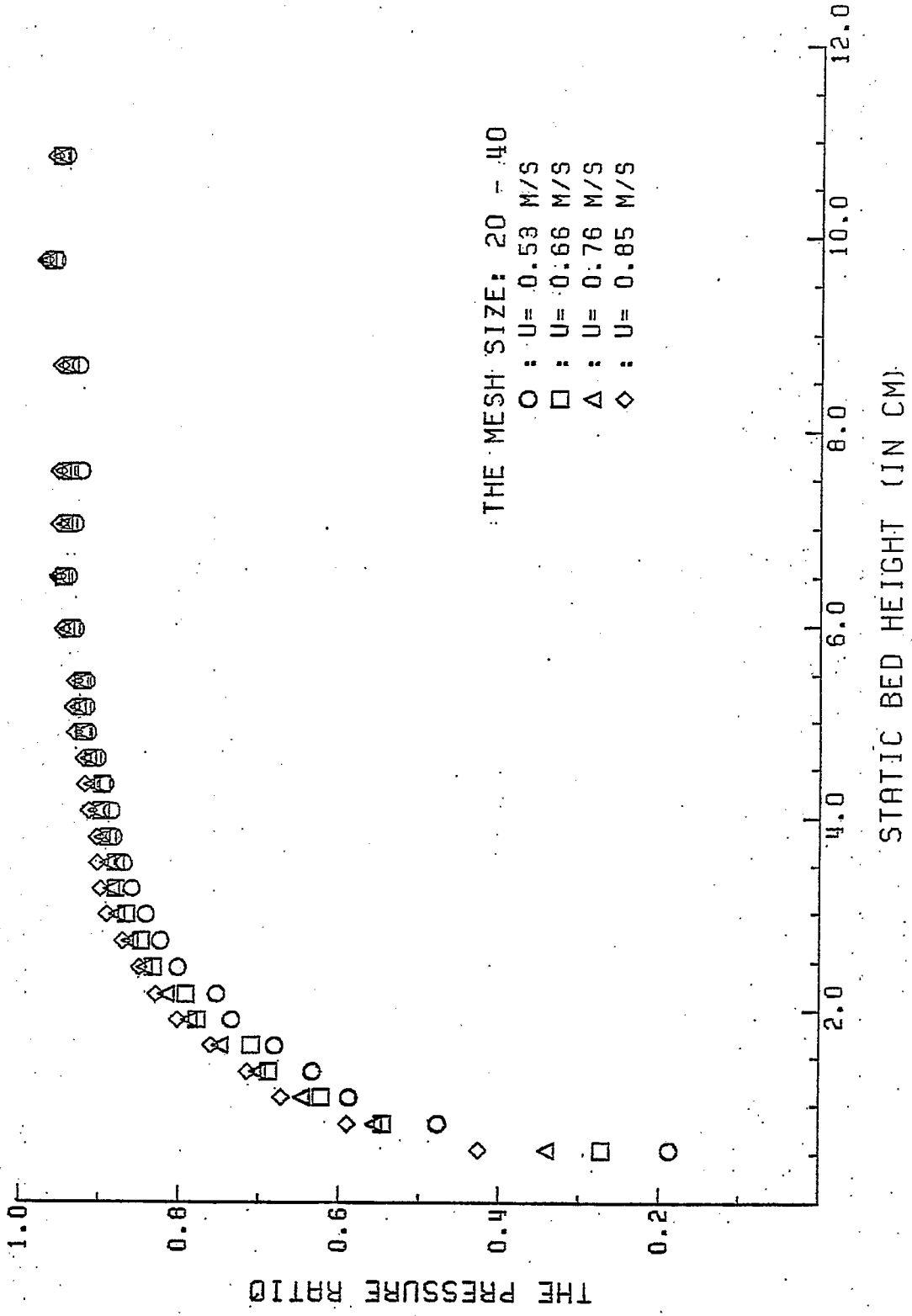


Figure 3.5(a) The Bed Pressure Drop in a Shallow Fluidized Bed of Spherical Alumina Particles (-20+40 Mesh).

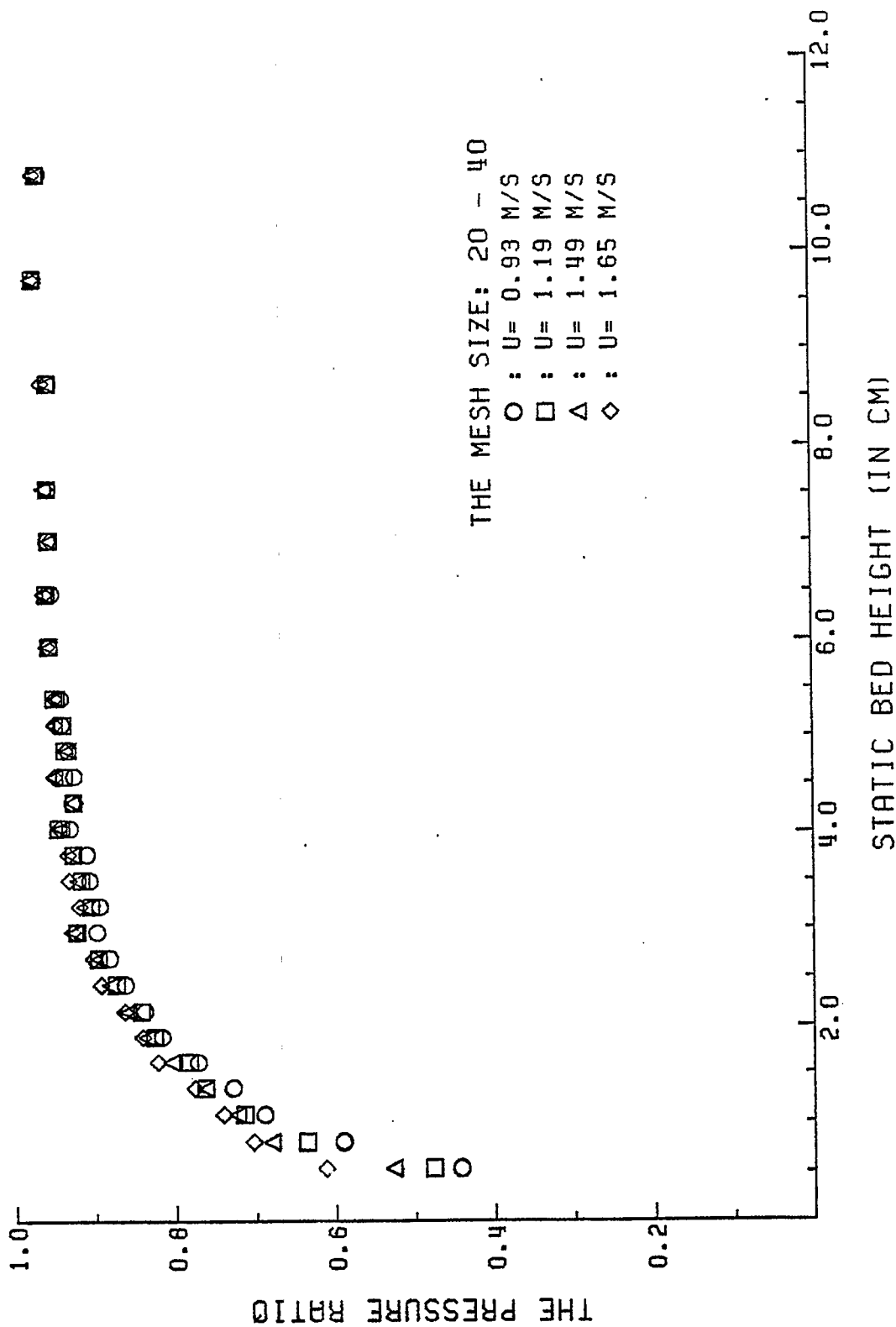


Figure 3.5(b) The Bed Pressure Drop in a Shallow Fluidized Bed of Spherical Alumina Particles (~20+40 Mesh).

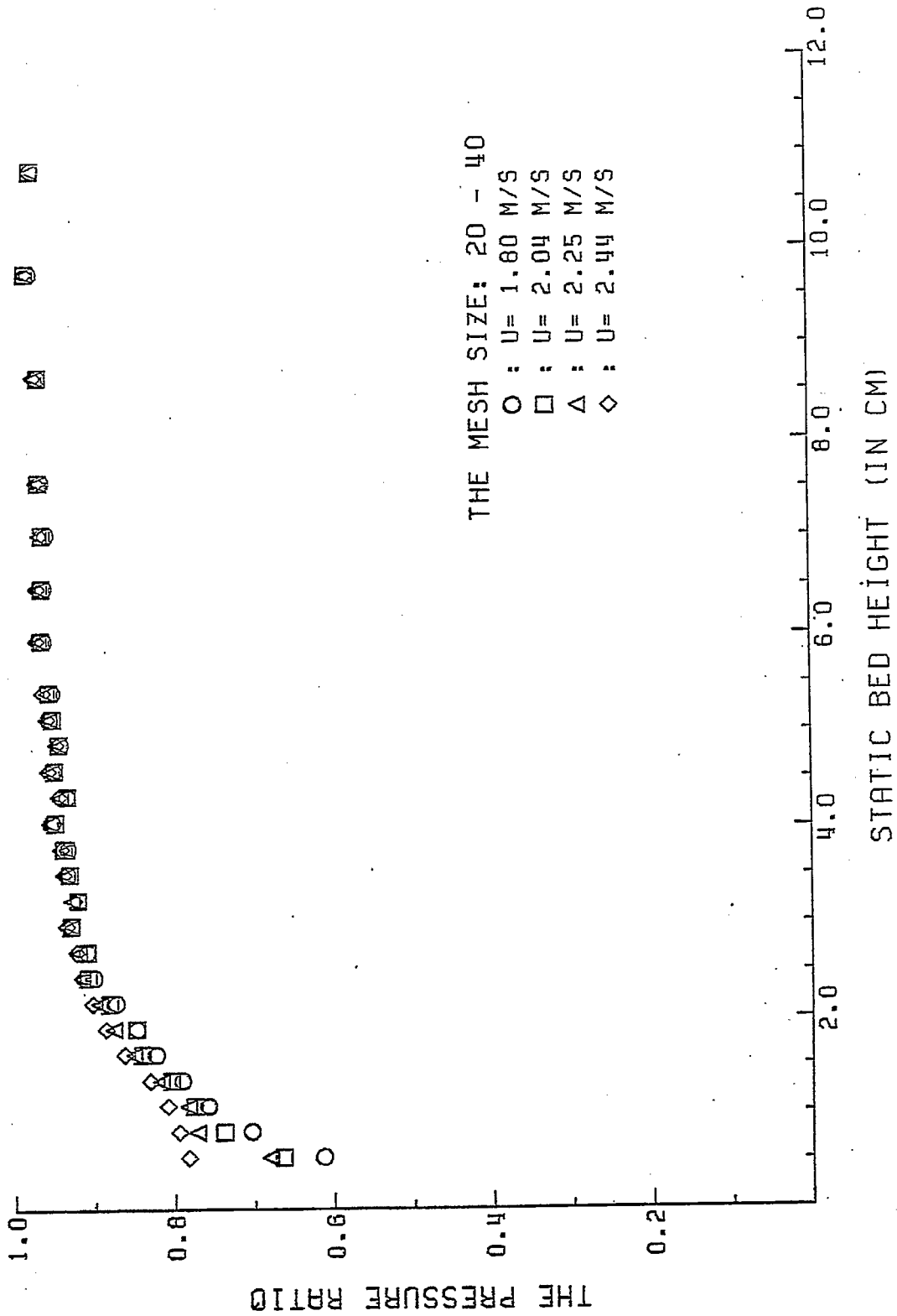


Figure 3.5(c) The Bed Pressure Drop in a Shallow Fluidized Bed of Spherical Alumina Particles (-20+40 Mesh).

Table 3.4

A Summary of Representative Investigations on Heat Transfer from Shallow Fluidized Beds to Immersed Heat-Transfer Surfaces

Author(s)	Bed Material and Particle Size (d_p , μm)	Bed Geometry and Dimension	Static Bed Height, cm	Superficial Fluidization Velocity, m/s	Heat-Transfer Surface	Elevation of Temperature Probe in Bed, cm
1. Atkinson (1974)	Zircon sand (138 μm) Silica sand (157 μm) Steel shot (432 μm)	Circular ($D_b=0.534$ m) Rectangular (102x305 107x305 mm)	2.5-7.9	0.08-1.40	horizontal bare and finned tubes ($D_t=1-5$ cm)	1.3-5.4
2. Pillai (1976)	Silica sand (243-755 μm) Silica carbide (255-787 μm)	Circular ($D_b=0.1$ and 0.14 m)	2.0-8.0	up to 1.5	sphere ($D=5,6,10$ and 15 mm)	50% of bed height
3. Andeen and Glicksman (1976)	Zircon sand (212-513 μm) Sand (360, 510 and 710 μm)	Square (609x609 mm)	0.5-3.0	0.3-2.4	horizontal bare tube ($D_t=19.2$ mm)	2
4. Al Ali and Broughton (1977)	Sand (151, 253 and 345 μm) Alumina (1100 μm)	Rectangular (600x150 mm)	2.8-5.0	0.1-1.1	horizontal bare tube ($D_t=14.3$ mm)	0.72-7.3
5. Abu Baker (1981)	Charcoal (165, 342, 480 μm)	Circular ($D_b=278$ mm)	0.7-13.0	0.1-0.8	horizontal bare tube ($D_t=30$ mm)	4.4-9.3

increased with decreasing tube elevation. Al Ali (1977) interpreted this experimental disagreement by noting that (a) in the entry region of the bed, particularly near the distributor plate, the bed temperature was different from that in the bulk region of the bed; (b) the heat transfer mechanisms in different elevations of the bed depth could be different. Al Ali (1977) also observed some interactive effects of particle properties and tube elevation on the bed-to-surface heat transfer coefficient. For example, he found that the maximum heat transfer coefficient increased with increasing tube elevation for small sand particles ($d_p = 151, 253, 345 \mu\text{m}$), but it decreased with increasing tube elevation for large alumina particles ($d_p = 1,100 \mu\text{m}$). Therefore, one may conclude that the quantitative effect of tube elevation on the bed-to-surface heat transfer coefficient is not well-established. Further, little is known about the interactive effects of tube elevation and other variables such as tube diameter, bed height and particle size on the bed-to-surface heat transfer.

The reported data have also revealed some discrepancy about the effect of static bed height on the bed-to-surface heat transfer coefficient. For example, Andeen and Glicksman (1976) found a maximum bed-to-surface heat transfer coefficient at a static bed height between 1.5 and 2.5 cm; but Al Ali and Broughton (1977) and Abu Baker (1981) both suggested that the bed-to-surface heat transfer coefficient would increase continuously with increasing static bed height. Therefore, there is a need to further examine experimentally the effect of static bed height on the bed-to-surface heat transfer.

Al Ali and Broughton (1977) were apparently the first to observe the "cloud zone effect" in shallow-bed heat transfer. In particular, they have observed much greater bed-to-surface heat transfer coefficient when the heat-transfer surface was placed in the cloud zone, in which an intensive gas bubbling was present. This reported investigation has suggested the importance of examining the quantitative effect of the elevation of heat-transfer surface on shallow-bed heat transfer.

The existing literature has indicated that no generally applicable heat-transfer correlations are available for shallow-bed design purposes. Little is known about the quantitative effects of particle properties, bed configurations and fluidization conditions on shallow-bed heat transfer. Therefore, a quantitative experimental study on shallow-bed heat transfer is being conducted in the present project.

3.2.2 Experimental System

The shallow bed used is essentially the same as the one shown previously in Figure 3.3 (page 50). It is a pyrex glass column with an inside diameter of 10.16 cm. The fluidized particles and their size ranges are identical to those specified in Table 3.2 (page 51). The air fluidizing velocity is determined by an orifice meter connected to a manometer, as shown in Figure 3.2.

The design of the bed heater and temperature probe is illustrated schematically in Figure 3.6. The temperature probe is suspended in the bed so that the heat-transfer tube elevation can be varied. A copper tube encloses the outside of the cartridge heater in order to reduce the temperature variation on the heater surface; and a brass foil is placed outside of the copper tube so as to maintain a smooth heating surface.

3.2.3 Experimental Results and Discussion

Table 3.5 summarizes the ranges of experimental variables and conditions in initial bed-to-surface heat transfer measurements in the shallow fluidized bed. The key results from the initial experiments are described below.

A. Minimum Fluidization Velocity and Superficial Gas Velocities

For each particle size range, the minimum fluidization velocity, u_{mf} , was determined by measuring the bed pressure drop at different superficial gas velocities. The results are illustrated in Figures 3.7(a)-(c). These figures were used to determine the range of superficial gas velocities within which the bed-to-surface heat transfer coefficient was measured.

B. Effect of Superficial Gas Velocity

The dependence of the bed-to-surface heat transfer coefficient on superficial gas velocity in a shallow fluidized bed of -40+60 mesh alumina particles with a laminated distributor plate is illustrated in Figure 3.8(a). When the heat-transfer tube elevation (i.e., the distance from the center line of the heater to the plate) is 20 mm or higher, the heat transfer coefficient is almost constant for each position. This is similar to the dependence observed in a deep bed. However, the data for the tube at 10 mm show an entirely different behavior: the heat transfer coefficient increases monotonically with increasing superficial gas velocity. This increase is more significant when using a laminated distributor plate compared to a perforated plate having a hole diameter of 1.5 mm and 2.2% open area, as illustrated in Figure 3.8(b). This

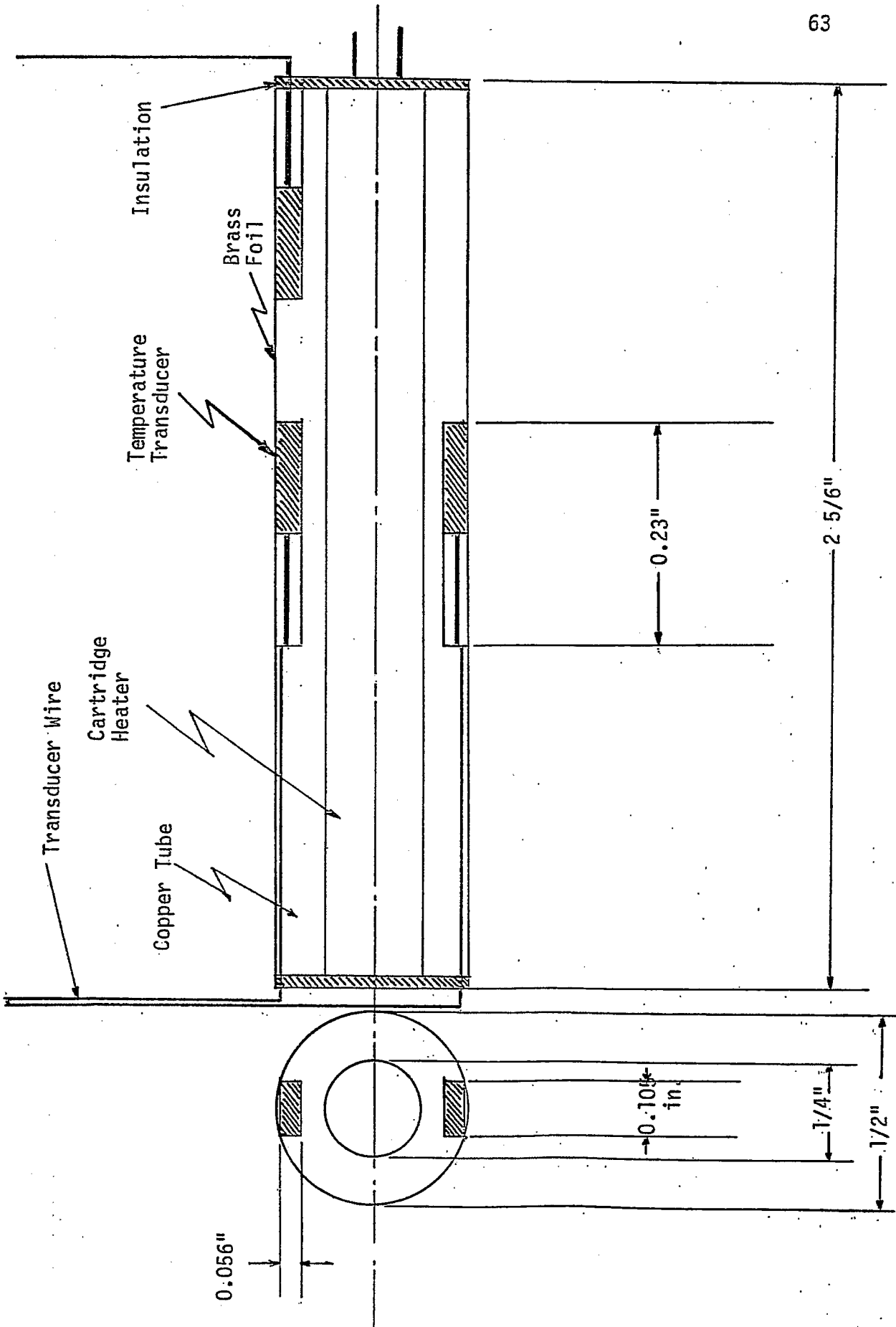


Figure 3.6 A Schematic Diagram of the Experimental System for Shallow-Bed Heat Transfer Studies

Table 3.5

Range of Experimental Variables and Conditions in Initial Bed-to-Surface Heat Transfer Measurements in a Shallow Fluidized Bed

Run Series	Distributor Type	Mean Alumina Particle Diameter (μm)	Static Bed Height, cm	Heat-Transfer Tube Elevation cm	Superficial Fluidization Velocity m/s
1	laminated	310	1-4	1-4	0.67-2.13
2	perforated	310	2-4	1-4	0.67-1.81
3	perforated	610	2-4	1-3	0.67-1.81

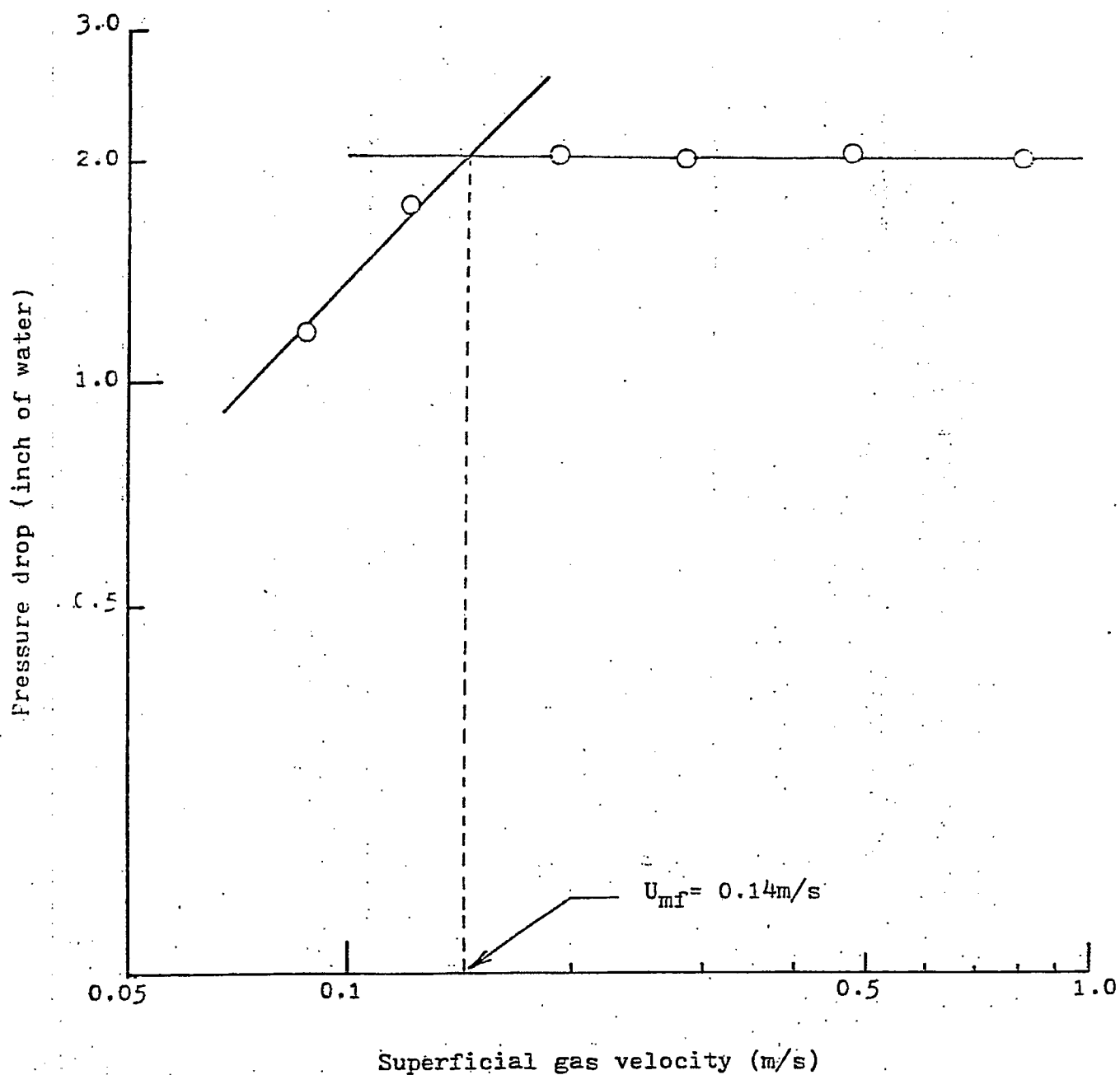


Figure 3.7(a) Minimum Fluidization Velocity of -40+60 Mesh Alumina Particles (Mean Particle Diameter = 310 μm).

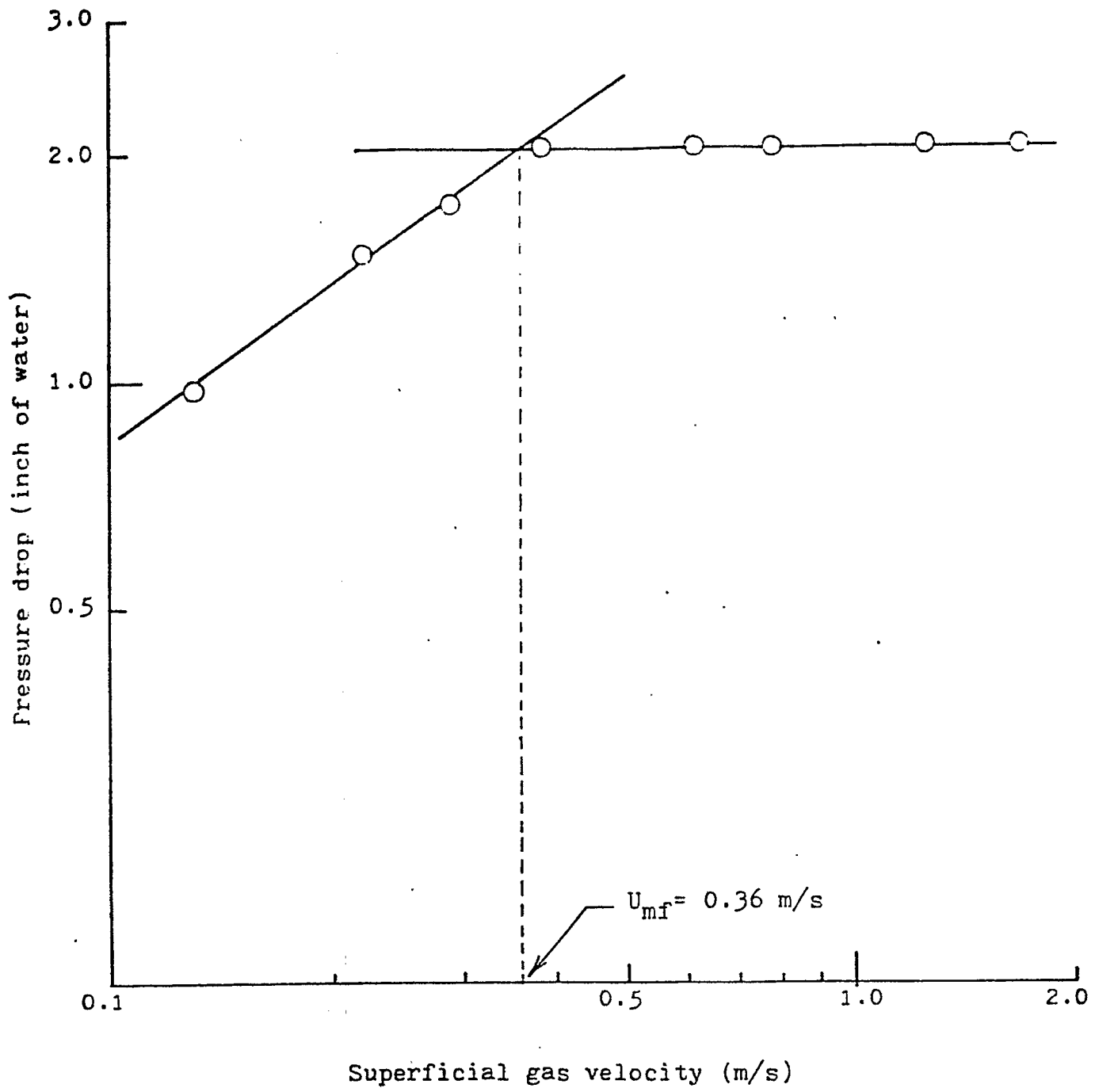


Figure 3.7(b) Minimum Fluidization Velocities of -10+20 Mesh Alumina Particles (Mean Particle Diameter = 610 μm)

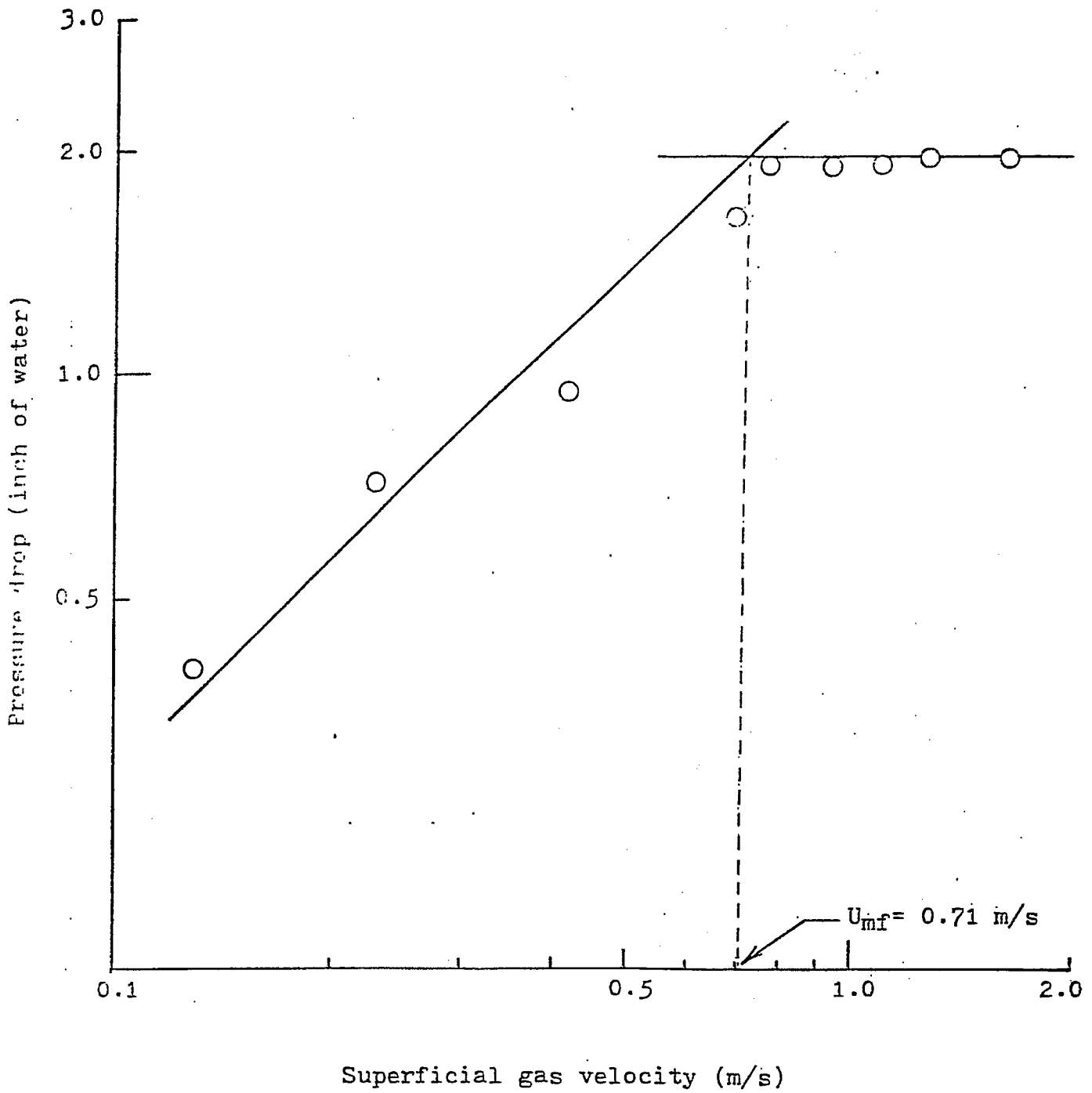


Figure 3.7(c) Minimum Fluidization Velocity of -12+20 Mesh Alumina Particles (Mean Particle Diameter = 1,100 μm)

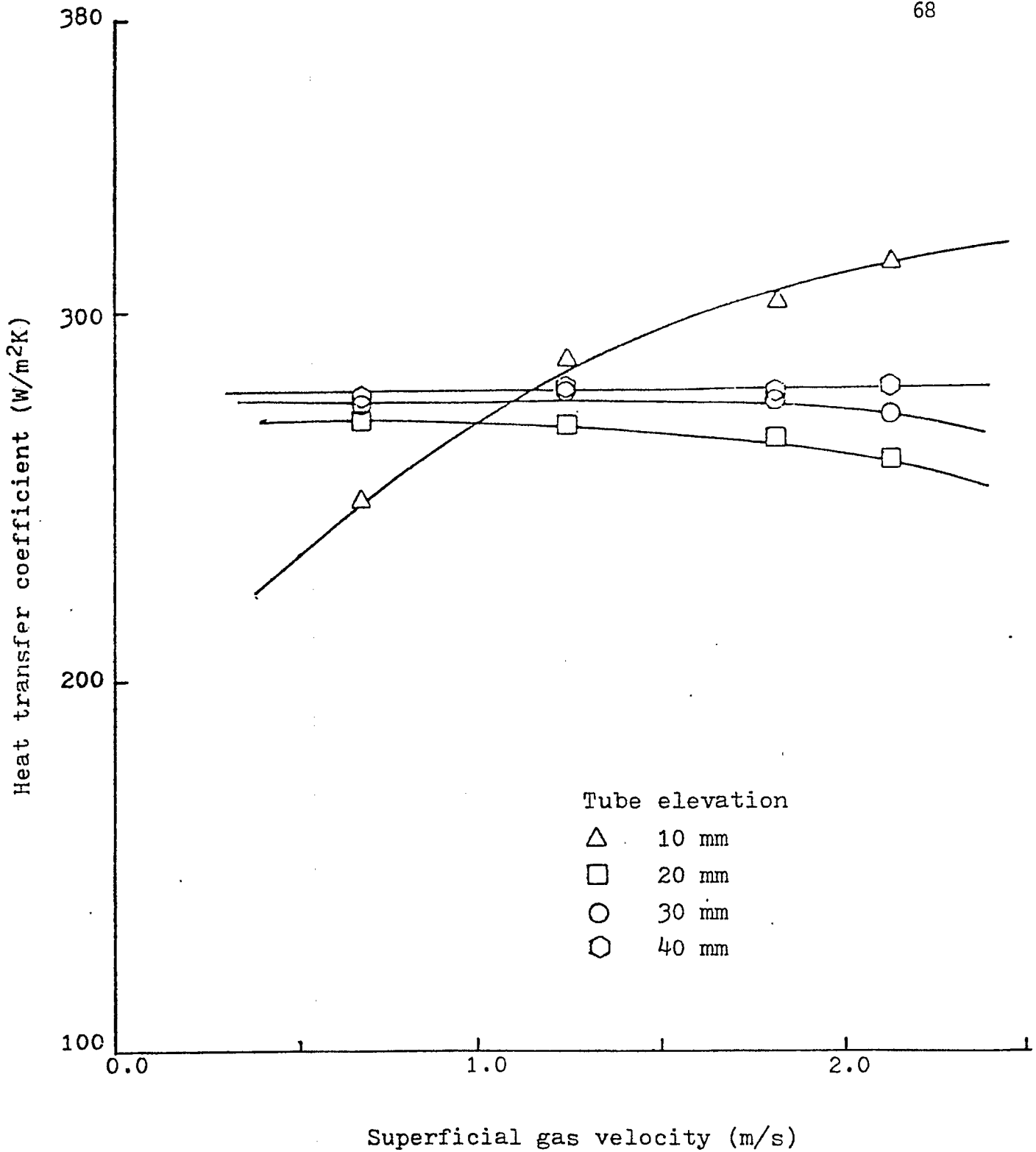


Figure 3.8(a) Effect of Superficial Gas Velocity on the Bed-to-Surface Heat Transfer Coefficient in a Shallow Fluidized Bed of -40+60 Mesh Alumina Particles with a Laminated Distributor Plate

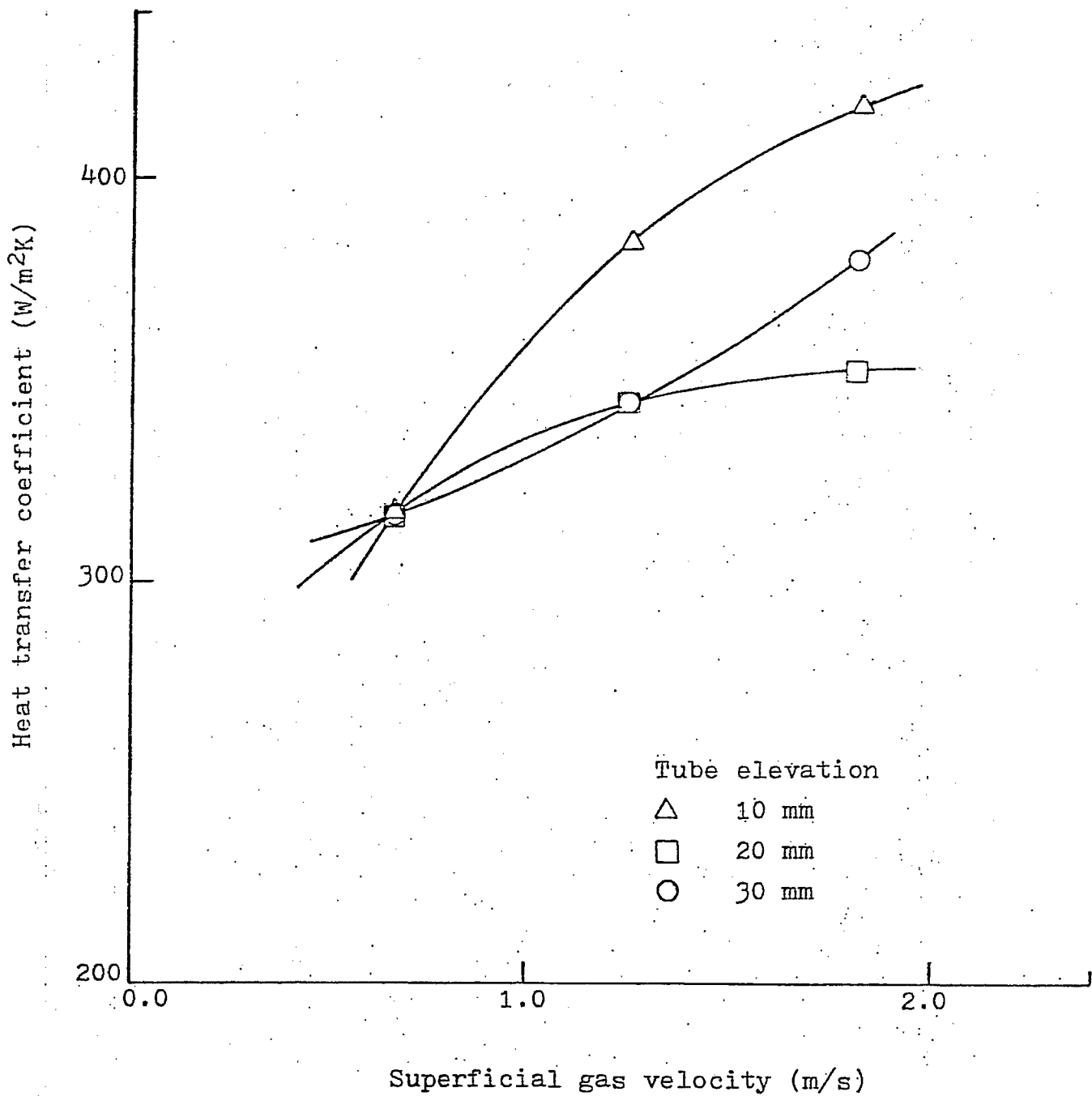


Figure 3.8(b) Effect of Superficial Gas Velocity on the Bed-to-Surface Heat Transfer Coefficient in a Shallow Fluidized Bed of -40+60 Mesh Alumina Particles with a Perforated Distributor Plate

special behavior may be attributed to the jet penetrating effect. For the perforated plate, the jet penetration depth, as calculated from the correlation of Zenz (1968), is about 30 mm for a superficial gas velocity at 1 m/s, which means that the tube is always immersed within the jet region in the experiments. For the laminated plate, the gas jet is much smaller due to the special structure of the plate. Therefore, the only case in which the jet effect may be observed is for a tube elevation of 10 mm, as shown in Figure 3.8(a).

In the jet region, the movement of the particles is so vigorous that the particle residence time becomes relatively short. Thus, the bed-to-surface heat transfer rate becomes larger than that outside the jet region. Since the jets penetrate further when the superficial gas velocity is increased, the jet effect becomes more significant as gas velocity is increased. As the jet region would usually occupy a large portion of a shallow bed, this special heat transfer behavior is worthy of further investigation. Note also that when the gas velocity is high, erosion of the heat-transfer surface could become a serious problem.

C. Effect of Static Bed Height

Figures 3.9(a)-(b) illustrate the effect of static bed height on the bed-to-surface heat transfer coefficient at different tube elevations in a shallow fluidized bed of -40+60 mesh aluminum particles. Figure 3.9(a) shows a maximum heat transfer coefficient at a static bed height of 30 mm when a perforated distributor plate is used. By contrast, Figure 3.9(b) demonstrates a maximum heat transfer coefficient at a static bed height of about 40 mm when a laminated distributor plate is used. As shown in both figures, a heat-transfer tube elevation of 10 mm appeared to give the highest heat transfer coefficient.

The data shown in Figures 3.9(a)-(b) suggest that the distributor design affects the bed-to-surface heat transfer in a shallow fluidized bed. At given fluidization conditions, an optimum static bed height apparently exists for each distributor design. Further work on solids mixing in shallow fluidized beds may be needed to quantitatively identify such an optimum static bed height.

D. Effect of Tube Elevation

The effect of heat-transfer tube elevation on the bed-to-surface heat transfer coefficient in a shallow bed of -40+60 mesh alumina particles is illustrated in Figures 3.10(a)-(c). The "cloud zone effect" in shallow-bed heat transfer, previously observed by Al Ali and Broughton (1977), can be seen from Figure

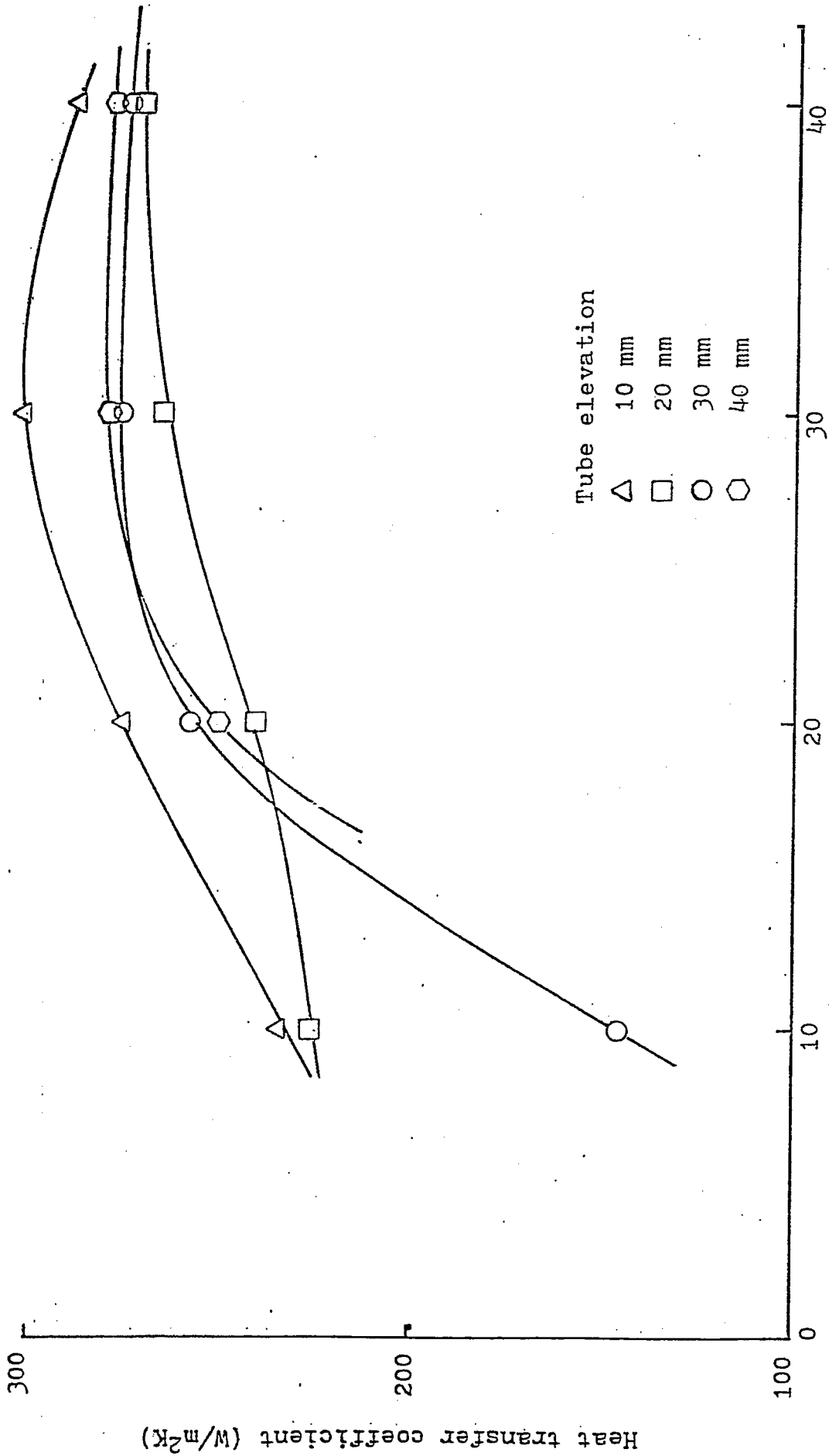


Figure 3.9(a) Effect of Static Bed Height on the Bed-to-Surface Heat Transfer Coefficient in a Shallow Fluidized Bed of -40+60 Mesh Alumina Particles with a Perforated Distributor Plate.

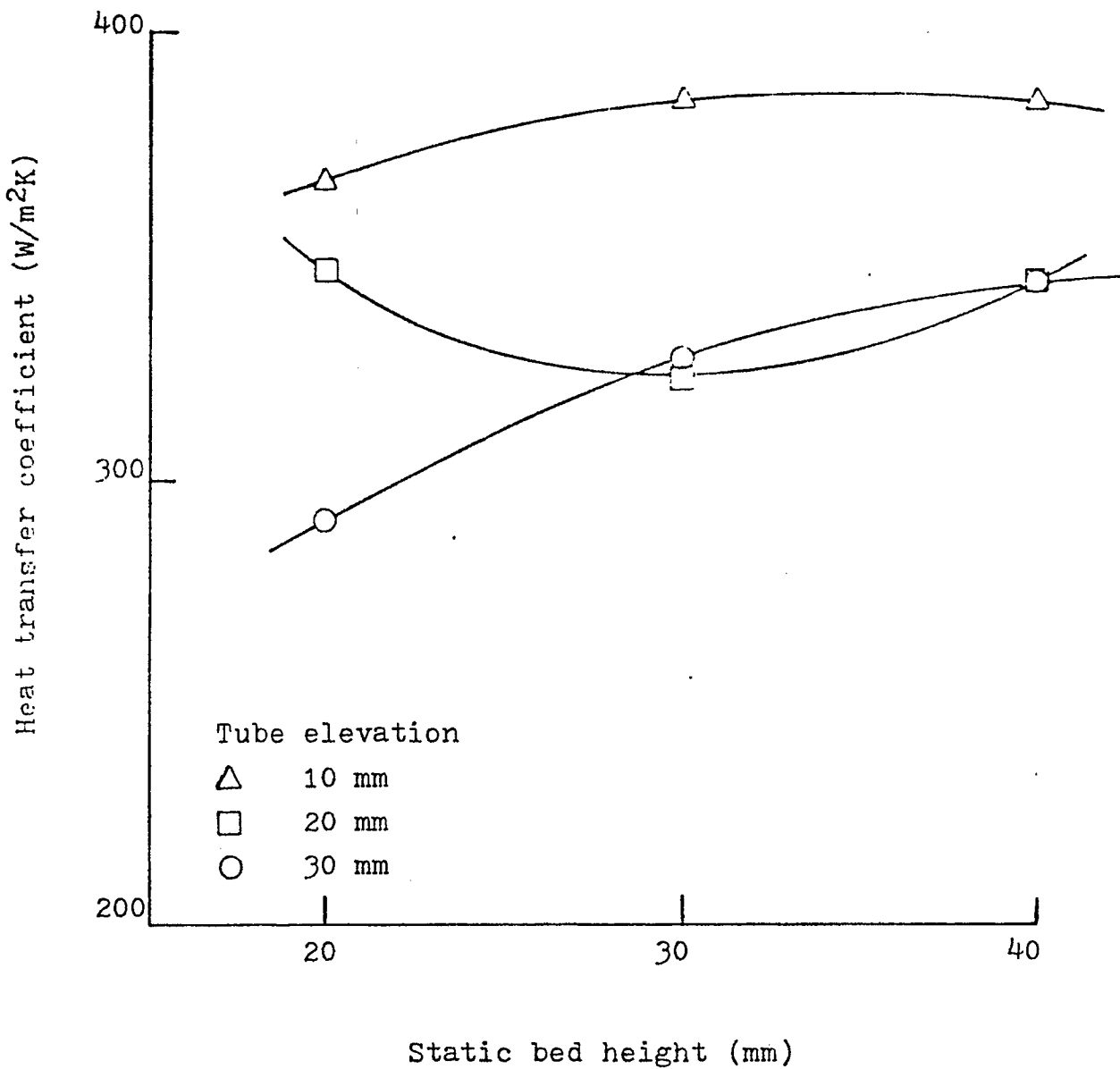


Figure 3.9(b) Effect of Static Bed Height on the Bed-to-Surface Heat Transfer Coefficient in a Shallow Fluidized Bed of -40+60 Mesh Alumina Particles with a Laminated Distributor Plate.

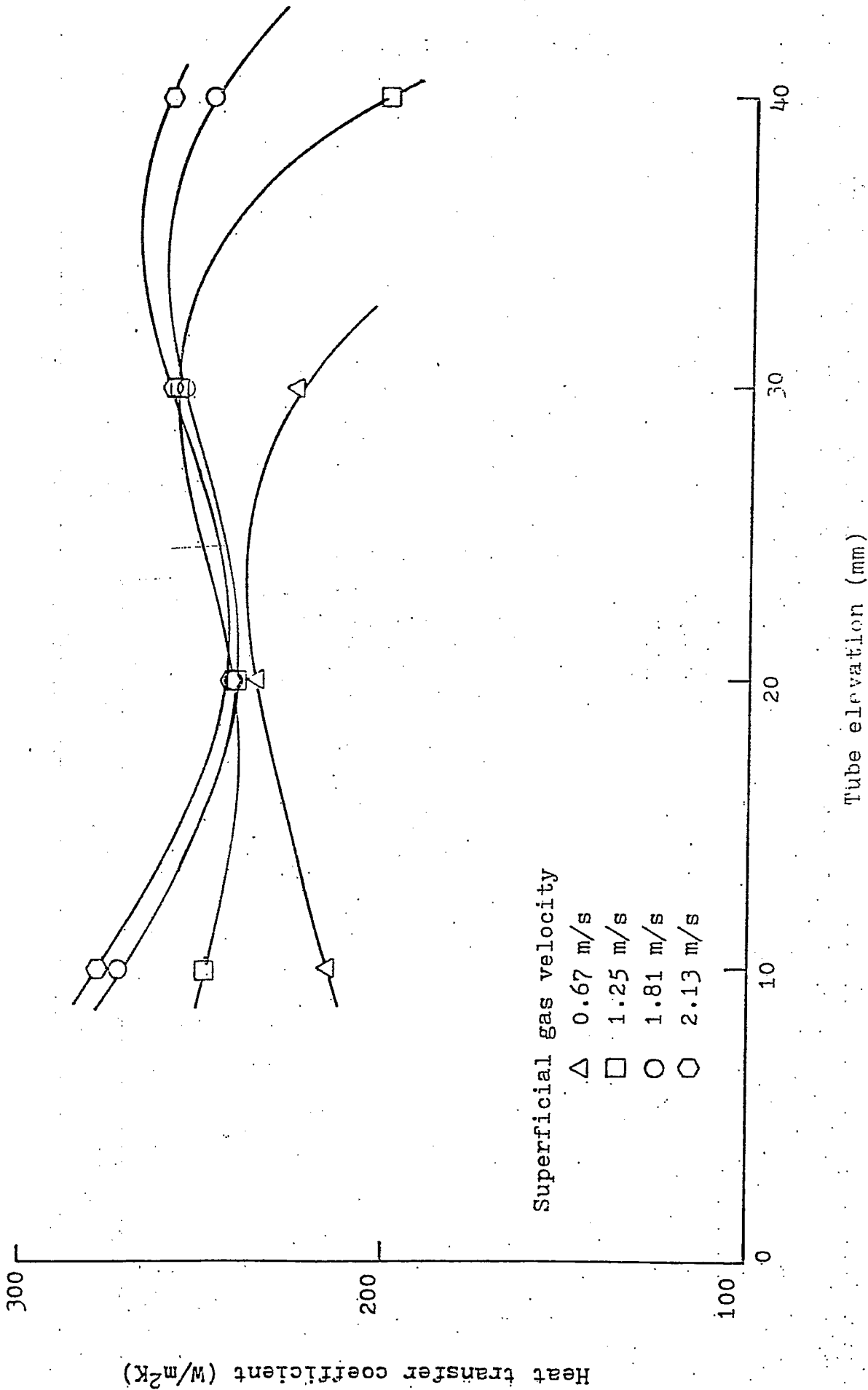


Figure 3.10(a) Effect of Heat-Transfer Tube Elevation on the Bed-to-Surface Heat Transfer Coefficient in a Shallow Fluidized Bed of -40+60 Mesh Alumina Particles with a Laminated Distributor Plate and at a Static Bed Height of 20 mm.

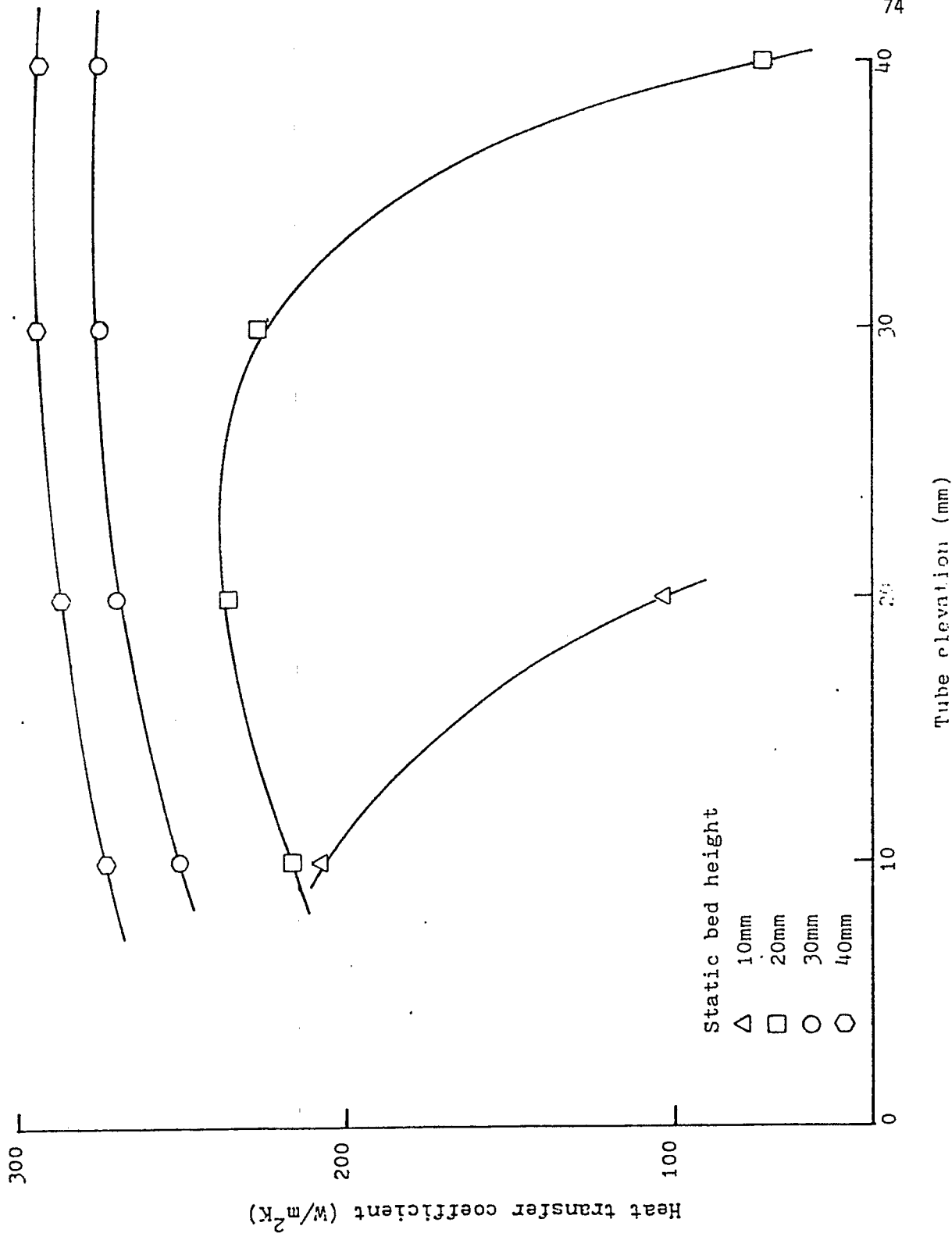


Figure 3.10(b) Effect of Heat-Transfer Tube Elevation on the Bed-to-Surface Heat Transfer Coefficient in a Shallow Fluidized Bed of -40+60 Mesh Alumina Particles with a Laminated Plate and at Superficial Gas Velocity of 0.67 m/s.

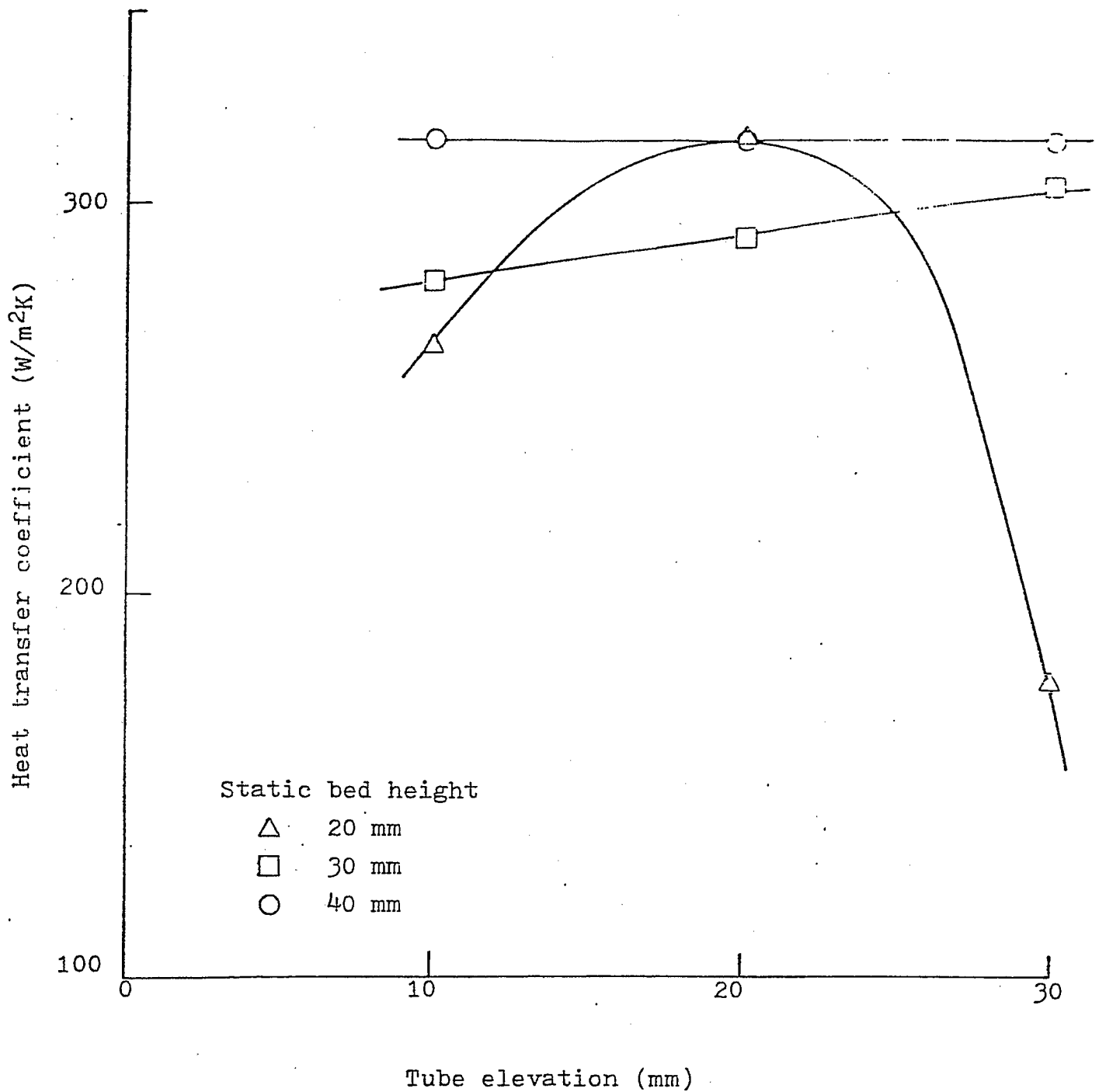


Figure 3.10(c) Effect of Heat-Transfer Tube Elevation on the Bed-to-Surface Heat Transfer Coefficient in a Shallow Fluidized Bed of -40+60 Mesh Alumina Particles with a Perforated Distributor Plate and at a Superficial Gas Velocity of 0.67 m/s.

3.10(a). At low superficial gas velocities, a maximum in the heat transfer coefficient is observed when the heat-transfer tube is placed above the static bed height of 20 mm, i.e., when the tube elevation is greater than 20 mm. This is apparently caused by the formation of a cloud-like region (with an intensive gas bubbling) in the bed by the splashed particles. When the gas velocity is increased, particles are splashed higher, leading to a maximum heat transfer coefficient at higher tube elevations.

Figure 3.10(b) shows that as the static bed height is increased, the increase in the bed-to-surface heat transfer coefficient due to the cloud-zone effect becomes less significant. This result also suggests that the cloud zone is indeed an important regime which affects both hydrodynamics and heat transfer in shallow fluidized beds.

Figure 3.10(c) illustrates the similar effect of static bed height on the bed-to-surface heat transfer coefficient when a perforated distributor plate was used. The result shows that the vigorous particle splashing caused by gas jets through the perforated plate leads to a notable increase in the heat transfer coefficient at higher heat-transfer tube elevations above the static bed height of 20 mm.

E. Effect of Particle Size and Distributor Type

Larger particles are known to have a lower bed-to-surface heat transfer coefficient than smaller particles, and this fact is confirmed by the typical experiment result shown in Figure 3.11. For even larger particles, the superficial gas velocity required may be so high that the gas convective component of the bed-to-surface heat transfer coefficient may become more significant. This effect will be investigated in the present project.

The effect of distributor type, previously illustrated in Figures 3.8(a)-(b), 3.9(a)-3.9(b) and 3.10(b)-(c), is further shown in Figure 3.11. At a given superficial gas velocity and with a fixed particle size range, this figure indicates a higher bed-to-surface heat transfer coefficient with a perforated distributor plate. As discussed before, the different penetration depths of gas jets through different distributor plates seem to significantly affect the bed-to-surface heat transfer, and several other distributor types should be used to further investigate this effect in shallow-bed heat transfer.

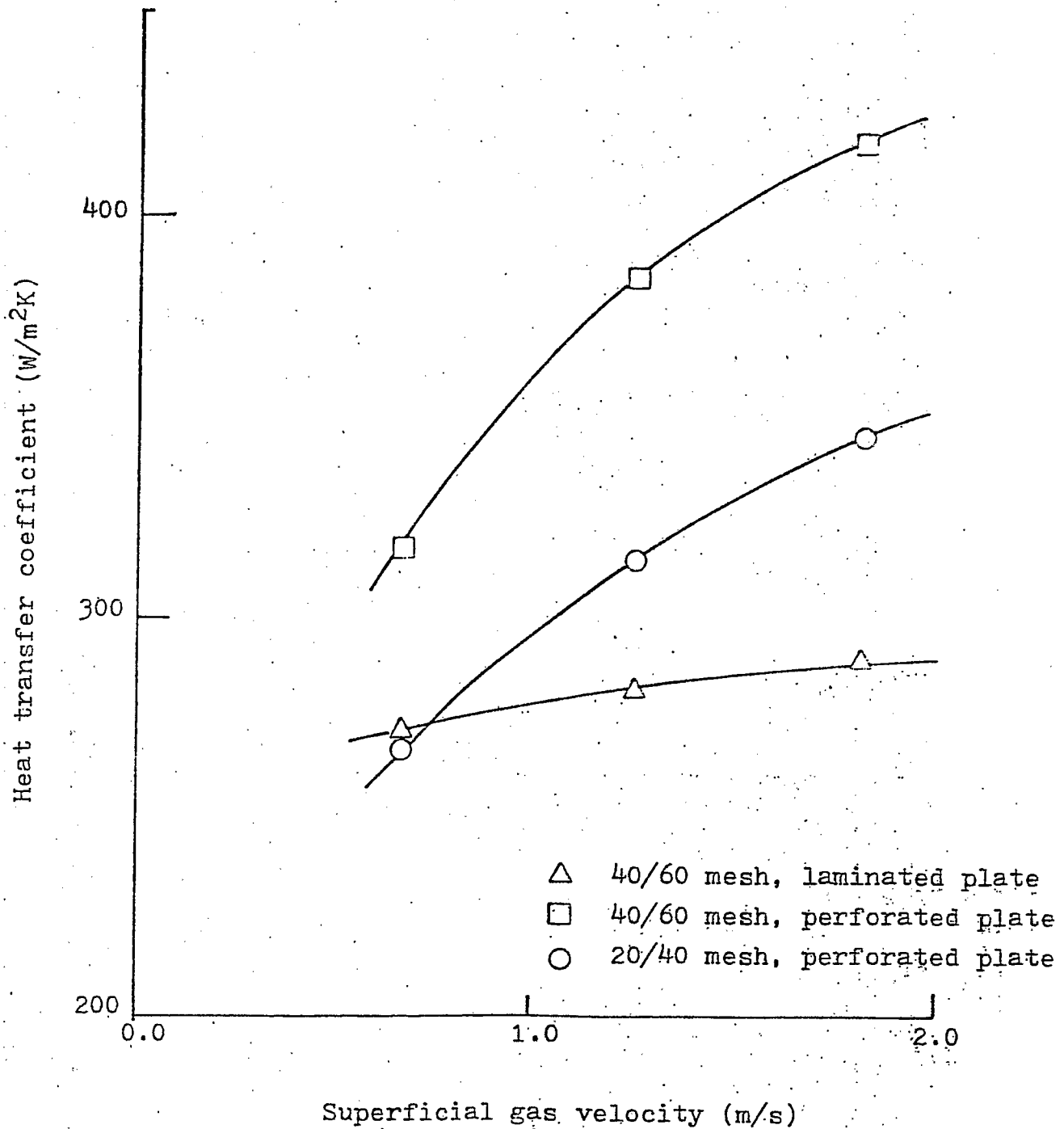


Figure 3.11 Effects of Particle Size and Distributor Type on the Bed-to-Surface Heat Transfer Coefficient in Shallow Fluidized Beds of Alumina Particles at Different Superficial Gas Velocities.

3.3 Heat Transfer in a Heat Tray

3.3.1 Experimental System

As discussed previously in Section 1.1, a key concept of the new fluidized-bed reactor (called "heat tray") being developed for the unsteady-state Fischer-Tropsch synthesis involves alternately exposing the iron catalyst to a large flow of CO-rich (H₂-lean) "supernatant gas" (S-gas) for a short period of time and to a smaller flow of H₂-rich "fluidizing gas" (F-gas) for a long period of time. An experimental heat tray has been designed and constructed for investigating the hydrodynamics and heat transfer in this fluidized-bed reactor. Initial experiments have been conducted to measure the heat transfer coefficient between the flowing supernatant gas and the fluidized bed.

Figures 3.12 and 3.13 show, respectively, a schematic diagram and a photograph of the heat tray system. In the system, building compressed air at a pressure of 80 psig flows through an one-inch pipe to a tee, where it is split to form the F-gas and S-gas streams. Stream flow rates are controlled and measured by separate globe valves and rotameters. The F-gas stream flows directly to the heat tray; and the S-gas stream is heated in a one-inch Sylvania in-line electric-resistance heater before entering the heat tray. The heater is controlled by a Superior Electric Company type 116 powerstat variable-transformer.

Both F-gas and S-gas streams exhaust to the atmosphere through a common exit nozzle which is fitted with a fine porous cloth to collect any entrained particles. Building water supply is circulated through the heat tray for cooling purposes. Water flow rate is measured with a standard rotameter. Temperature transducers, accurate to $\pm 0.1^{\circ}\text{C}$, are located on the water inlet, water exit, F-gas inlet, S-gas inlet and combined gas exhaust streams. A mobile transducer is used to monitor other temperatures, particularly those along different locations in the bed.

Figures 3.14(a)-(b) show the schematic diagrams of the front and side views of the heat tray. The heat tray is rectangular in plan view and is constructed from galvanized sheet metal. It is insulated by fiberglas insulation materials. It is mounted on an angle-iron bracket to facilitate tilting the bed at different angles from its horizontal position. This tilt will provide for solid circulation in the bed. As can be seen in Figure 3.14(a), the F-gas stream first enters a windbox at the bottom of the heat tray. A deflector plate, located in the windbox, evenly distributes the gas flow to the bed. The distributor used is a two-layer Dynapore laminate type constructed from stainless steel. The F-gas stream then fluidizes the solid particles above the immersed,

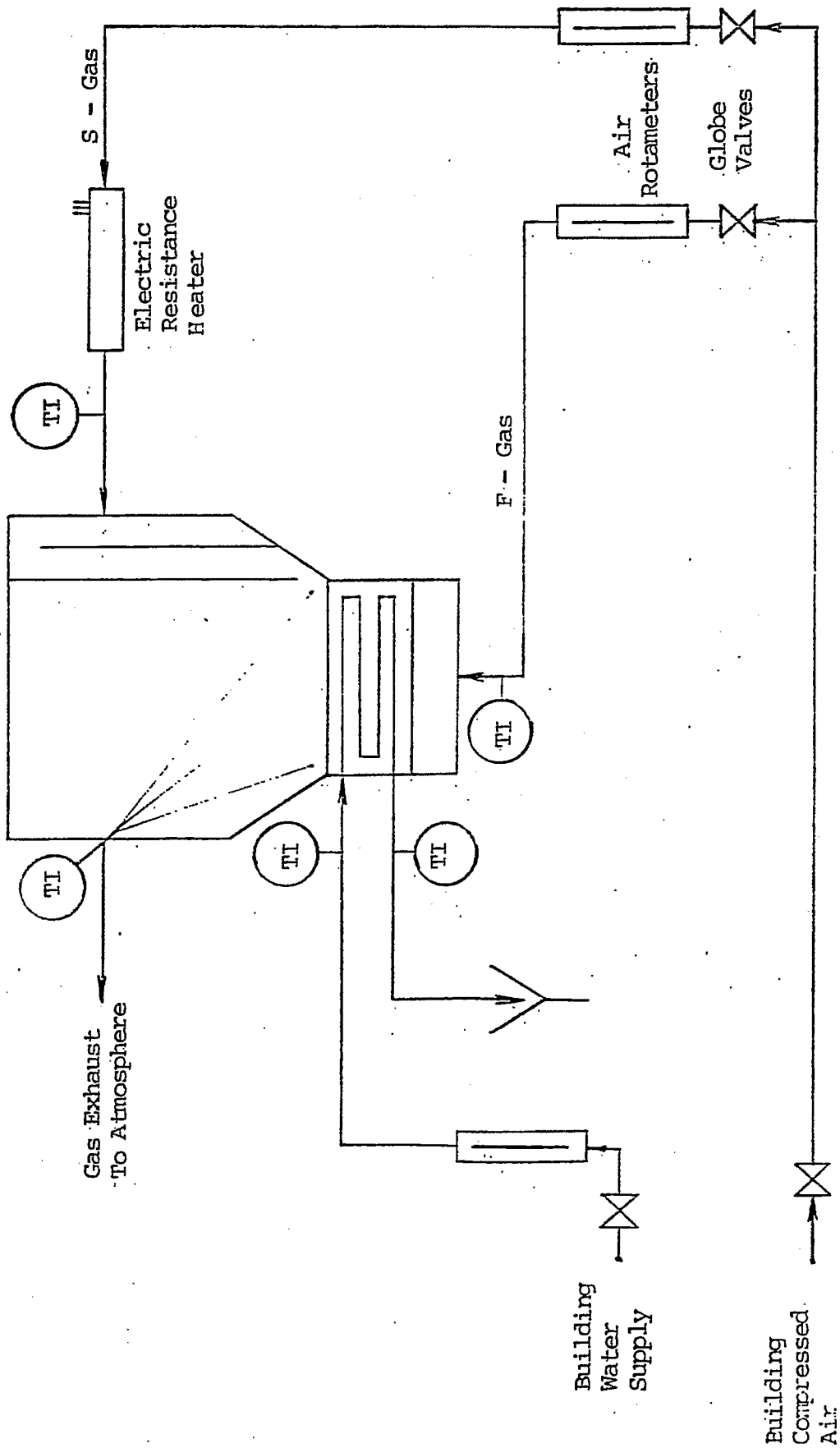


Figure 3.12 A Schematic Diagram of the Heat Tray System.

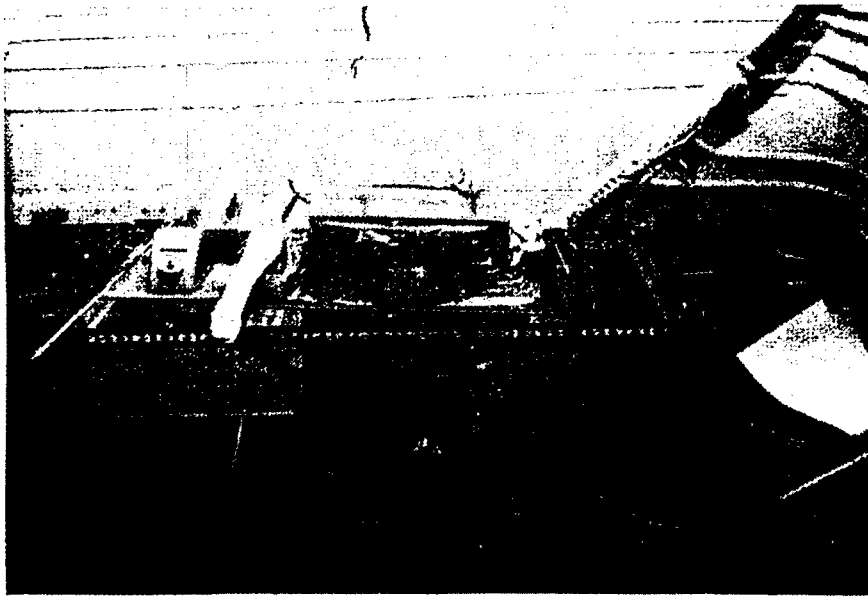


Figure 3.13 A Photograph of the Heat Tray System. Heat Tray and Support Bracket are Located Center Left, Air Supply at Far Left. Rotameters are Mounted on Support Grid Above Bench. The Following can be Viewed on the Heat Tray: F-Gas Feed (Bottom of Tray); Water Inlet and Outlet (Lower Right Corner of Tray); S-Gas Feed (Upper Right Corner of Tray); Gas Exit, Fitted With Cloth Particle Trap (Upper Left Corner of Tray).

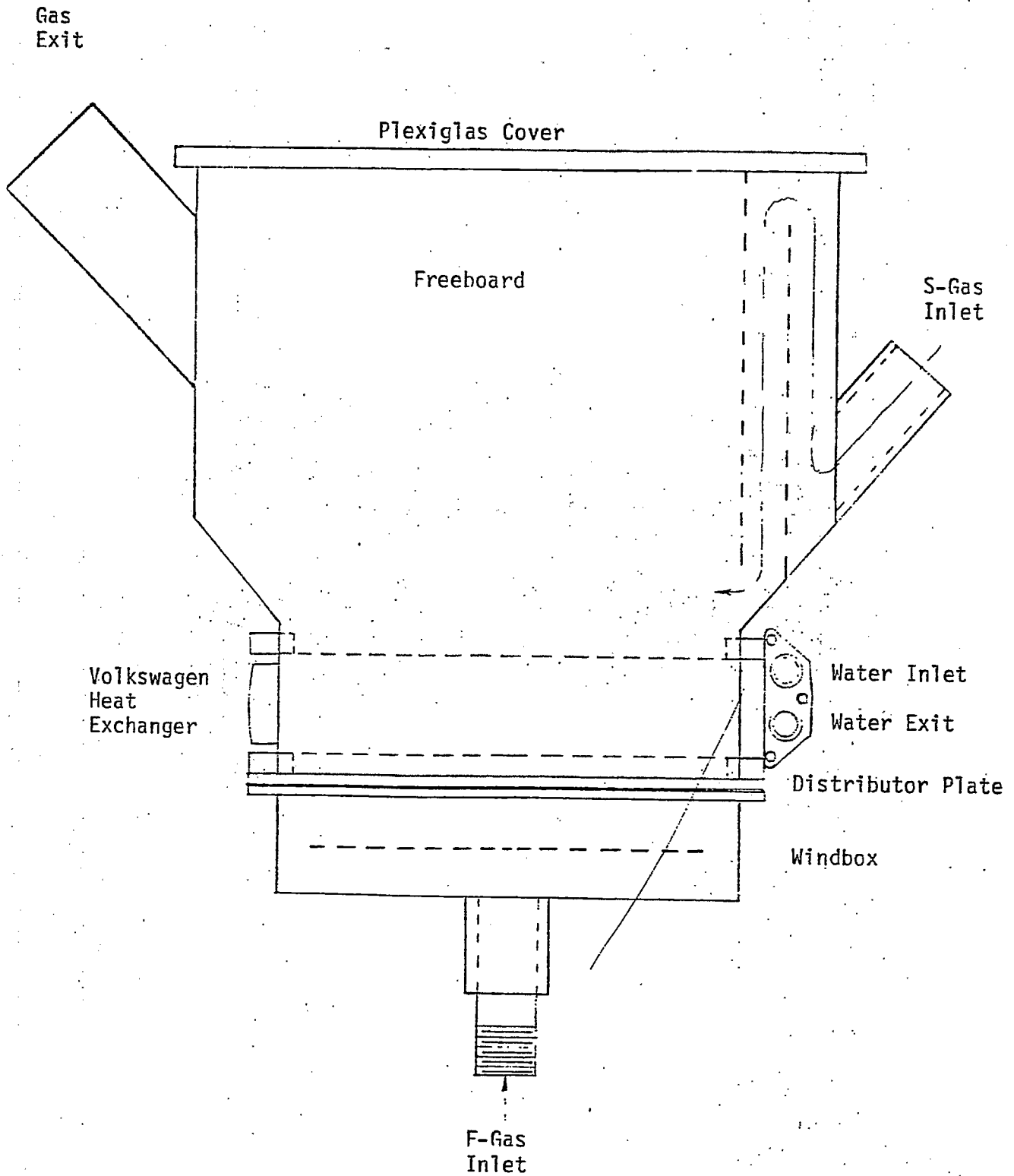


Figure 3.14(a) A Front View of the Heat Tray.

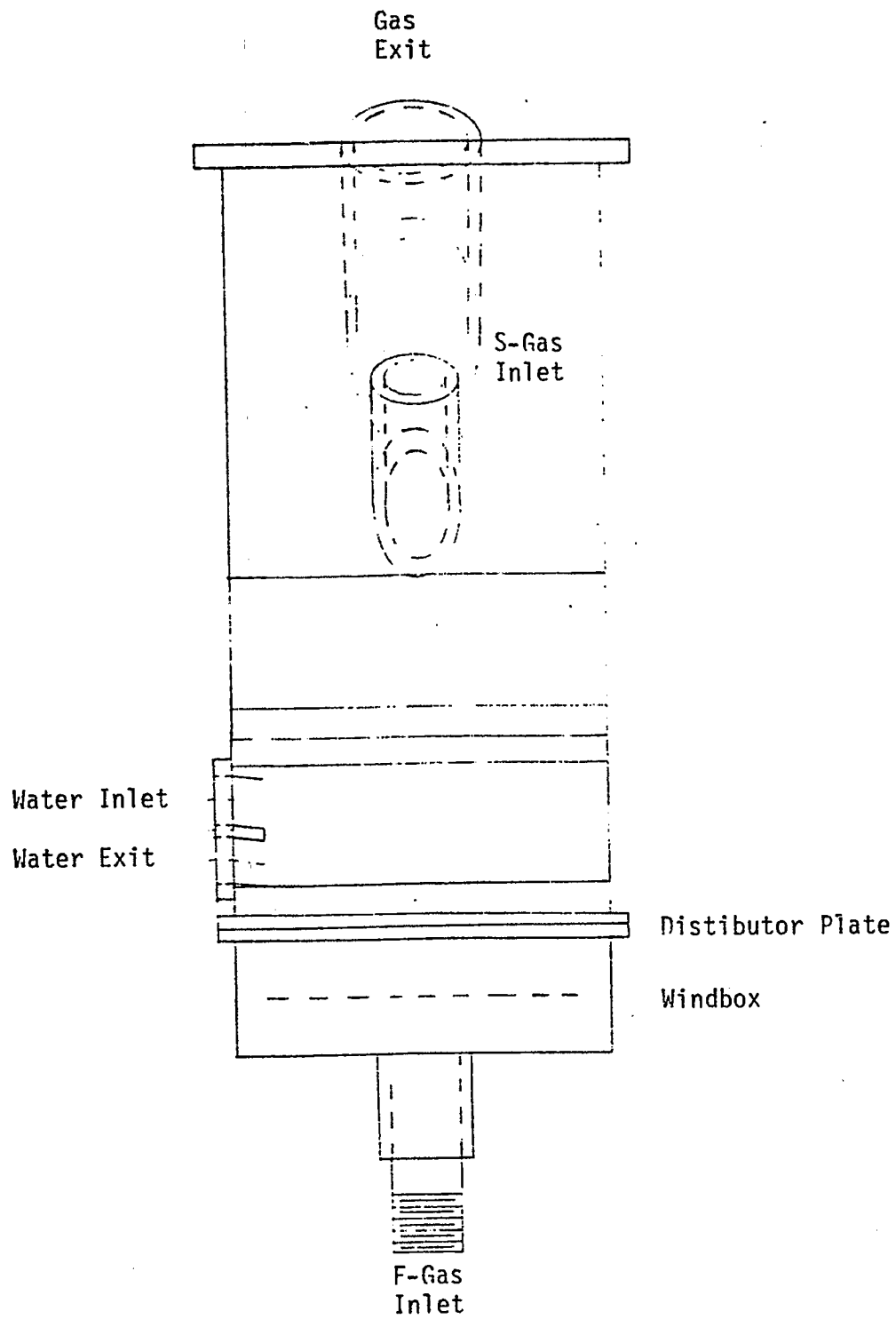


Figure 3.14(b) A Side View of the Heat Tray.

finned heat-transfer tubes which are part of a Volkswagen Rabbit heater. The S-gas stream enters the heat tray through a set of staggered sheet metal plates, which are designed to provide for an even gas flow and for an adjustable gas inlet height. Both the F-gas and S-gas streams are then mixed together in the freeboard zone of the bed and the combined stream exhausts through a common exit nozzle.

3.3.2 Experimental Results and Discussion

Initial experiments have been completed which provide the first data on the heat transfer coefficient between a flowing S-gas stream and a shallow fluidized bed in the heat tray system. The bed particles used in these experiments are spherical Norton Masterbeads, which have a mean diameter of 0.0123 to 0.0441 inches (313 to 1.120 μm) and a density of 229.1 lb/ft³ (3,670 kg/m³). Other information concerning the experimental variables and conditions is summarized in Table 3.6. The experimental results were analyzed using a set of working equations for heat transfer measurements in the heat tray, which are developed in detail in Section 5.3 of the Appendix.

Typical experimental results are illustrated in Figure 3.15, in which the heat transfer coefficients between the S-gas and the fluidized bed are plotted against the ratio of F-gas to S-gas mass flow rates at two S-gas inlet nozzle openings. Decreasing the F-gas flow rate or increasing the S-gas flow rate leads to higher heat transfer coefficients. In particular, the use of a small S-gas inlet nozzle opening at a high S-gas flow rate gives the highest heat transfer coefficient of about 1,240 Btu/hr-ft²°F (7,040 W/m²-°K). It appears that a smaller S-gas inlet nozzle opening results in S-gas injection closer to the bed surface and in more intimate contact between the S-gas and the bed.

Figure 3.16 illustrates the effect of S-gas inlet velocity on the heat transfer coefficient between the S-gas and the bed for both S-gas inlet nozzle openings. Increasing S-gas inlet velocities results in higher heat transfer coefficients.

The preliminary results described above show very high rates of heat transfer in the many thousands of watts per degree Kelvin per square meter of projected horizontal bed surface; and provide encouraging support of the new fluidized-bed reactor concept for Fischer-Tropsch synthesis, particularly in the use of immersed heat-transfer surface for recovering reaction heat in a shallow bed. Work is continuing to experimentally correlate the heat transfer coefficient with such variables as relative F-gas and S-gas flow rates, S-gas inlet velocity, and bed horizontal tilt angle. Provisions will also be made to reduce the freeboard height to promote better contact between the S-gas and the bed.

Table 3.6

Ranges of Experimental Variables and Conditions in Initial Measurements of Heat Transfer Coefficient Between A Flowing Supernatant Gas (S-Gas) Stream and A Shallow Fluidized Bed

Operating Variable	Level of Variable	
	(-)	(+)
1. F-gas mass flow rate, lb/hr	70	270
2. S-gas mass flow rate, lb/hr	70	270
3. Superficial fluidization velocity, ft/sec	0.63	2.43
4. Mean particle diameter, in. (μm)	0.0123 (313)	0.0441 (1,120)
5. Bed tilt, angle from horizontal, degrees	0 (level)	2.27
6. S-gas inlet nozzle opening, in.	0.79	0.98

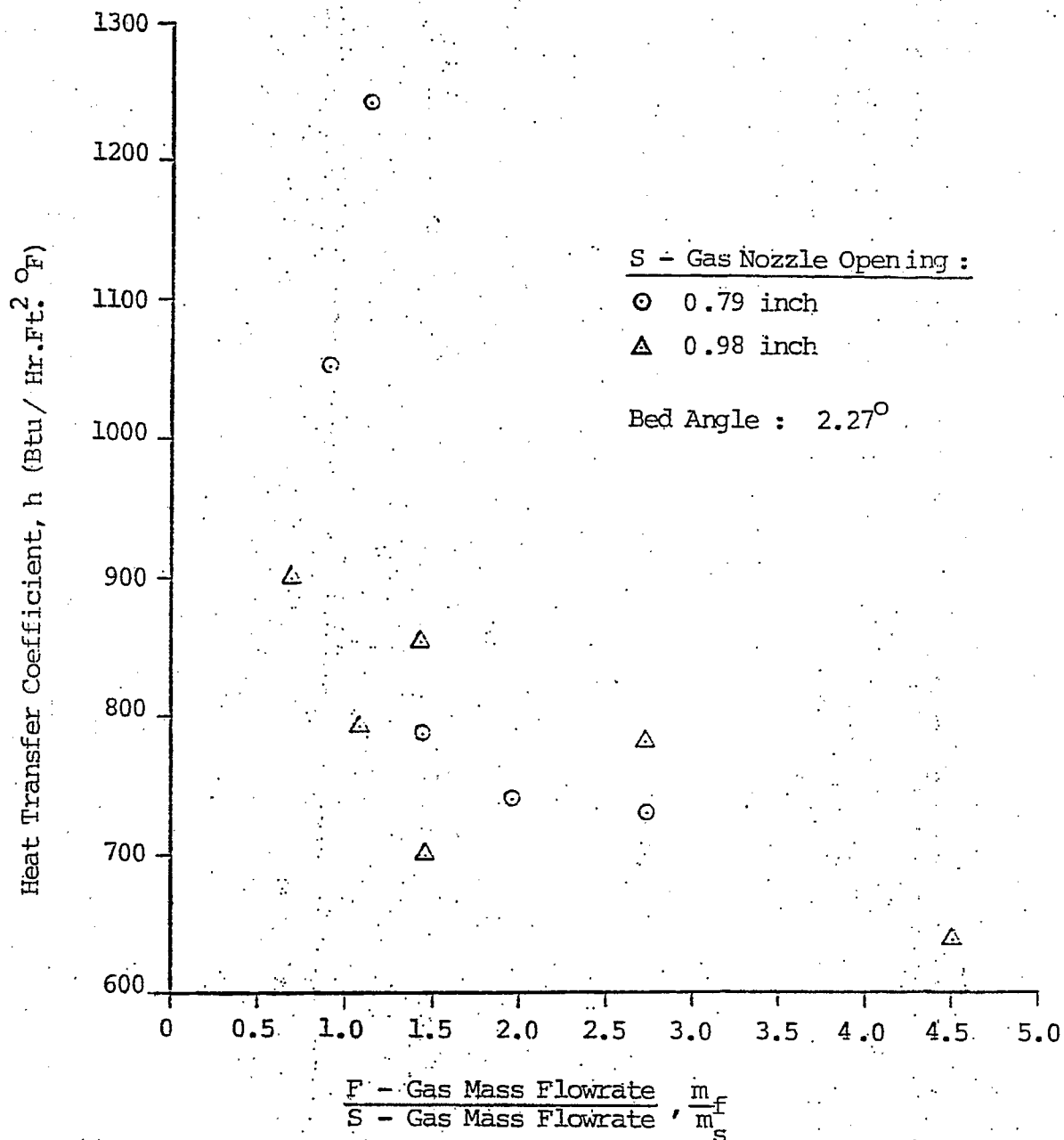


Figure 3.15 Effect of Ratio of F-gas to S-gas Mass Flow Rates on the Heat Transfer Coefficient Between a Flowing S-gas Stream and a Shallow Fluidized Bed of -40+60 Mesh Norton Masterbeads at Different S-gas Exit Nozzle Opening.

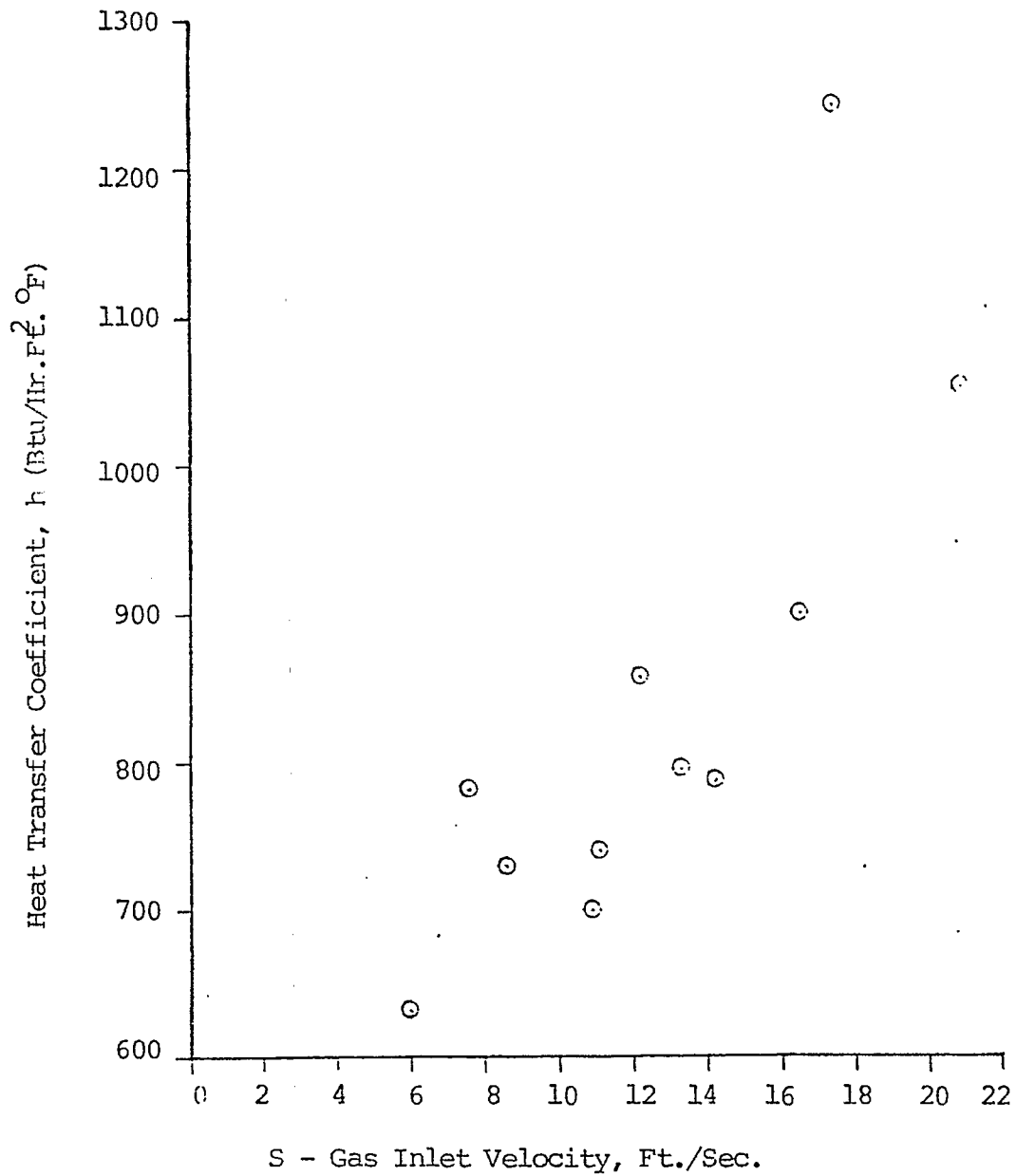


Figure 3.16 Effect of S-Gas Inlet Velocity on the Heat Transfer Coefficient Between a Flowing S-Gas Stream and a Shallow Fluidized Bed of -40+60 Mesh Norton Masterbeads.

4. LITERATURE CITED

- Abu Bakar, M. Y., "Heat Transfer Studies Between a Horizontal Tube and a Shallow Fluidized Bed," Ph.D. Thesis, University of Western Ontario, London, Canada. (1981).
- Al Ali, B. M. A. and J. Broughton, "Shallow Fluidized-Bed Heat Transfer," Applied Energy, 3, 101-114 (1977).
- Andeen, B. R. and L. R. Glicksman, "Heat Transfer to Horizontal Tubes in Shallow Fluidized Beds," ASME Paper 76-HT-67, presented ASME-AIChE Heat Transfer Conference, St. Louis, Missouri (1976).
- Atkinson, G. A., "Extended Surface Fluidized Bed Heat Transfer," Ph.D. Thesis, University of Aston in Birmingham, England, October (1974).
- Avidan, A., "Turbulent Fluid Bed Reactors Using Fine Powder Catalysis," Proceedings of the Joint Meeting of American Institute of Chemical Engineers and Chemical Industry and Engineering Society of China, Beijing, Vol. I, pp. 411-423, September (1982).
- Bell, A. T., "Catalytic Synthesis of Hydrocarbons over Group VIII Metals: A Discussion of the Reaction Mechanism," Catal. Rev.-Sci. Eng., 23, no. 1 and 2, 203-232 (1981).
- Bell, A. T. and L. L. Hegedus, editors, Catalysis Under Transient Conditions, ACS Symp. Series No. 178, American Chemical Society, Washington, DC (1982).
- Bennett, C. O., "The Transient Method and Elementary Steps in Heterogeneous Catalysis," Catal. Rev-Sci. Eng., 13, 121-148 (1976).
- Bennett, C. O., "Understanding Heterogeneous Catalysis Through the Transient Method," edited by A. T. Bell and L. L. Hegedus, pp. - , in Catalysis under Transient Conditions, ACS Symposium Series, No. 178, American Chemical Society, Washington, DC (1982).
- Biloen, P., "On the Mechanism of the Fischer-Tropsch Synthesis," Recueil, 32-38 (1979).

- Biloen, P., J. N. Helle, and W. M. H. Sachtler, "Incorporation of Surface Carbon into Hydrocarbons during Fischer-Tropsch Synthesis: Mechanistic Implications," J. Catalysis, 58, 95-107 (1979).
- Bonzel, H. P., and H. J. Krebs, "Enhanced Rate of Carbon Decomposition During Fischer-Tropsch Synthesis on K Promoted Fe," Surface Science, 109, L527-L531 (1981).
- Botterill, J. S. M. and M. van der Kolk, "The Flow Properties of Fluidized Solids," AIChE Symp. Ser., 67, No. 116, 70 (1971).
- Brady, R. C. III, and R. Pettit, "On the Mechanism of the Fischer-Tropsch Reaction. The Chain Propagation Step," J. Am. Chem. Soc., 103(5), 1287-1289 (1981).
- Dautzenberg, F. M., J. N. Helle, R. A. van Santen, and H. Verbeek, "Pulse-Technique Analysis of the Kinetics of the Fischer-Tropsch Reaction," J. Catalysis, 50, 8-14 (1977).
- Delvzarde, A., J. P. Hindermann, and R. Kieffer, "Carbon-Monoxide-Hydrogen Reactions; Possible Reaction Mechanisms in Heterogeneous Catalysis," J. Chem. Research, 934-948 (1981).
- Diffenbach, R. A., T. H. Johnson, and R. R. Schehl, "A Study of the Fischer-Tropsch Reaction Using On-Line Gas-Chromatographic Analysis," DOE/PETC/TR-82/10, July (1982).
- Dry, M. E., "Predict Carbonation Rate on Iron Catalyst," Hydrocarbon Processing, 92-94, February (1980).
- Eidus, Y. T., "The Mechanism of the Fischer-Tropsch Reaction and the Initiated Hydrodimerisation of Alkenes, from Radiochemical and Kinetic Data," Russian Chemical Reviews, 36,(5), 338-350 (1967).
- Feimer, J. L., P. L. Silveston, R. R. Hudgins, "Influence of Forced Cycling on the Fischer-Tropsch Synthesis," Preprints, 8th Canadian Symp. on Catalysis, Ontario. p. 104, May (1982).
- Henrici-Olive, G. and S. Olive, "The Fischer-Tropsch Synthesis: Molecular Weight Distribution of Primary Products and Reaction Mechanism," Angew. Chem. Int. Ed. Engl., 15(3), 136-141 (1976).
- Kehoe, P. W. K. and J. F. Davidson, "Continuously Slugging Fluidized Beds," Inst. Chem. Engrs. Symp. Ser., 33, 97-116 (1970).

- Kieffer, E. P. and H. S. van der Baan, "Transient Kinetics of the Fischer-Tropsch Synthesis," in Chemical Reaction Engineering-Boston, edited by J. Wei and C. Geogakis, pp. 200-212, American Chemical Society, Washington, DC (1982).
- Matsumoto, H. and C. O. Bennett, "The Transient Method Applied to the Methanation and Fischer-Tropsch Reactions over a Fused Iron Catalyst," J. Catalysis, 53, 331-344 (1978).
- McCarty, J. C. and H. Wise, "Hydrogenation of Surface Carbon on Alumina-Supported Nickel," J. Catalysis, 57, 406-416 (1979).
- McCarty, J. G., P. Y. Hou, D. Sheridan and H. Wise, "Reactivity of Surface Carbon on Nickel Catalyst: Temperature Programmed Surface Reaction with H₂ and H₂O," 7th North American Meeting of the Catalysis Society, Boston, MA, October (1981).
- Muetterties, E. L. and J. Stein, "Mechanistic Features of Catalytic Carbon Monoxide Hydrogenation Reactions," Chemical Reviews, 79, (6), 479-490 (1979).
- Niemantsverdriet, J. W., and A. M. van der Kraan, "On the Time-Dependent Behavior of Iron Catalysts in Fischer-Tropsch Synthesis," J. Catalysis, 72, 385-388 (1981).
- Nijs, H. H. and P. A. Jacobs, "On-Line Single Run Analysis of Effluents from a Fischer-Tropsch Reactor," Journal of Chromatographic Science, 19, 40-45 (1981).
- Pichler, H. "Twenty-five Years of Synthesis of Gasoline by Catalytic Conversion of Carbon Monoxide and Hydrogen," Advances in Catalysis, 4, 271-341 (1952).
- Pillai, K. K. "Heat Transfer to a Sphere Immersed in a Shallow Fluidized Bed," Letter in Heat Mass Trans., 3, 131 (1976).
- Ponec, V., "Some Aspects of the Mechanism of Methanation and Fischer-Tropsch Synthesis," Catal. Rev.-Sci. Eng., 18(1), 151-171 (1978).
- Pugh, P. R., "The Flow of Fluidized Solids," Ph.D. Thesis, University of Aston in Birmingham, England, October (1974).
- Reymond, J. P., P. Meriaudeau, B. Pommier, and C. O. Bennett, "Further Results on the Reaction of H₂/CO on Fused Iron by the Transient Method," Preprints, Division of Fuel Chemistry, American Chemical Society, 25, No. 2, 71-81 (1980).
- Rofer-DePoorter, G. K., "A Comprehensive Mechanism for the Fischer-Tropsch Synthesis," Chem. Rev., 81, 447-474 (1981).

- Schulz, H and A. Zeweldeen, "New Concepts and Results Concerning the Mechanism of Carbon Monoxide Hydrogenation. II. Evolution of Reaction Steps on the Basis of Detailed Product Composition and Other Data," Fuel Processing Technology, 1, 45-56 (1977).
- Shah, Y. T. and A. J. Perrotta, "Catalysts for Fischer-Tropsch and Isosynthesis," Ind. Eng. Chem., Prod. Des. Dev., Vol. 15, No. 2, pp. 123-131 (1976).
- Squires, A. M., "Applications of Fluidized Beds in Coal Technology in Alternative Energy Sources, J. P. Hartnett, editor, pp. 59-109, Academic Press, New York, NY (1976).
- Squires, A. M., "Contributions toward a History of Fluidization," Proceedings of the Joint Meeting of American Institute of Chemical Engineers and Chemical Industry and Engineering Society of China, Beijing, Vol. I, pp. 322-353, September (1982).
- Stockinger, J. H., "Quantitative Analysis of Gaseous Products Obtained in the Conversion of Methanol-to-Gasoline," Journal of Chromatographic Science, Vol. 15, pp. 198-202 (1977).
- Storch, H. H., N. Golumbic, and R. B. Anderson, The Fischer-Tropsch and Related Synthesis, John Wiley & Sons, Inc., New York (1951).
- Vannice, M. A., "The Catalytic Synthesis of Hydrocarbons from H₂/CO Mixtures over the Group VII Metals I.," Journal of Catalysis, Vol. 37, pp. 449-461 (1975).
- Vannice, M. A. "The Catalytic Synthesis of Hydrocarbons from Carbon Monoxide and Hydrogen," Catal. Rev. Sci. Eng., 14(2), 153-191 (1976).
- Wentrcek, P. R., B. J. Wood, and H. Wide, "The Role of Surface Carbon in Catalytic Methanation," J. Catalysis, 43, 363-366 (1976).
- Yerushalmi, J., N. T. Cankurt, D. Geldart and B. Liss, "Flow Regimes in Vertical Gas Solid Contact Systems," AIChE Symp. Ser., 74, No. 176, 1-13 (1978).
- Yerushalmi, J. and N. T. Cankurt, "Further Studies of the Regimes of Fluidization," Powder Technology, 187-205 (1979).
- Zenz, F. A., "Bubble Formation and Grid Design," in Fluidization, edited by J. M. Pirie, p. 136, Inst. Chem. Engrs., London (1968).
- Zenz, F. A. and D. F. Othmer, Fluidization and Fluid-Particle System, Reinhold, NY (1960).

5. APPENDICES

5.1 Safety Provisions for the Fischer-Tropsch Synthesis Microreactor System

5.1.1 Location of the Microreactor System

The vibrofluidized microreactor system described in Section 2.2 is located in the Laboratory for Coal Science and Process Chemistry ("coal lab"), Room 319A, on the third floor, northeast wing of Randolph Hall, Virginia Polytechnic Institute and State University. Above the microreactor system is the building roof, and below it is the Unit Operations Laboratory ("U.O. Lab"). Figure 5.1 shows a schematic of the location of the microreactor system ("reactor lab"). The system is surrounded by cinderblock wall on three sides, and by plywood on the other side and on the top, forming a "reactor box" as labelled in Figure 5.1. The dimension of this reactor box are 1.45 m x 1.32 m x 2.13 m (width x length x height), giving a total volume of 4.0768 m³. The laboratory surrounding this box, labelled as "reactor lab" in Figure 5.1, has the dimensions of 3.5 m x 7 m x 3.45 m or a total volume of 84.53 m³.

5.1.2 Ventilation of the Microreactor System

Ventilation for the entire reactor laboratory is provided by a large roof-fan which draws air from both the coal laboratory and the unit operations laboratory. This roof-fan draws air at a volumetric flow rate of approximately 9.46×10^{-3} m³/sec (0.334 ft³/sec or 20.04 cfm) at the grate of the reactor laboratory. Thus, the entire air content of the reactor laboratory would be replaced approximately once every two and one-half hours if there was no other air exit. However, an additional vent fan draws air from the reactor box at a faster rate of 9.91×10^{-2} m³/sec (3.5 ft³/sec or 2,100 cfm). This means that the air content in the reactor box can be replaced approximately once every 41 seconds. Also, the entire room air in the reactor laboratory is replaced about once every 7 minutes. Note that fresh air is drawn into the reactor laboratory via the unit operations laboratory and an air duct in the coal laboratory.

The reactor box has been caulked with silicone rubber at all of its joints and around the edges of the plexiglass at

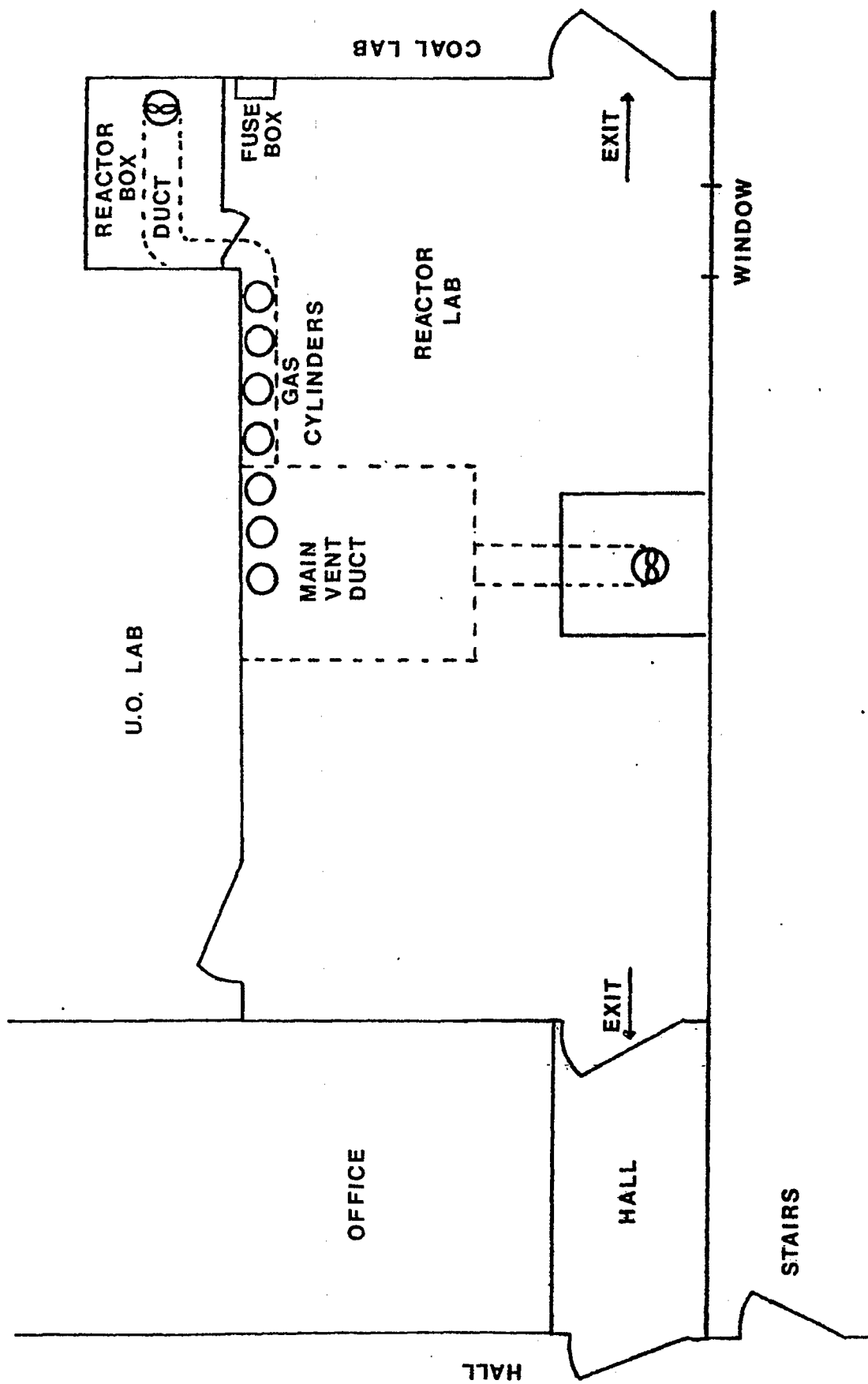


Figure 5.1. A Schematic of the Location of the Fischer-Tropsch Synthesis Microreactor System ("Reactor Lab").

the roof light. The small piece of plywood covering a vent hole in the wall has also been carefully caulked. The roof light is located on top of the reactor box and shines light through the plexiglass to eliminate any possibility of spark hazard.

Table 5.1 summarizes the estimated volumes of different components of the microreactor system and the estimated air renewal rates of the reactor box and the reactor laboratory. The volumetric flow rates of the reactant gases being used in initial experiments are as follows (see also Figure 2.3 and Table 2.2):

<u>Gas</u>	<u>Rate, mm³/sec</u>	<u>Duration, sec</u>	<u>Volume, mm³</u>
CO:H ₂ :Ar	2,500	2	5,000
H ₂	250	1	250
H ₂	14.7	17	250

The total volumetric flow rates of different reactant gases are:

<u>Gas</u>	<u>Rate, mm³/sec</u>	<u>Rate, cfm</u>
H ₂	1.09×10^{-5}	3.84×10^{-4}
CO	4.69×10^{-6}	1.65×10^{-4}
Ar	9.38×10^{-7}	3.29×10^{-5}

These volumetric flow rates suggest that if no fresh air were added to the reactor box for an hour, a total of 2.81×10^{-4} m³ of CO would have been accumulated in the reactor box containing the microreactor. This would correspond to a concentration of 0.007% by volume or approximately 69 ppm. Note that the American Conference of Governmental Industrial Hygienists has recommended a threshold limit value of 50 ppm for CO representing the concentration of CO in air to which nearly all workers may be continuously exposed without adverse effects.

The flammable limits of H₂ in air 4 to 75% by volume, depending upon the surrounding situations. Therefore, H₂ would have to build up inside the reactor box for approximately 250 hours before it would ignite.

Table 5.1
 Estimates of Microreactor System Volumes and
 Room Air Renewal Rates

System Description	Quantity	Volume (m ³) or Air Renewal Rate (m ³ /sec)
A. Microreactor System Components		
1. 1/4-inch 316SS tubing, 0.035-inch wall thickness	40 ft.	2.86×10^{-4}
2. 1/16-inch 316SS tubing, 0.028-inch wall thickness	12 ft.	2.21×10^{-6}
3. 500-ml reactant and inert gas reservoir	3	1.5×10^{-3}
4. 150-ml reactant and inert gas reservoir	1	1.5×10^{-4}
5. Microreactor	1	5.63×10^{-7}
6. Estimated Microreactor System Volume (components 1 to 5)		$1.94 \times 10^{-3} \text{ m}^3$
B. Reactor Box Volume		4.08 m^3
C. Reactor Laboratory Volume		84.53 m^3
D. Air Renewal Rates		
1. Reactor Box		$9.91 \times 10^{-2} \text{ m}^3/\text{sec}$
2. Reactor Laboratory		$9.46 \times 10^{-3} \text{ m}^3/\text{sec}$

5.1.3 High Temperature and Pressure Precautions

The vibrofluidized microreactor system is to be run at pressures up to 30 atm and parts of the system at temperatures up to 315°C. Thus, the upper limits of operating temperatures and pressures of different system components must be known. Those are summarized in Table 5.2.

5.1.4 Electrical System

All electrical switches and plugs are external to the reactor box. The only electrical devices located in the box are the solenoid valves, pressure and flow transducers, and CO detector, and the fluidized constant-temperature sand-bath. On-off switches for these devices are located on the control panel outside the box. The fuse box is located adjacent to the reactor box so that in case of an emergency, all electricity can be shut off immediately.

The Circle-Seal solenoid valves are activated by 28 VDC via a Zenith Z-89 microcomputer. The Atkomatic solenoid valve is actuated by 24 VDC via the microcomputer. The pressure transducers are excited using 10 VDC; and both the mass flow meters and CO detector require 120 VAC. The fluidized constant-temperature sand-bath uses 240 VAC.

5.1.5 Emergency Equipment

A Toxgard Model C carbon monoxide detector (Mine Safety Appliances Company) is mounted inside the reactor box as a first line of defense against CO leaks. This detector continuously samples the air by diffusion and reports concentration in ppm. If the limit is reached, both visual and audible alarms are tripped. The sensor life of this unit is about one year. The unit is powered by the 120 VDC building supply.

One 5-pound CO₂ fire extinguisher is located approximately 15 m from the reactor box inside the coal laboratory. At the same location is a first-aid kit and an eyewash station.

A sling air mask, available for rescue in toxic environments, is located on the wall outside of Room 155, Randolph Hall. A telephone is located inside the coal laboratory. Emergency telephone numbers are as follows:

Table 5.2

Upper Limits of Operating Temperatures and Pressures
for Different Components of the Vibrofluidized
Microreactor System

Component	Maximum Working Pressure at 70°F, (psi)	Maximum Working Pressure (psi) at Selected Temperature
1. High pressure air regulators	2,500	
2. Stainless steel tubing, 1/4-inch O.D.	5,906	5,433 at 315°C
3. Whitey 1/4 ball valves	3,000	
4. Whitey sample cylinders	1,800	
5. Nupro check valves	3,000	
6. Circle seal 2-way and 3-way solenoid valves	3,000	
7. Atkomatic solenoid valve	5,000	5,000 at 260°C (max)
8. Nupro metering valves:		
4 SG	2,000	
5 MG	1,000	
9. Flexible stainless steel hose	2,660	6,968 at 315°C
10. Brooks mass flow meters: 5810	3,000	
5811	1,500	
11. Circle-seal back-pressure regulator	1,000	

Table 5.2

(continued)

Component	Maximum Working Pressure at 70°F, (psi)	Maximum Working Pressure (psi) at Selected Temperature
12. Nupro filters	3,000	
13. Valco 6- and 10-port sampling valves		3,000 at 300°C (max)
14. Nupro in-line relief valves (350-600 psi adjustable)	3,000	

- | | |
|-------------------------------|------------|
| 1. Blacksburg Rescue Squad | 9-911 |
| 2. Blacksburg Fire Department | 9-552-2222 |
| 3. Campus Police | 6411 |
| 4. University Health Services | 6444 |
| 5. Montgomery County Hospital | 9-951-1111 |

5.1.6 Emergency Shutdown Procedures

A. Fire Emergency

1. Turn off the main valve on the hydrogen cylinder.
2. Turn off the main valve on the H₂:CO:Ar cylinder.
3. Call Blacksburg Fire Department at 9-552-2222.
4. Notify a close-by person to sound the fire alarm and evacuate the building.
5. If fire is small and confined in nature, steps may be taken to extinguish it with the CO₂ fire extinguisher.

B. Gas Leaks

1. Turn off all electricity to the experiment at the control panel of the fuse box.
2. Turn off the main valve on the hydrogen cylinder.
3. Turn off the main valve on the H₂:CO:Ar cylinder.
4. Locate leak site using nitrogen and repair the leak.
5. Pressure-test the system after leak repair.

C. Loss of Building Power

1. Turn off the main valve on the H₂:CO:Ar cylinder.
2. Turn off the main valve on the hydrogen cylinder.
3. Turn off the main valve on the nitrogen cylinder.
4. Turn off all meters and solenoid valves.
5. Wait for power restoration in another room.

5.2 Related Literature on the Fischer-Tropsch Synthesis

- Amelse, J. A., L. H. Schwartz and J. B. Butt, "Iron Alloy Fischer-Tropsch Catalysts. III." J. Catalysis, 72, 95-110 (1981).
- Anderson, R. B., R. A. Friedel and H. H. Storch, "Fischer-Tropsch Reaction Mechanism Involving Stepwise Growth of Carbon Chain," J. Chem. Phys., 19, No. 3, 313-319 (1951).
- Anderson, R. B., F. S. Karn, and J. F. Shultz, "Factors in Sulfur Poisoning of Iron Catalysts in Fischer-Tropsch Synthesis," J. Catalysis, 4, 56-63 (1965).
- Anderson, R. B., L. J. E. Hofer, E. M. Cohn, and B. Seligman, "Studies of the Fischer-Tropsch Synthesis. IX. Phase Changes of Iron Catalysts in the Synthesis," J. Am. Chem. Soc., 73, 944-946 (1951).
- Anderson, R. B., B. Seligman, J. F. Shultz, R. Kelly and M. A. Elliott, "Fischer-Tropsch Synthesis," Ind. Eng. Chem., 44, No. 2, 391-397 (1952).
- Anderson, R. B., J. F. Shultz, B. Seligman, W. K. Hall., and H. H. Storch, "Studies of the Fischer Tropsch Synthesis. VII. Nitrides of Iron as Catalysts," J. Am. Chem. Soc., 72, 3502-3508 (1950).
- Anderson, R. B., and Y. Chan, "Chain Growth in the Fischer-Tropsch Synthesis--A Computer Simulation of a Catalytic Process," Symposium on Advances in F-T Chemistry, Division of Petroleum Chemistry, Preprints, American Chemical Society, pp. 578-586 (1978).
- Anderson, R. B., "Schulz-Flory Equation," J. Catalysis, 55, 114-115 (1978).
- Anderson, R. B., "Reply to Rebuttal by G. Henrici-Olive' and S. Olive'," J. Catalysis, 60, 484 (1979).
- Araki, M., and V. Ponec, "Methanation of Carbon Monoxide on Nickel and Nickel-Copper Alloys," J. Catalysis, 44, 439-448 (1976).
- Atwood, H. E., "Kinetics for the Fischer-Tropsch Reaction," Report No. EPRI-AF-689, Electric Power Research Institute, Palo Alto, CA (1977).
- Atwood, H. E., and C. O. Bennett, "Kinetics of the Fischer-Tropsch Reaction over Iron," IEC Process Des. Dev., 18, No. 1, 163-170 (1979).

- Baird, M. J., R. R. Schehl, and W. P. Haynes, "Fischer-Tropsch Processes Investigated at the Pittsburgh Energy Technology Center since 1944," IEC Prod. Res. Dev., 19, No. 2, 175-191 (1980).
- Balaji, Gupta, R. B. Viswanathan, and M. V. C. Sastri, "Interaction of Hydrogen and Carbon Monoxide on Cobalt Catalysts: Part I." J. Catalysis, 26, 212-217 (1972)
- Bartholomew, C. H., and Pannell, R. B., "The Stoichiometry of Hydrogen and Carbon Monoxide Chemisorption on Alumina- and Silica-Supported Nickel," J. Catalysis, 65, 390-401 (1980).
- Beno, M. A., J. M. Williams, M. Tachikawa, and E. L. Muetterties, "Fischer-Tropsch Chemistry: Structure of a Seminal n^2 -CH Cluster Derivative, $H Fe_4(n^2-CH)(CO)_{12}$," J. Am. Chem. Soc., 102, No. 13, 4542-4544 (1980).
- Benziger, J. B., and R. J. Madix, "Reactions and Reaction Intermediates on Iron Surfaces II." J. Catalysis, 65, 49-58 (1980).
- Bilimoria, M. R. and J. E. Bailey, "Dynamic Studies of Acetylene Hydrogenation on Nickel Catalysts," Proc. 5th Intern. Sympos. Chem. React. Eng., Houston, p. 526 (1977).
- Blyholder, G. and P. H. Emmett, "Fischer-Tropsch Synthesis Mechanism Studies. II. The Addition of Radioactive Ketene to the Synthesis Gas," J. Phys. Chem., 64, 470 (1960).
- Blyholder, G., and A. J. Goodsel, "Infrared Spectra of C_2H_4 Adsorption and CO Insertion Reactions on an Fe Surface," J. Catalysis, 23, 374-378 (1971).
- Blyholder, G., D. Shihabi, W. V. Wyatt, and R. Bartlett, "Adsorption and Interaction of C_2H_4 , H_2 , CO, and Organic Acids on Fe, CO, and Ni," J. Catalysis, 43, 122-130 (1976).
- Bond, G. C., and B. D. Turnham, "The Kinetics and Mechanism of Carbon Monoxide Hydrogenation over Silica-Supported Ruthenium-Copper Catalysts," J. Catalysis, 45, 128-136 (1976).
- Bonzel, H. P. and G. Broden, "On the Adsorption and Dissociation of CO on Potassium Promoted Iron," Preprints, Symposium on New Tools in Catalysis, Division of Petroleum Chemistry, American Chemical Society, p. 1260 (1978).
- Bonzel, H. P. and H. J. Krebs, "Evidence for Adsorbed Hydrocarbon Intermediates During the Initial Stages of CO Hydrogenation on Iron," Preprints, Division of Fuel Chemistry, American Chemical Society, 25, No. 2, 19-27 (1980).

- Bonzel, H. P. and H. J. Krebs, "Evidence for Adsorbed Hydrocarbon Intermediates During the Initial Stages of CO Hydrogenation on Iron," Preprints, Div. of Fuel Chem., Amer. Chem. Soc., 25, No. 2, 19-26 (1980).
- Bossi, A., G. Carnisio, F. Garbassi, G. Giunchi, and G. Petrini, "Isotopic Equilibration of Carbon Monoxide Catalysed by Supported Ruthenium," J. Catalysis, 65, 16-24 (1980).
- Brady, R. C. III, R. Pettit, "Reactions of Diazo Methane on Transition Metal Surfaces and Their Relationship to the Mechanism of the Fischer-Tropsch Reaction," J. Am. Chem. Soc., 102, 6182-6184 (1980).
- Bridge, M. E., C. M. Comrie, and R. M. Lambert, "Hydrogen Chemisorption and the Carbon Monoxide-Hydrogen Interaction on Cobalt (0001)," J. Catalysis, 58, 28-33(1979).
- Broden, G., G. Gafner and H. P. Bonzel, "CO Adsorption on Potassium Promoted Fe (110)," Surface Science, 84, 295-314 (1979).
- Bub, G., and M. Baerns, "Prediction of the Performance of Catalytic Fixed Bed Reactors for Fischer-Tropsch Synthesis," Chem. Eng. Sci., 35, 348-355 (1980).
- Bussemeier, B., C. D. Frohning, and B. Cornils, "Lower Olefins via Fischer-Tropsch," Hydrocarbon Processing, 105-112, Nov. (1976).
- Caesar, P. D., J. A. Brennan, W. E. Garwood, and J. Ciric, "Advances in Fischer-Tropsch Chemistry," J. Catalysis, 56, 274-278 (1979).
- Castner, D. G., R. L. Blackadar, and G. A. Somorjai, "CO Hydrogenation over Rhodium Foil and Single Crystal Catalysts: Correlations of Catalyst Activity, Selectivity, and Surface Composition," Preprints, Div. Fuel Chem., Amer. Chem. Soc., 25, No. 2, 27-42 (1980).
- Collis, F. P., and J. A. Schwartz, "Selectivity Effects and Hydrocarbon-Chain Growth during Fischer-Tropsch Synthesis," J. Comp. Chem., 3, No. 2, 135-139 (1982).
- Dalla Betta, R. A., A. G. Piken, and M. Shelef, "Heterogeneous Methanation: Initial Rate of CO Hydrogenation on Supported Ruthenium and Nickel," J. Catalysis, 35, 54-60 (1974).
- Dalla Betta, R. A., and M. Shelef, "Heterogeneous Methanation: In Situ Infrared Spectroscopic Study of Ru/Al₂O₃ During the Hydrogenation of CO," J. Catalysis, 48, 111-119 (1977).

- Dalla Betta, R. A., and M. Shelef, "Heterogeneous Methanation: Absence of H₂-D₂ Kinetic Isotope Effect on Ni, Ru, and Pt," J. Catalysis, 49, 383-385 (1977).
- Darby, P. W., and C. Kemball, "Observations on the Fischer-Tropsch Synthesis over a Cobalt Catalyst at Low Pressure Using Gas Chromatography," Trans. Faraday Soc., 833-841 (1958).
- Deans, D. R., M. T. Huckle, and R. M. Peterson, "New Column System for Isothermal Gas Chromatographic Analysis of Light Gases (H₂, O₂, N₂, CO, CO₂, C₂H₄, C₂H₆, and C₂H₂) Employing a Column Switching Technique," Chromatographia, 4, 279-285 (1971).
- Deckwer, W. D., "FT Process Alternatives Hold Promise," Oil & Gas Journal, 198-213, Nov. 10 (1980).
- Deluzarche, A., J. P. Hindermann, R. Kieffer, A. Muth, M. Papadopoulos, and C. Tanielian, "Synthese de Fischer-Tropsch II." Tetrahedron Letters, No. 9, 797-800 (1977).
- Demitras, G. C. and E. L. Muetterties, "Metal Clusters in Catalysis-10. A New Fischer-Tropsch Synthesis," J. Am. Chem. Soc., 99, No. 8, 2796-2797 (1977).
- Dietz, W. A., "Response Factors for Gas Chromatographic Analyses," Journal of Gas Chromatography, 67-71, Feb. (1967).
- DiSanzo, F. P., "Characterization of High Boiling Fischer-Tropsch Liquids by Liquid and Gas Chromatography," Anal. Chem., 53, 1911-1914 (1981).
- Dry, M. E., "Advances in Fischer-Tropsch Chemistry," IEC Prod. Res. Des., 15, No. 4, 282-286 (1976).
- Dry, M. E., "Sasol's Fischer-Tropsch Experience," Hydrocarbon Processing, 121-124, Aug. (1982).
- Dry, M. E., J. A. K. DuPlessis, G. M. Leuteritz, "The Influence of Structural Promoters on the Surface Properties of Reduced Magnetite Catalysts," J. Catalysis, 6, 194-199 (1966).
- Dry, M. E. and L. C. Ferreira, "The Distribution of Promoters in Magnetite Catalysts," J. Catalysis, 7, 352-358 (1967).
- Dry, M. E. and G. J. Oostuizen, "The Correlation Between Catalyst Surface Basicity and Hydrocarbon Selectivity in the Fischer-Tropsch Synthesis," J. Catalysis, 11, 18-24 (1968).

- Dry, M. E., T. Shingles, and L. J. Boshoff, "Rate of the Fischer-Tropsch Reaction Over Iron Catalysts," J. Catalysis, 25, 99-104 (1972).
- Dry, M. E., T. Shingles, L. J. Boshoff, and C. S. van H. Botha, "Factors Influencing the Formation of Carbon on Iron Fischer-Tropsch Catalysts, II," J. Catalysis, 17, 347-354 (1970).
- Dry, M. E., T. Shingles, L. J. Boshoff and G. J. Oosthuizen, "Heats of Chemisorption on Promoted Iron Surfaces and the Role of Alkali in Fischer-Tropsch Synthesis," J. Catalysis, 15, 190-199 (1969).
- Dry, M. E., T. Shingles, and C. S. van H. Botha, "Factors Influencing the Formation of Carbon on Iron Fischer-Tropsch Catalyst, I," J. Catalysis, 17, 341-346 (1970).
- Dutartre, P. Bussiere, J. A. Dalmon, and G. A. Martin, "Activation of Hydrogen on Fe/MgO Catalysts Studied by Magnetic Methods and Mossbauer Spectroscopy," J. Catalysis, 59, 382-394 (1979).
- Dwyer, D., K. Yoshida, and G. A. Somorjai, "Hydrogenation of CO and CO₂ on Clean Rhodium and Iron Foils--Correlations of Reactivities and Surface Compositions," Preprints, Symposium on Advances in Fischer-Tropsch Chemistry, Div. of Petroleum Chemistry, Amer. Chem. Soc., 521-537 (1978).
- Dwyer, D. J. and G. A. Somorjai, "The Role of Readsorption in Determining the Product Distribution during CO Hydrogenation over Fe Single Crystals," J. Catalysis, 56, 249-257 (1979).
- Eisenlohr, K. H. and H. Gaensslen, "Motor Fuels from Coal--Technology and Economics," Fuel Processing Technology, 4, 43-61 (1981).
- Ekerdt, J. G., and A. T. Bell, "Evidence for Intermediates Involved in Fischer-Tropsch Synthesis over Ru," J. Catalysis, 62, 19-25 (1980).
- Ekerdt, J. G. and A. T. Bell, "Synthesis of Hydrocarbons from CO and H₂ over Silica-Supported Ru: Reaction Rate Measurements and Infrared Spectra of Adsorbed Species," J. Catalysis, 58, 170-187 (1979).
- Everson, R. C., E. T. Woodburn, and A. R. M. Kirk, "Fischer-Tropsch Reaction Studies with Supported Ruthenium Catalysts," J. Catalysis, 53, 186-197 (1978).

- Feimer, J. L., P. L. Silveston and R. R. Hudgins, "Steady-State Study of the Fischer-Tropsch Reaction," IEC Prod. Res. Dev., **20**, 609-615 (1981).
- Field, J. H., H. E. Benson, and R. B. Anderson, "Synthetic Liquid Fuels by Fischer-Tropsch Process," Chem. Eng. Prog., **56**, No. 4, 44-48 (1960).
- Field, J. H., J. J. Demeter, A. J. Forney, and D. Bienstock, "Development of Catalysts and Reactor Systems for Methanation," IEC Product Res. and Develop., **3**, No. 2, 150-153 (1964).
- Fischer, R. H. and R. E. Hildebrand, "Transportation Fuels from Synthesis Gas," Proceedings of the Symposium on Advances in Coal Utilization Technology, Institute of Gas Technology, pp. 331-344 (1979).
- Forsey, R. R., "A Dual-Column Gas Chromatographic Method for the Analysis of Light Gases," J. Gas Chromatography, **6**, 555 (1968).
- Fraenkel, D. and B. C. Gates, "Shape-Selective Fischer-Tropsch Synthesis Catalyzed by Zedlite-Entrapped Cobalt Clusters," J. Am. Chem. Soc., **102**, No. 7, 2478-2480 (1980).
- Friedel, R. A. and R. B. Anderson, "Composition of Synthetic Liquid Fuels. I. Product Distribution and Analysis of C₅-C₈ Paraffin Isomers from Cobalt Catalyst," J. Am. Chem. Soc., **72**, 1215-2307 (1950).
- Frohning, C. D., and B. Cornils, "Chemical Feedstocks from Coal," Hydrocarbon Processing, 143-146, Nov. (1974).
- Garrett, L. W. Jr., "Gasoline From Coal Via the Synthol Process," Chem. Eng. Prog., **56**, No. 4, 39-43 (1960).
- Gierlich, H. H., and M. Fremery, "Deactivation Phenomena of a Ni-based Catalyst for High Temperature Methanation," in Catalyst Deactivation, pp. 459-469. B. Delmon and G. F. Froment, editors, Elsevier Scientific Publishing Company, Amsterdam, Netherlands (1980).
- Goodman, D. W., R. D. Kelley, T. E. Madey, and J. M. White, "Measurement of Carbide Buildup and Removal Kinetics on Ni(100)," J. Catalysis, **64**, 479-481 (1980).
- Gray, D., M. Lytton, M. B. Neuwirth, "The Impact of Developing Technology on Indirect Liquefaction," Proceedings of Symposium on Advances in Coal Utilization Technology, Institute of Gas Technology, pp. 93-109 (1981).

- Grekel, H., K. L. Hujsak, and R. Mungen, "Contacting Efficiency in Hydrocarbon Synthesis," Chem. Eng. Prog., 60, No. 1, 56-60 (1964).
- Grenable, D. C., and M. M. Estadt, "The Chemistry and Catalysis of the Water Gas Shift Reaction," J. Catalysis, 67, 90-102 (1981).
- Haggin, J., "C₁ Chemistry Development Intensities," Chem. and Eng. News, 39-47, Feb. 23 (1981).
- Haggin, J., "Fischer-Tropsch: New Life for Old Technology," Chem. and Eng. News, 22-32, Oct. 26 (1981).
- Haggin, J., "Progress in C₁ Chemistry Aired," Chem. and Eng. News, 31-34, June 28 (1982).
- Hall, W. K., W. H. Tarn, and R. B. Anderson, "Studies of the Fischer-Tropsch Synthesis. XIII. Structural Changes of a Reduced Iron Catalyst on Reoxidation and on Formation of Interstitial Phases," J. Am. Chem. Soc., 56, 688 (1950).
- Hall, W. K., W. H. Tarn, and R. B. Anderson, "Studies of the Fischer-Tropsch Synthesis. VIII. Surface Area and Pore Volume Studies of Iron Catalysts," J. Am. Chem. Soc., 72, 5436-5443 (1950).
- Happel, J., I. Suzuki, P. Kokayeff, and V. Fthenakis, "Multiple Isotope Tracing of Methanation over Nickel Catalyst," J. Catalysis, 65, 59-77 (1980).
- Harney, B. M., and G. A. Mills, "Coal to Gasoline via Syngas," Hydrocarbon Processing, 67-71, Feb. (1980).
- Harney, B. M., G. A. Mills and L. M. Joseph, "High Quality Transportation Fuels from CO-H₂: A Competitive Option," Preprints, Symposium on Advances in Fischer-Tropsch Chemistry, Div. of Petroleum Chem., Amer. Chem. Soc., 573-577, March (1978).
- Haynes, W. P., M. J. Baird, R. R. Schehl, and M. F. Zarochak, "Fischer-Tropsch Studies in a Bench-Scale Tube Wall Reactor Using Magnetite, Raney Iron, and Taconite Catalysts," Preprints, Symposium on Advances in Fischer-Tropsch Chemistry, Div. of Petroleum Chem., Amer. Chem. Soc., 559-572, March (1978).
- Henrici-Olive, G. and S. Olive, "Letters to the Editors in Re: Fischer-Tropsch. Comments to Notes by R. B. Anderson (1) and R. J. Madon (2)," J. Catalysis, 60, 481-483 (1979).

- Henry, J. P., "Economics and Siting of Fischer-Tropsch Coal Liquefaction," Report No. DOE/ET/2625-9, U. S. Department of Energy, Washington, DC, July (1979).
- Herrmann, W. A., "Organometallic Aspects of the Fischer-Tropsch Synthesis," Angew. Chem., Int. Ed., Engl., 21, 117-130 (1982).
- Hoogendoorn, J. C., "New Applications of the Fischer-Tropsch Process," Proceedings of the Symposium on Clean Fuels from Coal II, Institute of Gas Technology, Chicago, pp. 343-358 (1975).
- Huang, C. P. and J. T. Richardson, "Alkali Promotion of Nickel Catalysts for Carbon Monoxide Methanation," J. Catalysis, 51, 1-8 (1978).
- Hugues, F., B. Besson, P. Bussiere, J. A. Dalmon, J. M. Basset, and D. Olivier, "Catalysis by Supported Iron Clusters: Unusual Selectivities in Fischer-Tropsch Synthesis and in Olefin Homologation. Considerations on the Mechanism of Fischer-Tropsch Synthesis," Nouveau Journal de Chimie, 5, No. 4, 207-210 (1981).
- Ichikawa, M., M. Sudo, M. Soma, T. Onishi, and K. Tamaru, "Catalytic Formation of Hydrocarbons (C₁-C₅) from Hydrogen and Carbon Monoxide over the Electron Donor-Acceptor Complex Films of Alkali Metals with Transition Metal Phthalocyanines or Graphite," J. Amer. Chem. Soc., 91, No. 6, 1538-1539 (1969).
- Jones, A., B. D. McNicol, "Comparison of the Fischer-Tropsch Synthesis of Hydrocarbons and the Haber Synthesis of Ammonia," J. Catalysis, 47, 384-388 (1977).
- Joyner, R. W., "Mechanism of Hydrocarbon Synthesis from Carbon Monoxide and Hydrogen," J. Catalysis, 50, 176-180 (1977).
- Kadelka, J., H. Loevenich, and W. Keim, "The Reactions of Fischer-Type Carbene Complexes with Ethene," J. Organometallic Chem., 231, 219-223 (1982).
- Karn, F. S., B. Seligman, J. F. Shultz, and R. B. Anderson, "Kinetics of the Fischer-Tropsch Synthesis on Iron Catalysts. I. Rate Data on Reduced and Nitrided Catalysts," J. Phys. Chem., 64, No. 4, 446-451 (1960).
- Karn, F. S., J. F. Shultz, and R. B. Anderson, "Kinetics of the Fischer-Tropsch Synthesis on Iron Catalysts Pressure Dependence and Selectivity on Nitrided Catalysts," J. Am. Chem. Soc., 64, 446-451 (1960).

- Kelley, R. D. and D. Wayne Goodman, "Catalytic Methanation Over Single Crystal Nickel and Ruthenium: Reaction Kinetics on Different Crystal Planes," Preprints, Div. Fuel Chem., Amer. Chem. Soc., 25, No. 2, 27-42 (1980).
- Kellner, C. S. and A. T. Bell, "Evidence for H₂/D₂ Isotope Effects on Fischer-Tropsch Synthesis over Supported Ruthenium Catalysts," J. Catalysis, 67, 175-185 (1981).
- Kellner, C. S., and A. T. Bell, "The Kinetics and Mechanism of Carbon Monoxide Hydrogenation over Alumina-Supported Ruthenium," J. Catalysis, 70, 418-432 (1981).
- Kibby, C. L., and T. P. Kobylinski, "Models of Product Distributions in Fischer-Tropsch Synthesis," Preprints, Symp. on Adv. in Synthetic Fuels, Div. of Pet. Chem., Amer. Chem. Soc., 1332-1335 (1978).
- King, D. L., "A Fischer-Tropsch Study of Supported Ruthenium Catalysts," J. Catalysis, 51, 386-397 (1978).
- King, D. L., "An in-Situ Infrared Study of CO Hydrogenation over Silica and Alumina-Supported Ruthenium and Silica-Supported Iron," J. Catalysis, 61, 77-86 (1980).
- King, R. B., A. D. King, Jr., M. Z. Iqbal, and C. C. Frazier, "Transition Metal Chemistry under High Carbon Monoxide Pressure: An Infrared Spectroscopic Study of Catalysis in the Fischer-Tropsch Reaction," National Technical Information Service, Publication Nos. SRO-933-1, SRO-933-2, SRO-933-3 (1977, 1978, 1979).
- Kolbel, H., and M. Ralek, "The Fischer-Tropsch Synthesis in the Liquid Phase," Catal. Rev. - Sci. Eng., 21, No. 2, 225-274 (1980).
- Kroeker, R. M., W. C. Kaska, and P. K. Hansma, "Formation of Hydrocarbons from Carbon Monoxide on Rhodium/Alumina Model Catalysts," J. Catalysis, 61, 87-95 (1980).
- Krupay, B. W., and Y. Amenomiya, "Alkali-Promoted Alumina Catalysts I." J. Catalysis, 67, 362-370 (1981).
- Kuchynka, K., J. Fusek, and O. Strouf, "Modelling of Fischer-Tropsch Catalytic Synthesis by Pattern Recognition Method. Chemisorption of Hydrogen on Metals," Collection Czechoslovak Chem. Commun., 46, 2328-2335 (1981).

- LeBlanc, J. R., D. O. Moore, and A. E. Cover, "Coal Can Be Gasoline," Hydrocarbon Processing, 133-138, June (1981).
- Le Roux, J. H., and L. J. Dry, "Fischer-Tropsch Waxes: VI. Distribution of Branches and Mechanism of Branch Formation," J. Appl. Chem. Biotechnol., 22, 719-726 (1972).
- Low, G. G., and A. T. Bell, "Studies of CO Desorption and Reaction with H₂ on Alumina-Supported Ru," J. Catalysis, 57, 397-405 (1979).
- Madon, R. J., and W. F. Taylor, "Fischer-Tropsch Synthesis on a Precipitated Iron Catalyst," J. Catalysis, 69, 32-43 (1981).
- Madon, R. J., "Reply to Comments by G. Henrici-Olive and S. Olive," J. Catalysis, 60, 485-486 (1979).
- Matsumoto, H., "The Catalytic Effect of Carbide Formation During Fischer-Tropsch Synthesis," Chemistry Letters, 1041-1044 (1981).
- Meyer, H. S., V. L. Hill, A. Flowers, J. Happel and M. A. Hnatow, "Direct Methanation--A New Method of Converting Synthesis Gas to Substitute Natural Gas," Preprints, Div. Fuel Chem., Amer. Chem. Soc., 27, No. 1, 109-115 (1982).
- McKee, D. W., "Interaction of Hydrogen and Carbon Monoxide on Platinum Group Metals," J. Catalysis, 8, 240-249 (1967).
- Niemantsverdriet, J. W., A. M. van der Kraan, W. L. van Dijk, and H. S. van der Baan, "Behavior of Metallic Iron Catalysts During Fischer-Tropsch Synthesis Studied with Mossbauer Spectroscopy, X-Ray Diffraction, Carbon Content Determination, and Reaction-Kinetic Measurements," J. Phys. Chem., 84, 3363-3370 (1980).
- Nijs, H. H., and P. A. Jacobs, "New Evidence for the Mechanism of the Fischer-Tropsch Synthesis of Hydrocarbons," J. Catalysis, 66, 401-411 (1980).
- Nijs, H. H., and P. A. Jacobs, "Metal Particle Size Distributions and Fischer-Tropsch Selectivity. An Extended Schulz-Flory Model," J. Catalysis, 65, 328-334 (1980).
- Novak, S., R. J. Madon and H. Suhl, "Models of Hydrocarbon Product Distributions in Fischer-Tropsch Synthesis. I," J. Chem. Phys., 74, No. 11, 6083-6091 (1981).

- O'Hara, J. B., A. Bela, N. E. Jentz, and S. K. Khaderi, "Fischer-Tropsch Plant Design Criteria," Chem. Eng. Prog., 65-67, Aug. (1976).
- O'Hara, J. B., F. E. Cumare, and S. N. Rippee, "Synthetic Fuels from Coal by Fischer-Tropsch," CEP Technical Manual, Coal Processing Technology, Amer. Inst. Chem. Eng., 2, 83-87 (1975).
- Ollis, D. F., and M. A. Vannice, "The Catalytic Synthesis of Hydrocarbons from H₂/CO Mixtures over the Group VIII Metals: Comments on Methanation Kinetics," J. Catalysis, 38, 514-515 (1975).
- Olsson, R. G. and E. T. Turkdogan, "Catalytic Effect of Iron on Decomposition of Carbon Monoxide: II. Effect of Additions of H₂, H₂O, CO₂, SO₂ and H₂S," Metal. Trans., 5, 21-26 (1974).
- Ott, G. L., T. Fleisch, and W. N. Delgass, "Carbon Deposition and Activity Changes over FeRu Alloys During Fischer-Tropsch Synthesis," J. Catalysis, 65, 253-262 (1980).
- Palmer, R. L., and D. A. Vroom, "Mass-Spectrometric Measurements of Enhanced Methanation Activity over Cobalt and Nickel Foils," J. Catalysis, 50, 244-251 (1977).
- Papic, M. M., "Coal Liquefaction via Sasol Fischer-Tropsch Synthesis," CIM Bulletin, 74, 60-64 (1980).
- Parkash, S., S. K. Chakrabartty, M. P. Rosynek, "Hydrocarbon Synthesis and Carbon Dioxide Adsorption on Iron Catalysts," Fuel Processing Technology, 3, 63-70 (1980).
- Parkash, S., T. Kotanigawa, and S. K. Chakrabartty, "Changes in Pore Structure of Precipitated Iron Oxide Catalysts During Pretreatment and Hydrocarbon Synthesis Reaction," Fuel Processing Technology, 5, 203-212 (1982).
- Ponec, V., Z. Knor, and S. Cerny, "Role of Chemisorption in Simple Catalytic Reactions," Discuss. Faraday Soc., 41, 149-161 (1966).
- Ponec, V. and W. A. Van Barneveld, "The Role of Chemisorption in Fischer-Tropsch Synthesis," IEC Prod. Res. Dev., 18, 268-271 (1979).
- Rabo, J. A., A. P. Risch, and M. L. Poutsma, "Reactions of Carbon Monoxide and Hydrogen on Co, Ni, Ru, and Pd Metals," J. Catalysis, 53, 295-311 (1978).

- Rao, V. U. S., R. J. Gormley, H. W. Pennline, L. C. Schneider and R. Obermyer, "Synthesis Gas Conversion to Gasoline Range Hydrocarbons over Medium Pore Zeolite Catalysts Containing 3d-Metals and Bimetallics," Preprints, Div. Fuel Chem., Amer. Chem. Soc., 25, No. 2, 119-126 (1980).
- Raupp, G. B. and W. N. Delgass, "Mossbauer Investigation of Supported Fe and FeNi Catalysts, I." J. Catalysis, 58, 337-347 (1979).
- Raupp, G. B., and W. N. Delgass, "Mossbauer Investigation of Supported Fe and FeNi Catalysts, II. Carbides Formed by Fischer-Tropsch Synthesis," J. Catalysis, 58, 348-360 (1979).
- Raupp, G. B. and W. N. Delgass, "Mossbauer Investigation of Supported Fe Catalysts, III. In Situ Kinetics and Spectroscopy during Fischer-Tropsch Synthesis," J. Catalysis, 58, 361-369 (1979).
- Renshaw, G. D., C. Roscoe, and P. L. Walker, Jr., "Disproportionation of CO. I. Over Iron and Silicon-Iron Single Crystals," J. Catalysis, 18, 164-183 (1970).
- Renshaw, G. D., C. Roscoe, and P. L. Waker, Jr., "Disproportionation of CO. II. Over Cobalt and Nickel Single Crystals," J. Catalysis, 22, 394-410 (1971).
- Reymond, J. P., P. Meriaudeau, B. Pommier, and C. O. Bennett, "Further Results on the Reaction of H₂/CO on Fused Iron by the Transient Method," J. Catalysis, 64, 163-172 (1980).
- Riekema, M. L., A. G. Vickers, E. C. Haun, and R. C. Koltz, "A Comparison of Fischer-Tropsch Reactors," Chem. Eng. Prog., 86-90, April (1982).
- Sachtler, J. W. A., J. M. Kool and V. Ponec, "The Role of Carbon in Methanation by Cobalt and Ruthenium," J. Catalysis, 56, 284-286 (1979).
- Sancier, K. M., W. E. Isakson, and H. Wise, "Carburization Studies of Iron Fischer-Tropsch Catalysts," ACS Symposium Series, No. 33, Amer. Chem. Soc., 129-145 (1979).
- Sanders, W. N., and J. B. Maynard, "Capillary Gas Chromatographic Method for Determining the C₃-C Hydrocarbons in Full-Range Motor Gasolines," Analy. Chem., 40, 527-535 (1968).
- Sastri, M. V. C., R. Balaji Gupta, and B. Viswanathan, "Interaction of Hydrogen and Carbon Monoxide on Cobalt Catalysts. Part II," J. Catalysis, 32, 325-332 (1974).

- Satterfield, C. N., G. A. Huff, Jr., and J. P. Longwell, "Product Distribution from Iron Catalysts in Fischer-Tropsch Slurry Reactors," IEC Proc. Des. Dev., 21, 465-470 (1982).
- Scherzer, J., and D. Fort, "Zeolite-Supported Metal Catalysts for Fischer-Tropsch Reactions. I. A New Preparation Method," J. Catalysis, 71, 111-118 (1981).
- Schlesinger, M. D., H. E. Benson, E. M. Murphy, and H. H. Storch, "Chemicals from the Fischer-Tropsch Synthesis," Ind. Eng. Chem., 46, 1322-1331 (1954).
- Schultz, H., "Future Sources of Organic Raw Materials," in CHEMRAWN I, pp. 167-183, Pergamon Press, NY (1978).
- Schultz, H. and A. Zein El Deen, "New Concepts and Results Concerning the Mechanism of Carbon Monoxide Hydrogenation. I. Organic Oxygen Compounds Produced During Medium-Pressure Synthesis with Iron Catalysts," Fuel Processing Technology, 1, 31-44 (1977).
- Sexton, B. A. and G. A. Somorjai, "The Hydrogenation of CO and CO₂ over Polycrystalline Rhodium: Correlation of Surface Composition, Kinetics and Product Distributions," J. Catalysis, 46, 167-189 (1977).
- Sharma, B. K., and K. A. Kini, "Adsorption of H₂ on Precipitated Fischer-Tropsch Iron Catalysts," Current Science, 45, No. 3, 98-99 (1976).
- Sharma, B. K., and P. S. M. Tripathi, "Crystal Field Surface Orbital-Bond Energy Bond Order Calculation for Hydrogen Chemisorption on Fischer-Tropsch Iron Catalyst," Indian J. Chem., 20A, 1105-1107 (1981).
- Shchel'tsyn, V. K., R. M. Flid, I. L. Vaisman, and T. P. Shapirovskaya, "Kinetics of the Gas-Phase Vinylation of α -pyrrolidone Using Basis Catalysts," Russian J. Phy. Chem., 42, No. 7, 869-872 (1968).
- Schlef, M., and R. A. Dalla Batta, "Reply to Comments on Heterogeneous Methanation: Absence of H₂-D₂ Kinetic Isotope Effect on Ni, Ru, and Pt," J. Catalysis, 60, 169-170 (1979).
- Shirazi, Z. H., and C. Stojanov, "Reaction Gas-Chromatography of Fischer-Tropsch Synthesis Products Including the Oxygen Containing Compounds," Pakistan J. Sci Ind. Res., 20, No. 1, 1-10 (1977).

- Shultz, J. F., M. Abelson, L. Shaw, and R. B. Anderson, "Fischer-Tropsch Synthesis: Nitrides and Carbonitrides of Iron as Catalysts," Ind. Eng. Chem., 49, No. 12, 2055-2060 (1957).
- Shultz, J. F., W. K. Hall, B. Seligman and R. B. Anderson, "Studies of the Fischer-Tropsch Synthesis. XIV. Hagg Iron Carbide as Catalysts," J. Am. Chem. Soc., 77, 213-221 (1955).
- Shultz, J. F., B. Seligman, J. Lecky, and R. B. Anderson, "Studies of the Fischer-Tropsch Synthesis. XII. Composition Changes of Nitrided Iron Catalysts During the Synthesis," J. Am. Chem. Soc., 74, 637-640 (1952).
- Shultz, J. F., B. Seligman, L. Shaw, and R. B. Anderson, "Effect of Nitriding on Three Types of Iron Catalysts," Ind. Eng. Chem., 44, 397-401 (1952).
- Singh, Manohar, "Why Not Use Fischer-Tropsch?," Hydrocarbon Processing, p. 138, June (1981).
- Singh, K. J. and H. E. Grenga, "Catalytic Decomposition of Carbon Monoxide on Single Crystalline Ruthenium," J. Catalysis, 47, 328-332 (1977).
- Stein, K. C., G. P. Thompson, and R. B. Anderson, "Iron Catalysts and the Fischer-Tropsch Synthesis," Ind. Eng. Chem., 49, 410 (1957).
- Stein, K. C., G. P. Thompson, and R. B. Anderson, "Studies of the Fischer-Tropsch Synthesis, XVII. Changes of Iron Catalysts During Pretreatment and Synthesis," J. Am. Chem. Soc., 61, 928-932 (1957).
- Stowe, R. A., and C. B. Murchison, "Upgrade F-T Liquids to Olefins and Aromatics," Hydrocarbon Processing, 147-150, Jan. (1982).
- Strouf, O., K. Kuchynka, and J. Fusek, "Modelling of the Catalytic Fischer-Tropsch Synthesis by Pattern Recognition. Chemisorption and Dissociation of Carbon Monoxide on Metals," Collection Czechoslovak Chem. Commun., 46, 2336-2344 (1981).
- Swart, J. S., G. J. Czajkowski, and R. E. Conser, "Sasol Upgrades," Oil and Gas Journal, 62-66 (1981).
- Tauster, S. J. and R. M. Koros, "Removal of Coke Precursors with Hydrogen: Studies with Alternating Pulses of Propane and Hydrogen," J. Catalysis, 27, 307-310 (1972).

- Ta-Yu, Chang, L. Nan-Tsuen, and C. Chun-Hao, "Report on Pilot Plant Synthesis of Liquid Fuels," Chem. Eng. Prog., 54, No. 3, 55-58 (1958).
- Thomson, W. J., J. M. Arndt, and K. L. Wright, "Applied Fischer-Tropsch Kinetics for a Flame Sprayed Iron Catalyst," Preprints, Div. Fuel Chem., Amer. Chem. Soc., 25, No. 2, 101-118 (1980).
- Trimm, D. L., "The Formation and Removal of Coke from Nickel Catalyst," Catal. Rev.-Sci. Eng., 16, No. 2, 155-189 (1977).
- Turkdogan, E. T., and J. V. Vinters, "Catalytic Effect of Iron on Decomposition of Carbon Moxoxide: I. Carbon Deposition in H₂-CO Mixtures," Metal. Trans., 5, 11-19 (1974).
- Unmuth, E. E., L. H. Swartz, and J. B. Butt, "Iron Alloy Fischer-Tropsch Catalysts, I. Oxidation-Reduction Studies of the Fe-Ni System," J. Catalysis, 61, 242-255 (1980).
- Unmuth, E. E., L. H. Schwartz, and J. B. Butt, "Iron Alloy Fischer-Tropsch Catalysts, II. Carburization Studies of the Fe-Ni System," J. Catalysis, 63, 404-414 (1980).
- Van Barneveld, W. A. A., V. Ponec, "Influence of Alloying on the Selectivity in Fischer-Tropsch Synthesis by Nickel-Copper Alloys," J. Catalysis, 51, 426-430 (1978).
- Vannice, M. A., "The Catalytic Synthesis of Hydrocarbons from H₂/CO Mixtures Over the Group VIII Metals, II. The Kinetics of the Methanation Reaction," J. Catalysis, 37, 462-473 (1975).
- Vannice, M. A., "The Catalytic Synthesis of Hydrocarbons from H₂/CO Mixtures Over Group VIII Metals, III," J. Catalysis, 40, 129-134 (1975).
- Vannice, M. A., "The Catalytic Synthesis of Hydrocarbons from H₂/CO Mixtures Over the Group VIII Metals, IV. The Kinetic Behavior of CO Hydrogenation Over Ni Catalysts," J. Catalysis, 44, 152-162 (1976).
- Vannice, M. A., "The Catalytic Synthesis of Hydrocarbons from H₂/CO Mixtures Over the Group VIII Metals. V. The Catalytic Behavior of Silica-Supported Metals," J. Catalysis, 50, 228-236 (1977).
- Vannice, M. A., "Solid State Chemistry of Energy Conversion and Storage," Advances in Chemistry Series, Amer. Chem. Soc., No. 163, 15-32 (1977).

- Vannice, M. A., and R. L. Garten, "The Influence of the Support on the Catalytic Behavior of Ruthenium in CO/H₂ Synthesis Reactions," J. Catalysis, 63, 255-260 (1980).
- Vannice, M. A., and R. L. Garten, "CO Hydrogenation Reactions Over Titania-Supported Nickel," J. Catalysis, 66, 242-247 (1980).
- Vannice, M. A. and R. L. Garten, "Metal-Support Effects on the Activity and Selectivity of Ni Catalysts in CO/H₂ Synthesis Reactions," J. Catalysis, 56, 236-248 (1979).
- Wedler, G., H. Papp, and G. Schroll, "The Interaction of Hydrogen and Carbon Monoxide on Polycrystalline Nickel Films at Temperatures up to 353 K," J. Catalysis, 38, 153-165 (1975).
- Weil, B. H. and J. C. Lane, The Technology of the Fischer-Tropsch Process, Constable and Co., Ltd., London (1949).
- White, G. A., T. R. Roszkowski and D. W. Stanbridge, "Predict Carbon Formation," Hydrocarbon Processing, 130-136, July (1975).
- Wilson, T. P., "Comments on Heterogeneous Methanation: Absence of H₂-D₂ Kinetic Isotope Effect on Ni, Ru, and Pt," J. Catalysis, 60, 167-168 (1979).
- Yokoyama, A. H. Komiyama, H. Inoue, T. Masumoto and H. Kimura, "The Fischer-Tropsch Synthesis by Amorphous Fe₂₀Ni₆₀P₂₀ and Fe₉₀Zr₁₀ Catalysts," Chemical Reaction Engineering, Advances in Chemistry Series, Amer. Chem. Soc., pp. 237-248 (1982).
- Zen El Deen, A., J. Jacobs, and M. Baerns, Proceedings of 5th International Sympos. Chem. React. Eng., Houston, pp. 26-36 (1977).

5.3 Development of Working Equations for Measurements of Heat Transfer Coefficient Between a Flowing Supernatant Gas and a Shallow Fluidized Bed in a Heat Tray

5.3.1 Heat Tray System Diagram and Simplifying Modeling Assumptions

Figure 5.2 shows a schematic diagram of the heat tray system used in the development of working equations for measurements of heat transfer coefficient between a flowing supernatant gas (S-gas) and a shallow fluidized bed. Figures 5.3 and 5.4 depict, respectively, the expanded versions of the upper half (freeboard) and lower half (fluidized bed) of the heat tray. The following simplifying assumptions are made in the modeling of this heat tray system.

(1) The system is well-insulated and at a steady state. There is no heat loss from the system. In other words, the system can be considered to be in a steady-state adiabatic operation.

(2) Heat capacities of the fluidizing and supernatant gas streams (F-gas and S-gas) and of the cooling water can be considered practically constant over the range of operating temperatures of the system.

(3) The temperature of the F-gas leaving the fluidized bed (T_f in Figure 5.3) can be considered as practically constant.

(4) The temperature of the flowing gas stream in the upper half (freeboard zone) of the heat tray (T in Figure 5.3) is only a function of the distance along the gas flow path (x direction), with $T = T_S$ (S-gas inlet temperature) at $x = 0$ and $T = T_g$ (combined F-gas and S-gas outlet temperature) at $x = a$.

(5) The heat transfer coefficient h between the flowing S-gas and the fluidized bed can be assumed to be practically constant.

5.3.2 Notations Used in Heat Transfer Model Development

- | | |
|---|---|
| A | the projected horizontal area of the fluidized bed, $a \cdot b$, m^2 or ft^2 |
| a | the length of the heat tray, Figure 5.3, m or ft |
| b | the depth of the heat tray, Figure 5.3, m or ft |
| c | the height of the freeboard zone in the heat tray, Figure 5.3, m or ft |

Differential Shell
Thickness Δx

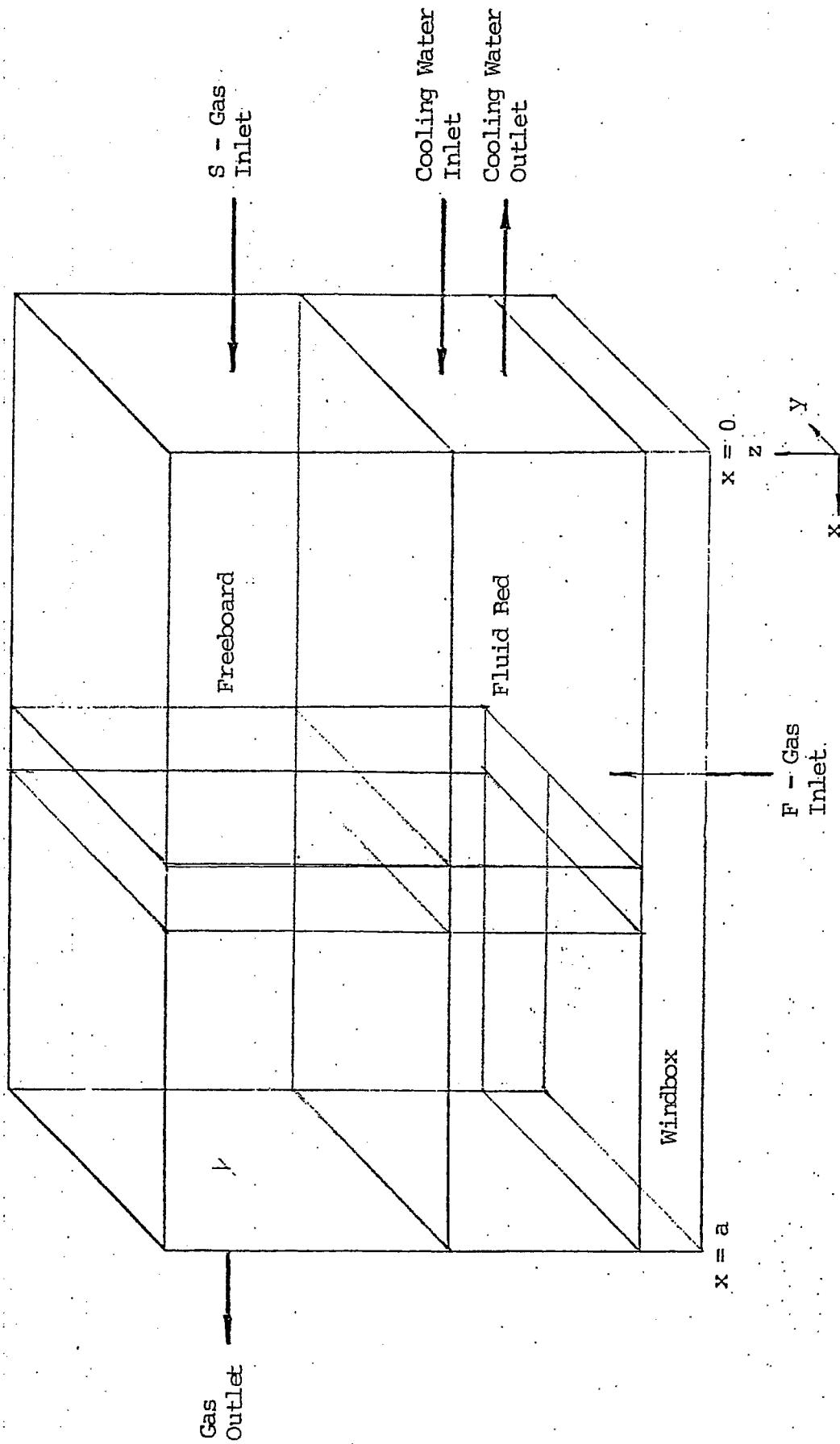


Figure 5.2 A Schematic Diagram of the Control Volume for Mass and Energy Balances for the Heat Tray

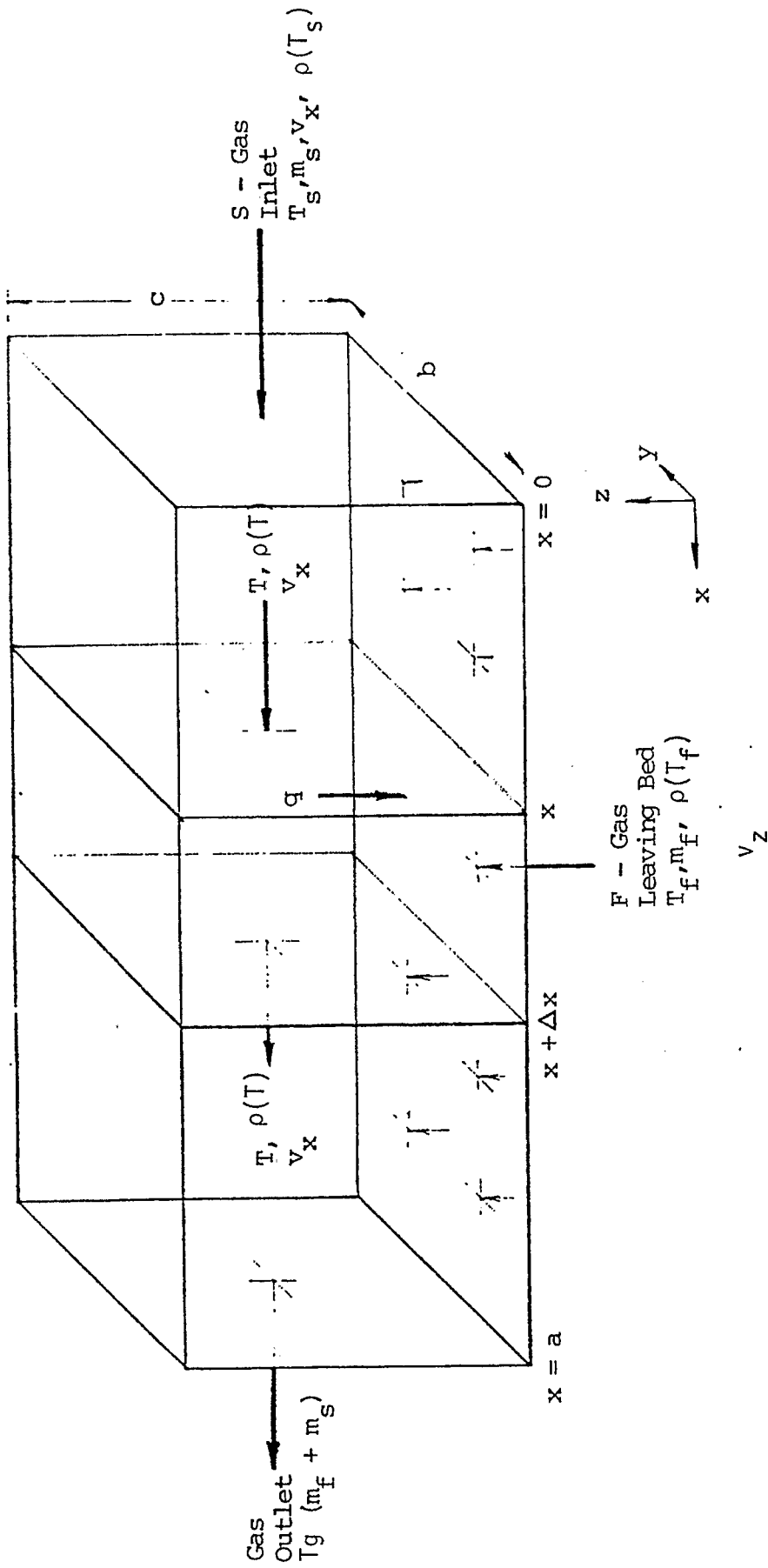


Figure 5.3 A Schematic Diagram of the Control Volume for Mass and Energy Balances for the Upper Half (Freeboard) of the Heat Tray

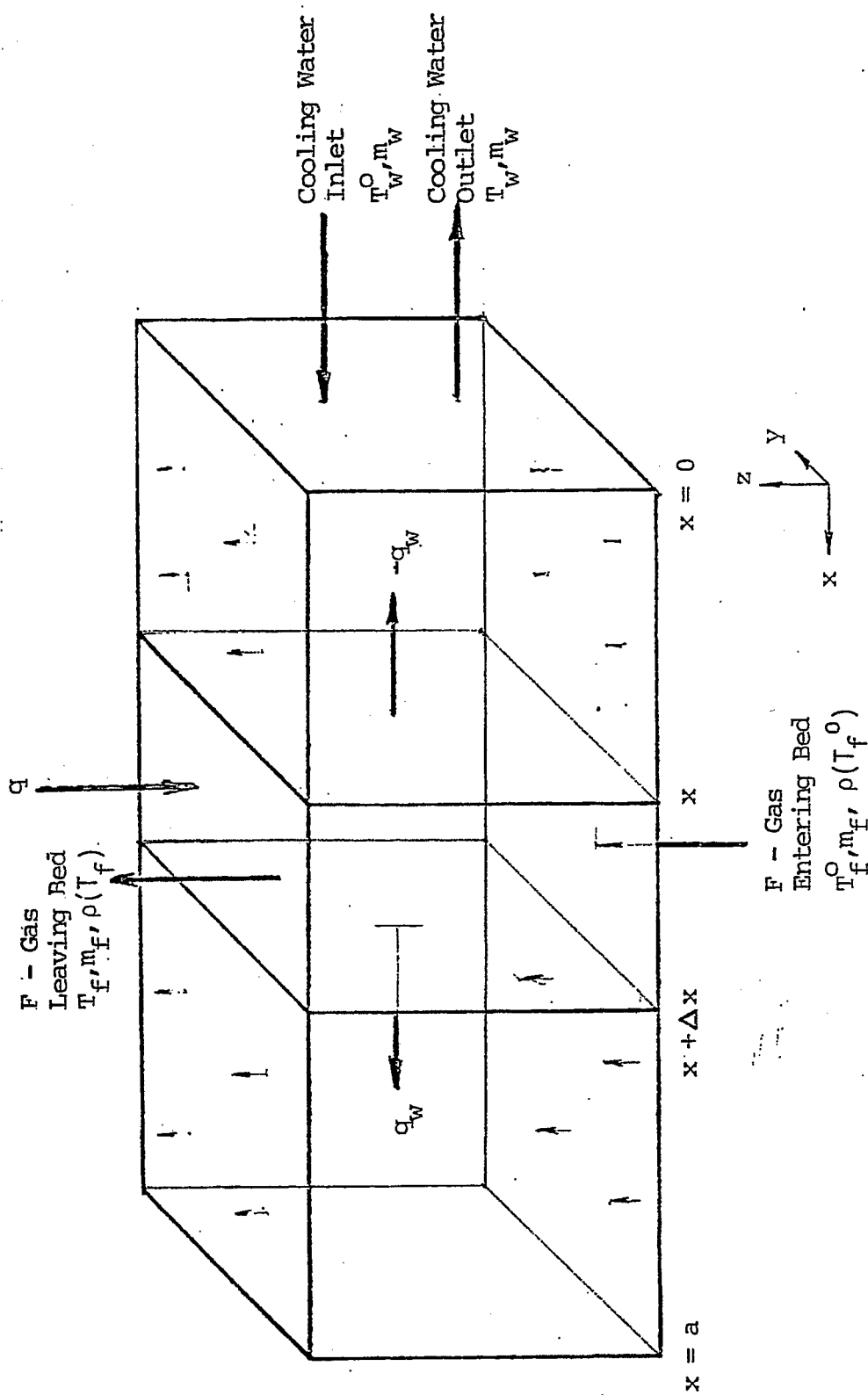


Figure 5.4 A Schematic Diagram of the Control Volume for Mass and Energy Balances for the Lower Half (Fluidized Bed) of the Heat Tray.

C_p	the heat capacity of the flowing gas
C_{pw}	the heat capacity of the cooling water, J/kg·°K or Btu/lb·°F
h	the heat transfer coefficient between the flowing supernatant gas (S-gas) and the shallow fluidized bed, W/m ² ·°K or Btu/ft ² ·hr·°F
I	an integration constant in the model development
m_f	the mass flow rate of the fluidizing gas (F-gas), hg/s or lb/s
m_s	the mass flow rate of the supernatant gas (S-gas), kg/s or lb/s
m_w	the mass flow rate of the cooling water, kg/s or lb/s
q	the heat flux transferred from the S-gas to the fluidized bed, W/m ² or Btu/hr·ft ²
q_w	the heat flux from the immersed heat-transfer tube in the fluidized bed to the cooling water
T	the temperature of flowing gas in the freeboard zone of the heat tray, °C or °F
T_f	the temperature of the fluidizing gas (F-gas) leaving the fluidized-bed zone of the heat tray, °C or °F
T_f^0	the temperature of the fluidizing gas (F-gas) entering the fluidized-bed zone of the heat tray, °C or °F
T_g	the temperature of the combined F-gas and S-gas stream leaving the freeboard zone of the heat tray, °C or °F
T_o	an arbitrary reference temperature in energy balance over the heat tray, °C or °F
T_s	the temperature of the supernatant gas (S-gas) entering the freeboard zone of the heat tray, °C or °F
T_w	the outlet temperature of the cooling water through the immersed heat-transfer tube in the fluidized bed, °C or °F
T_w^0	the inlet temperature of the cooling water through the immersed heat-transfer tube in the fluidized bed, °C or °F

- v_x the velocity of the flowing supernatant gas (S-gas) in the freeboard zone of the heat tray, m/s or ft/s
- v_z the velocity of the fluidizing gas (F-gas) in the fluidized-bed zone of the heat tray, m/s or ft/s
- x, y, z the coordinates used in modeling the heat tray system
- $\rho(T_i)$ the density of the gas stream at temperature T_i , kg/m³ or lb/ft³

5.3.3 The Upper Half or Freeboard Zone of the Heat Tray: Figure 5.3

Consider the rectangular differential volume defined by $\Delta x \cdot \Delta y \cdot \Delta z$ or $\Delta x \cdot b \cdot c$ shown in Figure 5.3. When mass inputs are equated to mass outputs, one obtains the steady-state mass balance on the rectangular differential volume $\Delta x \cdot b \cdot c$ of the freeboard zone of the heat tray as follows

$$v_z \rho(T_f) b \Delta x + \rho(T) v_x \Big|_x bc = \rho(T) v_x \Big|_{x+\Delta x} bc$$

Dividing each term by $\Delta x \cdot bc$, rearranging the result and taking the limit as Δx approaches zero then gives

$$v_z \rho(T_f) / c = \frac{d}{dx} [\rho(T) v_x]$$

Integrating both sides of the equation from $x = 0$ to $x = a$ and introducing the initial condition that at $x = 0$, $\rho(T) = \rho(T_s)$, one obtains the following expression

$$\rho(T) v_x = \frac{\rho(T_f) v_z}{c} x + \rho(T_s) v_x$$

Noting that $m_f = \rho(T_f) v_z b a$ and $m_s = \rho(T_s) v_x b c$, the above equation can be written as

$$v_x = \frac{1}{\rho(T) b c} \left(\frac{m_f}{a} x + m_s \right) \quad (1)$$

For the same rectangular differential volume shown in Figure 5.3, the contributions to the steady-state energy balance are as follows

Energy in by F-gas flow	$\rho(T_f)C_p v_z (T_f - T_o) \Delta x \cdot b$
Energy in by S-gas flow	$[\rho(T)C_p v_x (T - T_o)] \Big _x^{bc}$
Energy out by S-gas flow	$[\rho(T)C_p v_x (T - T_o)] \Big _{x+\Delta x}^{bc}$
Energy out by transfer from S-gas flow to fluidized bed	$q \Delta x \cdot b = h(T - T_f) \Delta x \cdot b$

By equating the sum of energy inputs to that of energy outputs, one obtains the steady-state energy balance on the rectangular differential volume $\Delta x \cdot b \cdot c$ of the freeboard zone of the heat tray as follows.

$$\rho(T_f)C_p v_z (T_f - T_o) \Delta x \cdot b + [\rho(T)C_p v_x (T - T_o)] \Big|_x^{bc}$$

$$= [\rho(T)C_p v_x (T - T_o)] \Big|_{x+\Delta x}^{bc} + h(T - T_f) \Delta x \cdot b$$

Dividing each term by $\Delta x \cdot bc$, rearranging the result and taking the limit as Δx approaches zero then gives

$$\frac{d}{dx} [\rho(T) v_x (T - T_o)] = \frac{-h(T - T_f)}{cc_p} + \frac{\rho(T_f) v_z (T_f - T_o)}{c}$$

$$= \frac{-h(T - T_f)}{cc_p} + \frac{m_f (T_f - T_o)}{abc}$$

In obtaining the last equation, the relationship $m_f = \rho(T_f) v_z b a$ has been used.

Next, by differentiating the left-hand side by parts and substituting Eq. (1) for v_x into the resulting expression, one obtains

$$\begin{aligned} (T-T_0) \frac{d}{dx} [\rho(T)v_x] + \rho(T)v_x \frac{dT}{dx} &= \frac{(T-T_0)m_f}{abc} + \left[\frac{m_f x}{abc} + \frac{m_s}{bc} \right] \frac{dT}{dx} \\ &= \frac{h(T-T_f)}{cc_p} + \frac{m_f(T_f-T_0)}{abc} \end{aligned}$$

Therefore, the change of the temperature of flowing gas stream in the freeboard zone of the heat tray is governed by

$$\frac{dT}{dx} = \frac{\left[\frac{m_f}{a} + \frac{hb}{c_p} \right] (T_f - T)}{\frac{m_f x}{a} + m_s}$$

Integrating both sides of this equation from $x = 0, T = T_s$ to $x = a, T = T_g$ gives the following relationship

$$\ln \left[\frac{T_g - T_f}{T_s - T_f} \right] = \left[\frac{-hA}{m_f c_p} - 1 \right] \ln \left[1 + \frac{m_f}{m_s} \right] \quad (2)$$

where $A = a \cdot b =$ the projected horizontal area of the fluidized bed. This relationship can also be written as:

$$h = \frac{-m_f c_p}{A} \left[\frac{\ln \left[\frac{T_g - T_f}{T_s - T_f} \right]}{\ln \left[1 + \frac{m_f}{m_s} \right]} + 1 \right] \quad (3)$$

In order to use Eq. (2) to find the heat transfer coefficient h , one needs to know the temperature T_f of the fluidizing gas (F-gas) leaving the fluidized-bed zone of the heat tray. This temperature can be found by making an energy balance over the fluidized-bed zone in terms of experimentally measurable variables.

5.3.4 The Lower Half or Fluidized Zone of the Heat Tray: Figure 5.4

Consider the rectangular differential volume defined by $\Delta x \cdot \Delta y \cdot \Delta z$ or $\Delta x \cdot b \cdot c$ shown in Figure 5.4. The contributions to the steady-state energy balance are as follows.

Energy in by
F-gas flow

$$\rho(T_f^0)C_p v_z^0 (T_f^0 - T_0) \Delta x \cdot b$$

Energy in by
transfer from
S-gas flow to
fluidized bed

$$q \Delta x \cdot b = h(T - T_f) \Delta x \cdot b$$

Energy out by
F-gas flow

$$\rho(T_f)C_p v_z (T_f - T_0) \Delta x \cdot b$$

Energy out by
transfer from immersed
heat transfer tube
to cooling water

$$-\left[q_w \Big|_x - q_w \Big|_{x+\Delta x} \right]$$

Based on these energy inputs and outputs, the steady-state energy balance on the rectangular differential volume $\Delta x \cdot b \cdot c$ of the fluidized-bed zone of the heat tray can be written as follows:

$$\begin{aligned} & \rho(T_f^0)C_p v_z^0 (T_f^0 - T_0) \Delta x \cdot b + h(T - T_f) \Delta x \cdot b \\ & = \rho(T_f)C_p v_z (T_f - T_0) \Delta x \cdot b - \left[q_w \Big|_x - q_w \Big|_{x+\Delta x} \right] \end{aligned}$$

Dividing each term by $\Delta x \cdot b \cdot c$, rearranging the result and taking the limit as Δx approaches zero then gives

$$\begin{aligned} \frac{dq_w}{dx} &= h(T - T_f)b + \left[\rho(T_f^0)C_p v_z^0 (T_f^0 - T_0) - \rho(T_f)C_p v_z (T_f - T_0) \right] b \\ &= h(T - T_f)b + \frac{m_f C_p (T_f^0 - T_f)}{a} \end{aligned}$$

Here, the relationship $m_f = \rho(T_f^0)v_z^0 b a = \rho(T_f)v_z b a$ has been used. By integrating both sides of the last equation from $x = 0, q = 0$ to $x = a, q = q_w$, one obtains the following expression

$$q_w = m_f C_p (T_f^0 - T_f) - m_s C_p (T_s - T_f) [(1 + \alpha)^{-\beta} - 1]$$

where $m_f = \rho(T_f)v_z ba$, $m_s = \rho(T_s)v_x bc$, $\alpha = m_f/m_s$, and

$$\beta = (hba)/(m_f C_p) = (ha)/(m_f C_p).$$

By defining $\gamma = q_w/(m_f C_p)$, the integrated equation for q_w can be rearranged to give the following explicit expression for the temperature T_f of the fluidizing gas (F-gas) leaving the fluidized-bed zone of the heat tray:

$$T_f = \frac{\gamma + \frac{T_s}{\alpha} [(1+\alpha)^{-\beta} - 1] - T_f^0}{\left[\frac{(1+\alpha)^{-\beta} - 1}{\alpha} \right] - 1} \quad (4)$$

5.3.5 The Working Equation for Measurements of Heat Transfer Coefficient Between a Flowing Supernatant Gas and a Shallow Fluidized Bed in a Heat Tray

The preceding results can be combined to give an explicit equation for finding the heat transfer coefficient h from experimentally measurable variables. First, Eq. (3) gives

$$-\beta \equiv \frac{-hA}{m_f C_p} = 1 + \frac{\ln \left[\frac{T_g - T_f}{T_s - T_f} \right]}{\ln [1+\alpha]}$$

where $\alpha = m_f/m_s = [\rho(T_f)v_z ba]/[\rho(T_s)v_x bc]$. This equation is the same as

$$\ln [1+\alpha]^{-(\beta+1)} = \ln \left[\frac{T_g - T_f}{T_s - T_f} \right]$$

or

$$T_f = \frac{T_s (1+\alpha)^{-(\beta+1)} - T_g}{(1+\alpha)^{-(\beta+1)} - 1} \quad (5)$$

Substituting Eq. (5) into Eq. (3) then gives

$$h = \frac{-m_f C_p}{A} \ln \left[\frac{[T_s - \gamma\alpha - T_g(1+\alpha)]}{\left[\frac{T_s + T_f^0 \alpha - \gamma\alpha}{(1+\alpha)} - T_g \right]} \right] \quad (6)$$

where

$$\gamma = \frac{m_w C_{pw} (T_w - T_w^0)}{m_f C_p}$$

$$\alpha = m_f / m_s = [\rho(T_f) v_z ba] / [\rho(T_s) v_x bc].$$

Eq. (6) is the final working equation for finding the heat transfer coefficient h from experimentally measurable variables in the heat tray.

SATISFACTION GUARANTEED

NTIS strives to provide quality products, reliable service, and fast delivery. Please contact us for a replacement within 30 days if the item you receive is defective or if we have made an error in filling your order.

▲ **E-mail: info@ntis.gov**

▲ **Phone: 1-888-584-8332 or (703)605-6050**

Reproduced by NTIS

National Technical Information Service
Springfield, VA 22161

This report was printed specifically for your order from nearly 3 million titles available in our collection.

For economy and efficiency, NTIS does not maintain stock of its vast collection of technical reports. Rather, most documents are custom reproduced for each order. Documents that are not in electronic format are reproduced from master archival copies and are the best possible reproductions available.

Occasionally, older master materials may reproduce portions of documents that are not fully legible. If you have questions concerning this document or any order you have placed with NTIS, please call our Customer Service Department at (703) 605-6050.

About NTIS

NTIS collects scientific, technical, engineering, and related business information – then organizes, maintains, and disseminates that information in a variety of formats – including electronic download, online access, CD-ROM, magnetic tape, diskette, multimedia, microfiche and paper.

The NTIS collection of nearly 3 million titles includes reports describing research conducted or sponsored by federal agencies and their contractors; statistical and business information; U.S. military publications; multimedia training products; computer software and electronic databases developed by federal agencies; and technical reports prepared by research organizations worldwide.

For more information about NTIS, visit our Web site at <http://www.ntis.gov>.

NTIS

**Ensuring Permanent, Easy Access to
U.S. Government Information Assets**



U.S. DEPARTMENT OF COMMERCE
Technology Administration
National Technical Information Service
Springfield, VA 22161 (703) 605-6000
